INVESTIGATION INTO THE FUNCTIONAL ROLE OF CHROMOPROTEINS IN THE
PHYSIOLOGY AND ECOLOGY OF THE HAWAIIAN STONY CORAL *MONTIPORA FLABELLATA*
IN KĀNEʻOHE BAY, OʻAHU

A DISSERTATION SUBMITTED TO THE GRADUATE DIVISION OF
THE UNIVERSITY OF HAWAIʻI AT MĀNOA
IN PARTIAL FULFILLMENT OF THE REQUIREMENTS FOR THE DEGREE OF
DOCTOR OF PHILOSOPHY

IN

MARINE BIOLOGY

DECEMBER 2019

By

Angela Richards Donà

Dissertation Committee:

Cynthia Hunter, Chairperson
Celia Smith
Kuʻulei Rodgers
Amber Wright
Philip Williams

Keywords: *Montipora flabellata*, chromoproteins, histology, confocal laser scanning microscopy, coral photophysiology, PAM fluorometry

ACKNOWLEDGMENTS

I would like to begin by thanking my committee chair, Dr. Cynthia Hunter. I originally came to Hawaii to work on coral disease—a continuation from my master's degree work—but when I decided I wanted to pivot to photobiology and coral pigments, she enthusiastically encouraged me to do so. She has been very supportive of my decision to learn an entirely new topic in coral physiology and I am grateful to her for allowing me to pursue the avenues of investigation that most interested me.

I am so grateful to Dr. Celia Smith for all the helpful input she has given me on this project. I have greatly appreciated her directness and encouragement, and I remain in awe of her ability to send me away after our meetings with many more questions than I had when I walked into her lab. Her enthusiasm for science and algae is inspiring, as is her vast knowledge and ability to communicate science.

Dr. Kuʻulei Rodgers is one of the warmest, most generous people I know. She took over the management of our lab when its founder Paul Jokiel passed away. Although she had many new responsibilities, she agreed to be on my committee, and I am grateful for that. It was a lot, I know, at a very bad time. She has supported me for several years, has given me many opportunities to contribute to lab projects, and even gave me the much-needed stiff kick-in-the-behind when it was time to finish. We have been on many field outings and work adventures and have had many good times together. I am amazed at how productive she is and how well she has held our lab together with so many projects and a ceaseless stream of requests for her help and time. She almost always says yes.

I feel tremendous gratitude for having had the opportunity to work with Dr. Paul Jokiel. I was so pleased when he welcomed me into the Point Lab ʻohana. He was a true pioneer of coral reef science and the work he did on the effects of ultraviolet radiation on reef organisms was highly influential in my decision to pursue photobiological questions. His presence and wisdom are greatly missed by all.

It is hard to believe how much impact Dr. Amber Wright has had on me and my work given the brief time I have known her. She became a committee member at a very late point in my graduate career, but her input has been immense. I cannot thank her enough for being available, helpful, and frankly, for getting me back on track when I needed it most.

I am grateful to Philip Williams for his kindness and generosity. He is a great instructor and was often so helpful when I just needed to talk things out. His presence on my committee was important and I truly appreciate his input and helpful comments.

Esther Peters was on my master's committee, was originally on my PhD committee until circumstances made that impossible and has been my mentor since the beginning of my science career. She is such an accomplished and respected scientist, an incredibly knowledgeable expert in the field of

ABSTRACT

The distinctly purple, stony coral *Montipora flabellata* Studer is endemic to Hawai‘i and stands out in bright contrast among the muted brown tones of most other coral species on the reef. Its unique coloration is due to the presence of non-fluorescent pigment protein complexes called chromoproteins (CPs). CPs absorb light energy in the yellow region of the photosynthetically active radiation (PAR) spectrum, which is potentially harmful to the mechanism of electron replacement in photosynthesis. These pigments, however, are separate and distinct from the brown photosynthetic pigments in the symbiotic dinoflagellates (zooxanthellae). Colonies appear uniformly brownish purple suggesting a homogeneous surface distribution of CPs that are as well-distributed as the symbionts. Pigment location across the colony surface provides some insight into the potential functions these pigments serve, i.e., growth enhancement, photoprotection, or an immune response, but this topic has not been explored in Hawaiian coral species. Several common corals in Hawai‘i have been extensively researched, but no studies have looked specifically at CP or fluorescent pigment (FP) function, and very little research has been conducted on *M. flabellata* for any purpose. The principal goal of the present investigation was to determine whether CPs in *M. flabellata* serve a photoprotective function. Since photoprotection entails blocking light energy before it reaches the symbionts, the CPs would necessarily be located between the coral tissue/seawater interface and the zooxanthellae, i.e., in the coral epidermis. I employed the use of histological staining techniques, light microscopy, and confocal laser scanning microscopy to locate CPs and FPs in coral epithelia. The investigation expanded to include basic information on anatomy, photosynthetic efficiency, and habitat requirements for *M. flabellata* when a lack of fundamental information on the species was exposed. This research fills some of the gaps in our knowledge of this species and by comparison several other common species in Kāne‘ohe Bay. Entire reef surveys from 22 patch reefs provide updated information on the distribution of *M. flabellata* in the lagoon region of the Bay. Analysis of *M. flabellata* histoslides provide evidence of CPs in the epidermis and a highly reduced number or lack of mucocytes. This trade-off suggests CPs are more important than production of mucus in *M. flabellata* and is consistent with a photoprotective function. Whole coral reflectance measurements provide details of coral host and symbiont pigment absorbance *in hospite*, while they also highlight the challenges of working with an intact, biological system. Photosynthetic parameters; F_v/F_m, ETR_{max}, ΔNPQ, and E_k, were characterized from rapid light curves (RLCs) using pulse amplitude-modulated (PAM) fluorometry and provided valuable information that improves our understanding of the photo-physiological functioning of the species and its relationship to the light environment. Best practices for PAM fluorometry use are discussed in detail since this powerful tool was extensively utilized during the investigation and important lessons were learned.

TABLE OF CONTENTS

LIST OF TABLES

LIST OF FIGURES

Chapter 1

Chapter 2

LIST OF ABBREVIATIONS

ANOM	analysis of means
ANOVA	analysis of Variance
AU	airy unit
BBW	basal body wall
CFP	cyan fluorescent pigment (or protein)
CGB	cnidoglandular band
Ci	cilia
Cn	cnidae
Coen	coenenchyme
CREL	Coral Reef Ecology Laboratory
CRN	CRIMP Buoy North
CRW	CRIMP buoy West
CRIMP	Coral Reef Instrumented Monitoring Platform
DD	diadinoxanthin
DN	dinoxanthin
EDTA	ethylenediaminetetraacetic acid
E_k	minimum saturating irradiance
Ep	epidermis
ETR	electron transport rate
FP	fluorescent pigment (or protein)
F_m	maximal fluorescence
F_v	variable fluorescence
Ga	gastrodermis
GFP	green fluorescent pigment (or protein)
GGC	granular gland cells
H&E	Hematoxylin & Eosin
HIMB	Hawai'i Institute of Marine Biology
HL	high light
LHCII	light harvesting complex II
LP	*Leptastrea purpurea*
LSM	laser scanning microscopy
MAA	mycosporine-like amino acids

Me	melanin granules
MF	*Montipora flabellata*
Mg	mesoglea
MP	*Montipora patula*
Mu	mucocyte
NPQ	non-photochemical quenching
Nu	nuclei
OEC	oxygen-evolving complex
PAM	pulse amplitude-modulated (fluorometry)
PAR	Photosynthetically Active Radiation
PC	*Porites compressa*
PFD	photon flux density
PR	patch reef
PSII	Photosystem II
RFP	red fluorescent pigment (or protein)
RLC	rapid light curve
ROS	radical oxygen species
SBE	Sand bar East
SBS	Sand bar West
SBW	surface body wall
Sp	spirocyte
Sy	symbiont
UVR	ultra-violet radiation

INTRODUCTION

The Hawaiian endemic coral *Montipora flabellata* Studer derives its purple or blue coloration from pigment protein complexes called chromoproteins (CPs). CPs are highly similar in structure to fluorescent proteins (FPs) although they do not fluoresce and are easily observed in daylight. When present, FPs and CPs are generally located at colony growing tips and margins or tend to be highly focal and patterned across the colony surface. The different locations and patterning likely indicate different functions. For instance, FPs and/or CPs at branch tips are believed to aid in coral growth (D'Angelo et al. 2012) and some patterning may signify an immune response, i.e., in Trematodiasis in *Porites* spp. corals (Palmer et al. 2009). The uniformity of the often bright, purple CPs across the entirety of the colony surface in *M. flabellata* indicates the possibility of yet another function. This investigation was devised to determine the functional role of CPs in *M. flabellata* and whether these pigments influence the ecology of this coral in Kāneʻohe Bay, Oʻahu.

Montipora flabellata is the sixth most abundant coral in the main Hawaiian Islands (Rodgers et al. 2015) but it is not common on all reefs. It is known to inhabit reef environments with high water flow and colonies have been documented on Hawaiʻi, Maui, Oʻahu, Kauaʻi, Molokaʻi, and Kahoʻolawe (Coral Reef Assessment and Monitoring Project; CRAMP). In 1970-1972 extensive coral distribution surveys were conducted in Kāneʻohe Bay and presence of *M. flabellata* colonies were documented in the major incoming and outgoing channels and outside the barrier reef. Colonies were not found on patch reefs in the lagoon or on the coastal fringing reefs (Maragos 1972), but in August 2014, pale and bleached *M. flabellata* colonies were observed on patch reefs within the lagoon portion of the Bay. The lavender and white *M. flabellata* colonies were surrounded by fully pigmented colonies of other species. These observations indicated that *M. flabellata* was highly vulnerable to elevated seawater temperatures and provided evidence that the species was present in a previously undocumented area. A literature search on *M. flabellata* yielded little information, exposing a major gap in our understanding of the ecology and physiology of this important Hawaiian coral species. In the present investigation, I sought to fill some of that gap by conducting distribution surveys in Kāneʻohe Bay, verifying the species' suggested requirement for high water flow habitat, and determining the function of the highly prominent chromoproteins.

Corals from the order Scleractinia are the primary reef-building organisms on most coral reefs. Also termed stony corals, these autogenic engineers (Jones et al. 1994) build the underlying structures of their tropical ecosystems with energy produced by their symbiotic dinoflagellate partners (zooxanthellae) from the family Symbiodiniaceae. This partnership is arguably the most productive in the marine environment (Trench 1993). Abundant solar irradiance fuels this productivity resulting in a living reef

structure that supports a myriad of reef-associated organisms and ecosystem services. The importance of the mutualistic relationship is as well-documented as it is extraordinary; the microscopic algae actually inhabit the gastrodermal cells of the coral and provide nearly all of their photosynthate to the coral host (Falkowski et al. 1984). The products of zooxanthellate photosynthesis contribute up to 100% of coral's reduced carbon needs but the dependence on photosynthate also limits coral growth to the tropical photic zone where light is consistent year round (Yonge et al. 1931; Kawaguti 1944; Goreau 1959; Falkowski et al. 1984). It is widely believed that sessile corals receive the greatest benefit from this relationship, however, coral metabolic processes may also supply zooxanthellae with required inorganic nutrients (Muscatine and Porter 1977; Falkowski et al. 1984). Importantly, these intracellular guests reside in a homogeneous light environment that is superb in reflecting and diffusing incident solar irradiance. Light energy that reaches the surface of a stony coral is eventually captured by the algal photosynthetic machinery with high efficiency (Enrıquez et al. 2005; Marcelino et al. 2013). The enhanced light environment, however, can be problematic for zooxanthellae when light is supersaturating, particularly when other stressors are present. Because supersaturating light conditions are likely to occur for many hours each day, the ability to divert excess solar irradiance is fundamental to symbiont survival.

Zooxanthellae are coccoid, single-celled dinoflagellates with unique physiological adaptations for life as intracellular symbionts. When free-living, zooxanthellae cells are biflagellate—one transverse and one longitudinal flagellum—however, while in residence within the coral gastrodermal cells, they are non-motile and lack flagella (Freundenthal 1962; Stat et al. 2006). A single, multi-lobed chloroplast lines the interior surface of the algal cell in a reticulate pattern in densities calibrated to the light environment (Rowan and Powers 1991; Stat et al. 2006). Within chloroplasts exist an array of pigments that collectively function to maximize photosynthesis. Pigments are located within light harvesting protein complexes embedded in stacked and unstacked regions of thylakoid membranes and may protrude outward from the thylakoid membrane to increase the likelihood of absorbing incoming photons. Once captured, that energy is shuttled through resonance energy transfer from pigment to pigment until it reaches a highly specialized chlorophyll *a* reaction center pigment in Photosystem II (PSII; Ke 2001). Similarly, when light is supersaturating, the energy may be absorbed by photoprotective pigments and carried away from the reaction center and released as heat. Chlorophyll *a* (Chl *a*) is ubiquitous in all photosynthetic organisms, serves the critical function of primary electron donor in the light reactions of photosynthesis, and may also function as a light-harvesting pigment. Chlorophyll c_2 and Peridinin—an oxygen-containing carotenoid—harvest photons and funnel the energy through resonance energy transfer to the specialized Chl *a* reaction center. The carotenoid, β, β-carotene is a light-harvesting accessory pigment but also serves a photoprotective role by quenching excited states of Chl *a* and oxygen (radical oxygen species; ROS) that can be harmful to the cell. Diadinoxanthin and dinoxanthin are epoxide-

2

containing carotenoids that are activated by the concentration of protons in the thylakoid lumen to protect reaction center Chl *a*. This process of de-epoxidation of diadinoxanthin and the epoxidation of dinoxanthin is called the xanthophyll cycle and is an important method for alleviating light stress (Brown et al. 1999; Garcia-Mendoza et al. 2002; Kuffner 2005). Corals that are regularly exposed to high irradiance are likely to maintain a higher ratio of photoprotective to light-harvesting pigments as compared to deep or shaded corals. Zooxanthellae produce these photoprotective pigments to prevent photoinhibition. Photoinhibition is the loss of function in PSII and occurs when the rate of inactivation exceeds the rate of repair (Ohad et al. 1984; Takahashi et al. 2004). Repair may entail *de novo* synthesis of the important D1 protein, requiring time and energy that will not be dedicated to photosynthesis. Recent evidence suggests that the first step leading to photodamage begins in the oxygen-evolving complex (OEC; Ohnishi et al. 2005; Hakala et al. 2006; Tyystjärvi 2008). The OEC performs the fundamental task of splitting water to replace the oxidized electron in the PSII reaction center (RC). Without electron replacement, electron transport ceases, halting photosynthesis while incoming irradiance continues. These processes take place and are regulated within the symbiont cells.

CPs and FPs are coral host pigments and are not among the photosynthetic pigments within symbiont cells. The uniformity of CPs across the entire surface of *M. flabellata* colonies appears consistent with a photoprotective function (Salih et al. 2000; Smith et al. 2013), and would constitute an additional, coral-facilitated, method to protect the symbiotic partners. While the colony surface distribution of the CPs is generally uniform, the vertical distribution within coral epithelia is not known. In this investigation, the determination of CP function in *M. flabellata* explicitly sought to determine whether they are photoprotective. To function as photoprotectants, CPs must absorb potentially damaging light energy before it reaches the symbionts. CPs must, therefore, be physically located in coral epithelia, i.e., in the epidermis, in a manner which permits them to "screen" the symbionts. To determine CP and FP location, I utilized numerous histological staining techniques and light microscopy, as well as confocal laser scanning microscopy on numerous coral fragments from various Hawaiian species with a particular focus on *M. flabellata*.

Another key factor determining the potential for CPs and FPs to be photoprotective is whether they absorb light at wavelengths that are relevant to zooxanthellae absorbance, i.e., in a region of the photosynthetically active radiation (PAR) spectrum that is potentially harmful to the symbionts. The proposed photoprotective role of CPs has been disputed due to its high and narrow absorbance band in a region of the PAR spectrum where symbionts absorb minimally (Mazel et al. 2003; D'Angelo et al. 2008). Strong CP absorbance in this range, therefore, would not alleviate light energy stress since very little is absorbed by zooxanthellae. Evidence suggests, however, that yellow PAR wavelengths are particularly damaging to the OEC, and secondarily, to PSII as electron transport breaks down (Takahashi

3

et al. 2010; Zavafer et al. 2015). An important goal of this investigation was to determine whether CPs (and FPs) are suitable as photoprotectants by characterizing their absorbance maxima in *M. flabellata, M. patula* Verrill, *Leptastrea purpurea* Dana, and *Porites compressa* Dana. Coral tissue, presence of UVR-absorbing mycosporine-like amino acids (MAAs; Teai et al. 1997; Banaszak et al. 2000; Oren and Gunde-Cimerman 2007), and the intact clusters of symbionts present challenges to understanding the results of absorbance measurements from whole coral fragments (Enrıquez et al. 2005; Vásquez-Elizondo et al. 2017). Unlike measurements of extracted and homogenized zooxanthellae, intact cells in the living coral organism are subject to pigment self-shading and for some of the deeper cells, the "package effect" (Duysens 1956; Morel and Bricaud 1981; Kirk 2010). To tease out the contributions of the CPs and FPs in whole coral absorbance at 560-590 nm, I leveraged the minimal absorbance by the zooxanthellae at these wavelengths and developed a method to compare the relative absorbance by corals and zooxanthellae to arrive at coral CP absorbance values for use in further analyses. Unifying photosynthetic efficiency measurements with CP and FP absorbance to test the potential for measurable effects of CPs on the performance of the symbionts was a logical next step.

Light energy that reaches the light harvesting pigments in a photosynthetic organism will undergo one of three competing processes: it will drive photochemistry (photosynthesis), it may re-emit as light at a longer wavelength (fluorescence), or it may be dissipated as heat (non-photochemical quenching; NPQ). These processes occur in competition with approximately 20-25% of absorbed photons utilized for photochemistry, 70–75% utilized for photoprotection, and up to 5% will fluoresce (Maxwell and Johnson 2000; Govindjee 2004; Taiz and Zeiger 2010). Measurement of these processes in live samples is possible with pulse amplitude-modulated (PAM) fluorometry due to the competitive nature of these pathways and is a commonly-used method to characterize photosynthetic efficiency in plants and algae. To better understand how the proposed photoprotective CPs and FPs may affect the zooxanthellae I endeavored to characterize the photosynthetic efficiency and compare it to CP and FP absorbance in *M. flabellata* and the three aforementioned Hawaiian species. The method was designed to be minimally invasive and non-destructive with near simultaneous measurements via rapid light curves (RLCs) with a Diving-PAM (Heinz Walz GmbH, Germany) and a modular spectrometer. In this manner, the coral fragments could be returned to the reef unaltered.

A major advantage to running RLCs is the relatively non-invasive nature of the PAM data collection (Ralph and Gademann 2005). The use of PAM on whole coral fragments, however, is complicated by the highly reflective skeleton underlying the photosynthetic symbionts. Not all light energy will be absorbed by the symbionts; some will bypass the photosynthetic cells and will be reflected off the coral skeleton in numerous directions as diffuse, lower energy light (Enrıquez et al. 2005; Kirk 2010; Marcelino et al. 2013). The reflected light may be absorbed by pigments on the undersides of

symbiont cells or by lower tier symbionts, deeper in the coral tissue. The reflected light also travels within the skeleton at distances determined by microstructures that form the skeletal framework (Marcelino et al. 2013). Light travels further in thin, rapidly built skeleton, i.e., in branching corals, as compared to thick, slowly built skeletal structures in massive or mounding corals (Enrıquez et al. 2005; Marcelino et al. 2013). To alleviate the complications associated with ambient light interference, data collection is ideally done with dark-acclimated specimens to record the strongest fluorescence signal from which to derive values of F_v/F_m (optimal quantum yield), a measurement of photosynthetic efficiency (Schreiber 2004). While working with individual fragments during this investigation, it was believed that light reflected off the coral skeleton could impact the dark-acclimated status of the remaining areas of the fragment, rendering the subsequent RLCs invalid. To verify the legitimacy of this concern, I used data from two experiments and over 300 individual coral fragments to test the effects of initial measurements on subsequent measurements during RLCs with PAM. Having a strong understanding of the benefits and potential complications of this powerful tool as applied to corals, is highly valuable, particularly given the minimally invasive nature of PAM fluorometry.

As the term implies, photoprotection involves protection of the symbiotic zooxanthellae from irradiance, but it does not indicate protection from thermal stress. Thylakoid membrane lipids within zooxanthellate chloroplasts are the initial foci of damage when seawater temperatures increase beyond a particular threshold (Tchernov et al. 2004). Additionally, increased temperatures inhibit the repair of damaged D1 proteins in PSII (Takahashi et al. 2004, 2009). Solar irradiance may also work synergistically with high seawater temperatures to accelerate zooxanthellae degradation and loss (Fitt et al. 2001). When impaired, zooxanthellae may be expelled from coral gastrodermis (Jaap 1979; Ralph et al. 2001; Davy et al. 2012) or digested (Davy et al. 2012; Richards Dona 2012). As symbiont pigment and cell concentrations decrease, downwelling light reflecting off the coral skeleton increases with a concomitant increase in diffuse light energy absorbed by the remaining zooxanthellae (Enrıquez et al. 2005; Marcelino et al. 2013). Reduced water motion may also play a role in bleaching susceptibility since this reduces the rate of waste and material exchange at the coral surface (Nakamura and Van Woesik 2001; Nakamura et al. 2003; Jokiel 2004). Corals generally rely more on heterotrophic feeding when bleached (Grottoli et al. 2006), and a reduction in food supply due to slack water flow could be catastrophic. Corals with high water flow requirements are thus even more vulnerable if water flow is reduced during bleaching events. To shed light on potential causes of the species' high bleaching susceptibility, I sought to verify the assumption that *M. flabellata* requires high water flow habitat by conducting distribution surveys within Kāneʻohe Bay and by comparing water flow where colonies were present vs. where they were not.

The main focus of this research was to determine the functional role of CPs in *M. flabellata* and to understand whether these pigments influence the habitat requirements of this coral in Kāneʻohe Bay. This project began in the summer of 2014, when this species was observed showing signs of thermal stress, acting as harbinger of the widespread bleaching that was to follow and continue into 2016 in Hawaiʻi. The event exposed the high vulnerability of this species to seawater temperature increases and the paucity of information on the species in general. This dissertation fills some of the knowledge gap for *M. flabellata* with comparisons to other common corals in Kāneʻohe Bay. It provides valuable information for implementation of PAM fluorometry on corals, and proposes that photosynthetic parameters should be essential and integral components of all investigations that aim to determine how species thrive or survive in particular reef habitats and why they may be vulnerable to bleaching. In the context of a warming planet, understanding the differences between thermal and light energy stressors, and their interactions, will ultimately yield better actionable goals for coral reef management. This information and the techniques described in this dissertation can have broad application for coral reef research worldwide and highlight the importance of understanding the photobiological characteristics of individual coral species, particularly of endemics.

References

Banaszak A, LaJeunesse T, Trench R (2000) The synthesis of mycosporine-like amino acids (MAAs) by cultured, symbiotic dinoflagellates. J. Exp. Mar. Bio. Ecol. 249:219–233

Brown B, Ambarsari I, Warner M, Fitt W, Dunne R, Gibb S, Cummings D (1999) Diurnal changes in photochemical efficiency and xanthophyll concentrations in shallow water reef corals: Evidence for photoinhibition and photoprotection. Coral Reefs 18:99–105

Coral Reef Assessment and Monitoring Project (CRAMP) http://cramp.wcc.hawaii.edu. Website accessed: 11/20/2019

D'Angelo C, Denzel A, Vogt A, Matz MV, Oswald F, Salih A, Nienhaus GU, Wiedenmann J (2008) Blue light regulation of host pigment in reef-building corals. Mar. Ecol. Prog. Ser. 364:97–106

D'Angelo C, Smith EG, Oswald F, Burt J, Tchernov D, Wiedenmann J (2012) Locally accelerated growth is part of the innate immune response and repair mechanisms in reef-building corals as detected by green fluorescent protein (GFP)-like pigments. Coral Reefs 31:1045–1056

Davy SK, Allemand D, Weis VM (2012) Cell biology of cnidarian-dinoflagellate symbiosis. Microbiology and Molecular Biology Reviews. 76:229–261

Duysens LNM (1956) The flattening of the absorption spectrum of suspensions, as compared to that of solutions. Biochem. Biophys. Acta 19:1–12

Enrıquez S, Méndez E, Iglesias-Prieto R (2005) Multiple scattering on coral skeletons enhances light absorption by symbiotic algae. Limnol. Ocean. 50:1025–1032

Falkowski PG, Dubinsky Z, Muscatine L, Porter JW (1984) Light and the bioenergetics of a symbiotic coral. Bioscience 34:705–709

Fitt W, Brown B, Warner M, Dunne R (2001) Coral bleaching: interpretation of thermal tolerance limits and thermal thresholds in tropical corals. Coral Reefs 20:51–65

Freudenthal HD (1962) *Symbiodinium* gen. nov. and *Symbiodinium microadriaticum* sp. nov. a zooxanthella: taxonomy, life cycle and morphology. J. Protozoan. 9:45–52

Garcia-Mendoza E, Matthijs HCP, Schubert H, Mur LR (2002) Non-photochemical quenching of chlorophyll fluorescence in *Chlorella fusca* acclimated to constant and dynamic light conditions. Photosynth. Res. 74:303–15

Govindjee (2004) Chlorophyll a fluorescence: a bit of basics and history. In: Papageorgiou GC, Govindjee (eds.) Chlorophyll a Fluorescence. A Signature of Photosynthesis. Springer, Dordrecht, pp 1–42

Grottoli AG, Rodrigues LJ, Palardy JE (2006) Heterotrophic plasticity and resilience in bleached corals. Nature 440:1186–9

Hakala M, Rantamäki S, Puputti EM, Tyystjärvi T, Tyystjärvi E (2006) Photoinhibition of manganese enzymes: Insights into the mechanism of photosystem II photoinhibition. J. Exp. Bot. 57:1809–1816

Jaap WC (1979) Observations on zooxanthellae expulsion at Middle Sambo Reef, Florida Keys. Bull. Mar. Sci. 29:414–422

Jokiel PL (2004) Temperature Stress and Coral Bleaching. In: Rosenberg E, Loya Y (eds.) Coral Health and Disease. Springer, Dordrecht, pp 401–425

Jones C, Lawton J, Shachak M (1994) Organisms as ecosystem engineers. Oikos 69:373–386

Ke B (2001) Photosynthesis: An Overview. Photosynthesis: Photobiochemistry and Photobiophysics. Kluwer Academic Publishers, Dordrecht, pp 1–46

Kirk JTO (2010) Light and photosynthesis in aquatic ecosystems, third edition. Cambridge University Press, New York

Kuffner IB (2005) Temporal variation in photosynthetic pigments and UV-absorbing compounds in shallow populations of two Hawaiian reef corals. Pac. Sci. 59:561–580

LaJeunesse T (2002) Investigating the biodiversity, ecology, and phylogeny of endosymbiotic dinoflagellates in the genus *Symbiodinium* using the ITS region: in search of a "species" level. J. Phycol. 880:866–880

Maragos J (1972) A Study of the Ecology of Hawaiian Reef Corals. Doctoral Dissertation. University of Hawaii at Manoa

Marcelino LA, Westneat MW, Stoyneva V, Henss J, Rogers JD, Radosevich A, Turzhitsky V, Siple M, Fang A, Swain TD, Fung J, Backman V (2013) Modulation of light-enhancement to symbiotic algae by light-scattering in corals and evolutionary trends in bleaching. PLoS One 8:e61492

Maxwell K, Johnson GN (2000) Chlorophyll fluorescence - a practical guide. J. Exp. Bot. 51:659–668

Mazel CH, Lesser MP, Gorbunov MY, Barry TM, Farrell JH, Wyman KD, Falkowski PG (2003) Green-fluorescent proteins in Caribbean corals. Limnol. Oceanogr. 48:402–411

Morel A, Bricaud A (1981) Theoretical results concerning light absorption in a discrete medium, and application to specific absorption of phytoplankton. Deep. Res. 28A:1375–1393

Muscatine L, Porter JW (1977) Reef corals: mutualistic symbioses adapted to nutrient-poor environments. BioScience 27:454–459

Nakamura T, Van Woesik R (2001) Water-flow rates and passive diffusion partially explain differential survival of corals during the 1998 bleaching event. Mar. Ecol. Prog. Ser. 212:301–304

Nakamura T, Yamasaki H, Van Woesik R (2003) Water flow facilitates recovery from bleaching in the coral *Stylophora pistillata*. Mar. Ecol. Prog. Ser. 256:287–291

Ohad I, Kyle DJ, Arntzen CJ (1984) Membrane protein damage and repair: removal and replacement of inactivated 32-kilodalton polypeptides in chloroplast membranes. J. Cell Biol. 99:481–485

Ohnishi N, Allakhverdiev SI, Takahashi S, Higashi S, Watanabe M, Nishiyama Y, Murata N (2005) Two-step mechanism of photodamage to photosystem II: Step 1 occurs at the oxygen-evolving complex and step 2 occurs at the photochemical reaction center. Biochemistry 44:8494–8499

Oren A, Gunde-Cimerman N (2007) Mycosporines and mycosporine-like amino acids: UV protectants or multipurpose secondary metabolites? FEMS Microbiol. Lett. 269:1–10

Palmer CV, Roth MS, Gates RD (2009) Red fluorescent protein responsible for pigmentation in trematode-infected *Porites compressa* tissues. Biol. Bull. 216:68–74

Ralph PJ, Gademann R (2005) Rapid light curves: A powerful tool to assess photosynthetic activity. Aquat. Bot. 82:222–237

Ralph PJ, Gademann R, Larkum AWD (2001) Zooxanthellae expelled from bleached corals at 33°C are photosynthetically competent. Mar. Ecol. Prog. Ser. 220:163–168

Richards Donà A (2012) Investigation into pathological responses of two phenotypes of the Scleractinian coral, *Montastraea faveolata*, to putative marine *Vibrio* pathogens. Master's Thesis. State University of New York, Stony Brook University

Rodgers KS, Jokiel PL, Brown EK, Hau S, Sparks R (2015) Over a decade of change in spatial and temporal dynamics of Hawaiian coral reef communities. Pac. Sci. 69:1–13

Rowan R, Powers DA (1992) Ribosomal RNA sequences and the diversity of symbiotic dinoflagellates (zooxanthellae). Proc. Natl. Acad. Sci. U. S. A. 89:3639–43

Salih A, Larkum A, Cox G, Kühl M, Hoegh-Guldberg O (2000) Fluorescent pigments in corals are photoprotective. Nature 408:850–3

Schreiber U (2004) Pulse-Amplitude-Modulation (PAM) Fluorometry and Saturation Pulse Method: An Overview. In: Papageorgiou G., Govindjee (eds) Chlorophyll a Fluorescence. Springer, Dordrecht, pp 279–319

Smith E, D'Angelo C, Salih A, Wiedenmann J (2013) Screening by coral green fluorescent protein (GFP)-like chromoproteins supports a role in photoprotection of zooxanthellae. Coral Reefs 32:463–474

Stat M, Carter D, Hoegh-Guldberg O (2006) The evolutionary history of *Symbiodinium* and scleractinian hosts - Symbiosis, diversity, and the effect of climate change. Perspect. Plant Ecol. Evol. Syst. 8:23–43

Takahashi S, Milward SE, Yamori W, Evans JR, Hillier W, Badger MR (2010) The solar action spectrum of Photosystem II damage. Plant Physiol. 153:988–93

Takahashi S, Nakamura T, Sakamizu M, Van Woesik R, Yamasaki H (2004) Repair machinery of symbiotic photosynthesis as the primary target of heat stress for reef-building corals. Plant Cell Physiol. 45:251–255

Takahashi S, Whitney SM, Badger MR (2009) Different thermal sensitivity of the repair of photodamaged photosynthetic machinery in cultured *Symbiodinium* species. Proc. Natl. Acad. Sci. U. S. A. 106:3237–3242

Tchernov D, Gorbunov MY, de Vargas C, Narayan Yadav S, Milligan AJ, Häggblom M, Falkowski PG (2004) Membrane lipids of symbiotic algae are diagnostic of sensitivity to thermal bleaching in corals. Proc. Natl. Acad. Sci. U. S. A. 101:13531–13535

Teai T, Drollet J, Bianchini J (1997) Widespread occurrence of mycosporine-like amino acid compounds in scleractinians from French Polynesia. Coral Reefs 1994:169–176

Trench RK (1993) Microalgal-invertebrate symbioses: A review. Endocytobiosis Cell Res. 9:135–175

Tyystjärvi E (2008) Photoinhibition of Photosystem II and photodamage of the oxygen evolving manganese cluster. Coord. Chem. Rev. 252:361–376

Vásquez-Elizondo RM, Legaria-Moreno L, Pérez-Castro MÁ, Krämer WE, Scheufen T, Iglesias-Prieto R, Enríquez S (2017) Absorptance determinations on multicellular tissues. Photosynth. Res. 132:311–324

Zavafer A, Cheah MH, Hillier W, Chow WS, Takahashi S (2015) Photodamage to the oxygen-evolving complex of Photosystem II by visible light. Sci. Rep. 5:16363

CHAPTER ONE

DISTRIBUTION AND PHYSIOLOGY OF THE HAWAIIAN CORAL <u>MONTIPORA FLABELLATA</u> IN KĀNEʻOHE BAY, OʻAHU

Angela Richards Donà

Abstract

The vibrantly colorful stony coral *Montipora flabellata* Studer is endemic to Hawaiian reefs and exclusively inhabits shallow reefs with high water flow and/or wave action where solar irradiance is often supersaturating. Although a common habitat trait for all known colonies, it remains unclear whether high water flow is an absolute requirement or whether *M. flabellata* simply competes well under those conditions. This investigation sought to update the distribution of this species in the lagoon area of Kāneʻohe Bay and to determine the importance of high water flow to colony survival. To this end, three independent lines of inquiry were explored. First, I surveyed 22 shallow patch reefs from the north, central, and south Bay regions to quantify colony presence and size class. Second, I conducted experiments to compare water flow and sedimentation between three nearby sites: two sites with confirmed colony presence and the third site without. Third, I examined coral fragments histologically to determine whether physiological characteristics at the cellular and tissue level could explain the species' exclusive presence in high water flow habitats. The present surveys documented that *M. flabellata* occurs in the lagoon and is abundant at the lagoon-side entrances to the Ship's and Sampan channels, contrary to previously documented *M. flabellata* presence only outside the Bay and within the channels. The water flow and sedimentation experiments suggest that water flow is variable throughout the year and significantly higher where *M. flabellata* colonies are present. Interestingly, sedimentation was also higher where colonies were present. Histological analyses of healthy-appearing *M. flabellata* fragments showed consistently low numbers of mucocytes in the epidermis, which would hinder surface sediment removal and may explain the species' exclusive occurrence on reefs with high water flow. All other species examined histologically (*M. patula*, *M. capitata*, *Porites evermanni*, *Pocillopora meandrina*) showed normal to profuse numbers of mucocytes. The histological data strongly suggest that *Montipora flabellata* relies on high water flow to prevent or remove surface sediment in Kāneʻohe Bay—where suspended particulate matter is a common seawater attribute. Additional histological analysis of several Kāneʻohe Bay *M. flabellata* specimens revealed that chromoproteins (CPs) fill the apical surface of the epidermis, particularly in the polyps, which supports a role in photoprotection. A photoprotective role is consistent with the absence of mucocytes, since these would provide wide areas for solar irradiance to penetrate through the epidermis unfiltered to the gastrodermis where symbiotic algae occur. This research provides evidence that *Montipora flabellata* colonies are physiologically limited to high water flow reefs as a result of the biological trade-offs associated with solar protection versus surface debris removal. This research also supports the view that *M. flabellata* possesses traits unique to the species. These results improve our understanding of the ecology of this poorly-studied, endemic Hawaiian coral species and its novel solution to the stress of high light environments.

Introduction

Montipora flabellata is the sixth most abundant coral in the main Hawaiian Islands (Rodgers et al. 2015) and is considered an endemic species. Often brightly colored, these purple or blue corals stand out visually among the primarily muted, brown tones common on Hawaiian reefs (Fig. 1.1). Although morphologies may vary somewhat, *M. flabellata* grows mainly by encrusting over hard substrate, rubble, shell, and sand. Along the colony surface, fine-scale skeletal protrusions called papillae project outward in seemingly random fashion giving the coral an overall rough, rutted appearance. Papillae are distinguishable from verrucae because they are smaller than the coral polyps, unlike verrucae, which are larger (Veron and Stafford-Smith 2000). Papillae may be in the form of tiny knobs or they may fuse together to form irregular ridges that can give the colony (or sections thereof) a crumpled paper effect. Polyps are small— approximately 0.5 mm in diameter—and numerous, and are tightly packed among the papillae. Importantly, papillae enhance the light-scattering capabilities of this coral, effectively dispersing sub-surface irradiance for its photosynthetic algal symbionts (Enrıquez et al. 2005; Marcelino et al. 2013).

Montipora flabellata inhabits high water motion environments—often at reef crests where wave action is powerful—thus these colonies are found in shallow water areas where solar irradiance is often supersaturating (Maragos 1972). Survival in this unremitting environment requires investment in strong physical structure (Rodgers et al. 2015), and/or a low reef profile, and presumably, some form of solar protection. *Montipora flabellata* may possess all of these attributes since it appears to be competitive for reef space under these conditions. Unlike most other corals, however, *M. flabellata* appears unable to remove surface sediment (ARD pers. obs.) and it is reportedly highly susceptible to thermal bleaching (ARD pers. obs.; Jokiel and Brown 2004). Thermal bleaching is the result of warmer-than-normal seawater temperatures and normal solar irradiance that act synergistically to cause the expulsion (or digestion; Titlyanov et al. 1996) of algal symbionts from coral tissues. Reduced water flow is also recognized as a major contributor to coral bleaching (Nakamura and Van Woesik 2001; Nakamura et al. 2003). The high bleaching susceptibility of this species may potentially be explained by its inability to function optimally when increased seawater temperatures and reduced water flow overlap in time.

In 2014, unprecedented thermal stress caused a multi-year, mass bleaching event that affected coral reefs worldwide. The event was larger in magnitude and spatial scale than the previously-observed major bleaching events in Hawai'i in 1996 and 2002 (P. Jokiel, pers. comm). Compounding the effect of increasing temperatures was a prolonged slackening of the trade winds that normally drive surface water flow. *Montipora flabellata* was the first coral species to show incontrovertible signs of bleaching stress throughout Kāne'ohe Bay, O'ahu as early as August 2014 (Fig. 1.2). It was interesting to observe that this coral species, despite a clear adaptation to live in high light environments, was among the most vulnerable

when seawater temperatures reached and persisted at atypically high levels. The unique characteristics of this coral species (pigmentation, habitat preference, and observed vulnerability to bleaching conditions) provided the impetus for deeper and broader exploration of its physiological and ecological traits.

Bleaching of *M. flabellata* colonies was significant across Kāne'ohe Bay during the prolonged thermal event that continued into 2016. Additionally, strong rainfall poured freshwater onto reefs just prior to the warming event and wiped out vast sections of several very large colonies on patch reef 44 (PR44) in the north bay (Bahr et al. 2015). The ability to study this coral species was in doubt as many colonies appeared unlikely to survive through the warm period and the species was under consideration for protected status under the Endangered Species Act. In late 2015, a large, bleached colony from PR1 (Moku o Lo'e) was collected and fragmented for recovery and observational studies. After ten months, approximately 74% of the fragments had survived and were returned to the reef.

Montipora flabellata corals, like all scleractinian corals, are made up of sac-like polyps resting in skeletal corallites connected externally by coenenchyme and internally by gastrovascular canals. They are perforate—gastrovascular canals connect *through* the skeleton rather than simply over it—and their polyps are diminutive (approximately 0.5 mm in diameter) and unevenly and tightly spaced. The coral skeleton is thin, loosely built, and porous; corallites and walls are poorly-defined. The loose and ill-defined skeleton is characteristic of a rapidly-built structure as expected for a highly competitive species (Darling et al. 2012).

The most visually distinguishing characteristic of the coral *M. flabellata* is its color. Often bright purple (Kāne'ohe Bay, O'ahu and North Shore, Kaua'i) or blue (Pupukea, North Shore, O'ahu) these vibrant colors come from non-fluorescent chromophore-protein complexes called chromoproteins (CPs) that are distinct from the coral symbiont's photosynthetic pigments. CPs (and fluorescent pigments; FPs) are thought to be produced by the coral host and are generally referred to as "host" pigments. CPs in *M. flabellata* have a mostly uniform distribution over the colony surface and may become more vibrant during warmer months (ARD pers. obs). In most other Hawaiian coral species, colors other than brown can be fluorescent or non-fluorescent and are generally isolated in particular areas of the coral colony, i.e., growing margins, tips of branches, and wounds, supporting growing evidence that these coral pigments serve a functional role in growth and immunity (Palmer et al. 2009; D'Angelo et al. 2012). CPs are also present in a morphologically similar species, *Montipora patula*, but are visible exclusively in the polyps (Fig. 1.3). CP uniformity in *M. flabellata* is distinctive and suggests a colony-wide function.

In contrast to a strict preference for high water flow habitat, *M. patula* appears to tolerate medium and sometimes low water flow conditions. Like *M. flabellata*, *M. patula* colonies also tend to inhabit shallow reef, but they did not demonstrate the same level of bleaching susceptibility that *M. flabellata*

colonies did in 2014. It is unclear why these similar species occupy different water flow habitats, and specifically, what physiological attributes permit *M. patula* to tolerate low water flow.

This investigation was exploratory, multi-faceted, and integrated both field, laboratory, and light microscopy research components. It included numerous surveys and water clarity measurements at patch reefs throughout Kāne'ohe Bay, and habitat water flow and sedimentation comparisons. Histological characterizations of cells and epithelia from *M. flabellata* and its closest congener, *M. patula,* were undertaken to examine whether cellular attributes were consistent with habitat parameters and importantly, whether the chromoproteins could be visualized. A suite of staining techniques and decalcification methods were used to detect CPs in the coral tissue and determine their specific location in the coral epithelia. Localization of CPs in the epidermis would suggest an ability to physically block particular wavelengths of solar energy that might otherwise harm the algal symbionts. Furthermore, it was proposed that a lack of epidermal mucocytes and/or cilia in *M. flabellata* could explain the species' observed inability to remove surface sediment and restriction to high water flow habitats.

Methods

Distribution Surveys

Twenty-two patch reefs—spanning from the Ship's Channel to the Sampan Channel in Kāne'ohe Bay—were surveyed for the presence of *Montipora flabellata* colonies to provide an updated distribution of this species within the bay (Fig 1.4). All surveys were conducted on snorkel with the aid of one assistant; reefs were chosen based on weather and accessibility at the time of the surveys. Secchi disk measurements were taken to determine water clarity at each patch reef prior to the survey (Preisendorfer 1986). Several large reefs in the northernmost part of Kāne'ohe Bay were too deep to access on snorkel and were thus not considered part of the study. Similarly, reefs in the south bay are subject to very long water residence times (Maragos 1972; Lowe et al. 2009) making the habitat unsuitable for this coral species.

Surveys began on the southwestern "corner" of each reef. A compass point was taken heading perpendicular to the reef and set the direction for outward swims while 180 degrees from that point marked the direction for return swims. Surveyors remained approximately two meters apart and each visually scanned an area of roughly one meter to each side while swimming across the reef. When the edge of the reef was reached, the furthest point surveyed was marked as a pivot point and both snorkelers shifted along the reef edge to begin the return swim. In this manner, a creeping line pattern was followed

until the entire reef had been surveyed (Fig. 1.5). When *M. flabellata* colonies were found, they were photographed, the length of longest dimension was measured, and all were recorded by size class (<5 cm; 5–10 cm; 10–20 cm; 20–40 cm; 40–80 cm; 80–160 cm; >160 cm). Colonies were considered individual if growing margins were more than a hand's width apart (approximately 8 cm). To avoid losing direction while measuring and recording *M. flabellata* colonies, a weighted, highly visible marker was placed on the reef to signal the point from which the surveys were to resume. Depending on the size of the reef, surveys were concluded in approximately one to four hours.

At other times subsequent to the quantitative surveys, reconnaissance in Kāneʻohe Bay for *M. flabellata* was done covering areas where strong water flow is common, particularly in the north Bay and in the area of the Sampan Channel. In one instance, reefs on both sides of the Sampan Channel, and closer to Mokapu Peninsula, were explored by boat on a calm day. One researcher drove the boat over the reefs, while a glass-bottom look box was used to search for colonies. Additionally, a thorough search was done by two researchers on snorkel in the large area shoreward of Kapapa Island.

Water Flow and Sedimentation Comparisons

Clod cards and sediment traps were deployed at three sites in Kāneʻohe Bay, at the Coral Reef Instrumented Monitoring Platform (CRIMP) buoy, Patch Reef 14 (PR14), and Patch Reef 15 (PR15), to determine relative water flow and sedimentation load for comparison between sites (Doty 1971; Jokiel and Morrissey 1993). The main channel-facing sides of PR14 and PR15 are roughly equidistant from the CRIMP buoy site (~750 m) and are approximately 115 meters distant from one another (Google Earth, 2019). These nearby sites represented reef areas where the likelihood of reproductive connectivity was high thus the lack of colonies on PR15 could not be explained by absence of gamete arrival for settlement.

Concurrent with deployment, two clod card controls were put in a 5-gallon bucket of ambient temperature seawater and left undisturbed. Clod cards were made from Plaster of Paris poured into ice trays with each individual cube glued to a ~2 x 4 in semi-rigid plastic card. Prior to use, the clods were thoroughly dried, labeled, and weighed twice. Average weight was recorded. Two clod cards were deployed per site and each was secured to a brick with thick rubber bands and placed adjacent to a *Montipora flabellata* colony. Submersion times were recorded, and each clod card remained on the reef for 22 to 24 h. Time of retrieval, the following day, was recorded and two replacement clods were secured to the brick. This was done over the course of four days for a total of three deployments.

Sediment traps were made from 2.5" diameter PVC pipe with PVC caps glued to the bottom for a total length of 6 in. Two traps were cable-tied together and to a thinner open-ended central pipe. Long

rebar sections (~ 60 in) were hammered into non-living reef substrate perpendicular to the upper surface and the thin, central PVC pipe was slipped onto the rebar, positioning the open end of the traps upward. The traps were deployed on day one and retrieved on day four at all three sites. Each trap was immediately capped to avoid sample loss.

The clod cards and sediment traps were deployed in November 2016 and in April 2017. The retrieved clod cards were rinsed in fresh water and dried in a Blue M laboratory oven (Thermal Product Solutions, PA, USA) at 100 °C for a minimum of seven (7) hours. Sediment was rinsed from the traps with filtered seawater and captured on 1.2 µm Whatman GF/C 42.5 mm diameter glass microfiber filters (GE Healthcare, MA, USA) . Excess water was removed from the filters using vacuum pumps and Millepore filter holders. When sediment appeared dry the sediment-laden filters were carefully removed and put in the 100 °C oven to dry completely with the clod cards. All dry clod card and sediment samples were weighed twice to adjust for humidity differences and the mean was recorded. The difference in clod card weight before and after deployment was calculated and was used to determine the daily rate of diffusion in grams hr^{-1} for each replicate. The mean daily diffusion rate for each set of replicates was determined and used for analysis.

Post-Bleaching Coral Recovery and Growth

A large section of an extensively bleached *M. flabellata* colony on PR1 (Moku O Loʻe) was collected by Dr. Paul Jokiel in late September 2015 and placed in the Coral Reef Ecology Lab (CREL) 660-gallon flow-through seawater mesocosms to recover. The colony was sampled at a time when most of the *M. flabellata* in Kāneʻohe Bay were bleached and their local survival was in question. *Montipora flabellata* is believed to be highly sensitive to slack water conditions so this collection provided an opportunity to add critical new information including what levels of water flow would be necessary to maintain fragments in good apparent health, and for how long fragments could survive tank conditions.

The colony was fragmented into 216 pieces, approximately 3 cm^2 each, and all were placed randomly in flat plastic netted trays in three seawater tables under shade cloth that reduced the incident solar radiation by approximately 76%, measured with a LiCor LI-1250 photometer with a LI-193 4π sensor (LI-COR Biosciences, NE, USA). Thirty larger fragments approximately 10-15 cm^2, were also maintained for observation.

Fragments were glued with reef-safe polyacrylate superglue (Bulk Reef Supply, USA) to small, numbered, 1.5 x 1.5 in plastic bases. Each specimen was kept free of algae growth with weekly cleanings and were examined for lesions, flatworms, and sedimentation. Cleanings consisted of algae removal from the base and exposed skeleton with a toothbrush; sediment was removed from tissue daily by pressure

rinse using a turkey baster. This also proved effective for removing predatory polyclad flatworms residing in coral pits and crevices. Additionally, 36 total fragments from two additional colonies were added to the project and maintained as described for a total of 248 fragments. In early December 2015 all fragments had regained pigmentation and shading was reduced to approximately 58% for all tables.

In March 2016, an additional method was devised to test whether sediment-smothering of coral fragments could be avoided by hanging corals vertically in the water tables. In this manner no contact was made between the coral and the sides or bottom of the tank. Thirty-six fragments were randomly selected to be transferred from individual bases to group tiles; each fragment was epoxied with several others to an 8 x 8 cm tile. Fragments were maintained until August 2016, at which time all were assembled on tiles and returned to PR1.

Water temperature was measured daily, particularly in the first months of the project, with a digital thermometer (UEi Test Instruments) at the inflow end of each water table. Fragments were rotated every week from one table to the next to avoid subjecting any particular group to unknown effects of an individual water table. Fragment growth was determined using the utility balance method for buoyant weighing following Jokiel et al. (1978) with equation 1:

$$W_a = 1.54W_w \qquad (1)$$

where W_a is the weight of the aragonite skeleton, 1.54 is a derived value for the weight of the seawater displaced, and W_w is the buoyant weight as measured. Seawater density of 1.03 (22–30 °C with salinity constant at 35 ppm) was used.

Statistical Analyses

Statistical analyses were done for clod card dissolution and sediment weight at three sites in Kāneʻohe Bay at two time points using Welch's Analysis of Variance (ANOVA) test after running a standard One-way ANOVA on independent observations of data with acceptably Normal distributions. Analysis of Means (ANOM) for Variances-Levene showed variances within limits, however, Levene's test for equal variances for one of the months was not acceptable. Welch's Test was thus used for all related datasets as this allowed for variances to be unequal. All statistics were carried out using SAS JMP Pro 14.0.0.

Histology

Several coral fragments from five species (*M. flabellata* n = 3, *M. patula* n = 2, *M. capitata* n = 2, *Porites evermanni*, n = 2, *Pocillopora meandrina* n = 2) collected in Kāneʻohe Bay were processed for histology by Dr. Esther Peters and Valerie Nguyen in the Histology Laboratory, George Mason University, Fairfax, Virginia. These fragments were fixed in buffered aqueous zinc formalin solution (Z-fix; Anatech, MI, USA) in 50 mL screwcap tubes for one week. The bulk of the fixative was poured off and one Kimwipe (Kimtech, Kimberly-Clark, GA, USA) was placed in each tube to absorb the remaining fixative and prevent the corals from drying out. At the time of fixation, the fragments had been maintained together in flow-through seawater tables for approximately one month and appeared healthy. The fragments were processed for light microscopy using three decalcifying solutions: 10% Ethylenediaminetetraacetic Acid (EDTA), Immunocal, and Formical (StatLab, TX, USA) and six different staining techniques: Harris's hematoxylin and alcoholic eosin (H&E), periodic acid-Schiff reagent/alcian blue, Cason's trichrome, Fontana-Masson, Movat's modified pentachrome, and Giemsa (Table 1.1). Analysis of the prepared slides was carried out on a Leica Diastar compound microscope at 4x, 10x, 20x, 40x, 63x, and 100x magnifications. Calibration of the stage micrometer (OMAX 0.1 mm, 0.01 mm) with an eyepiece reticle was done for the purpose of measurements. Values for divisions at each magnification were recorded. Photomicrographs were taken with a Nikon D300 camera housing attached to a DD20NLT 2.0x digital SLR coupler (Diagnostic Instruments, LTD). Each section on each slide was scanned several times thoroughly to characterize cells and epithelia, detect and report presence of gonads, nematocysts, and other unique structures, and describe in detail all basic attributes of *M. flabellata*. The other species were used for comparison. Oblique and sagittal sections were examined on each slide for each stain/fixative combination (Peters et al. 2005). Mucocytes were measured and counted in ImageJ software, version 1.52a from photomicrographs of *M. flabellata* and *M. patula,* scanning 14,193 linear μm of epidermis in *M. patula* and 11,720 linear μm in *M. flabellata*.

Histological slides, stained with Masson's trichrome, of 10 *M. flabellata* colonies collected from Kāneʻohe Bay at two separate timepoints were obtained from another researcher at HIMB. In coral histology, Masson's trichrome is generally used to differentiate connective tissue (mesoglea) from the epidermis and gastrodermis. In the medical and veterinary fields, it is often used to stain hemoglobin (a chromoprotein) bright red. The tissue taken for these slides were sampled from visibly healthy regions of purple-pigmented colonies. The colonies were sampled in the field in November 2017 and January 2018 and fragments were immediately fixed in 4% paraformaldehyde. Two to three slides per colony were scanned at least twice for analysis.

Results

Surveys

A total of 359 *M. flabellata* colonies were counted on 22 patch reefs. Presence of *M. flabellata* was fairly well-distributed between the Ship's and Sampan channels (PR11–PR43) and colonies were particularly abundant near the Sampan Channel on PR11 and PR14. At least one colony of *Montipora flabellata* was found on 14 of the 22 reefs surveyed (64%). Over 100 colonies, distributed across size classes from <5 to 80 cm, were found on two reefs whereas only four reefs had more than 20 colonies present and most reefs had less than ten colonies (Fig 1.6). Only one colony of *M. flabellata* was observed in the >160 cm category and was located on PR43 (Fig. 1.7). This massive colony was the largest observed in Kāne'ohe Bay in 2014 (Table 1.2).

No colonies were observed during post-survey reconnaissance trips to the areas near Mokapu Peninsula or Kapapa Island. Numerous colonies of *M. flabellata* were observed on patch reefs 44, 50, and 51, and on the large reef area seaward of reefs 42 and 43 (Fig. 1.4) during trips to the north Bay. Colonies were also observed on a small coral peninsula that extends from the southern end of the sandbar just seaward of PR14, near the National Oceanographic and Atmospheric Administration (NOAA) Coral Reef Instrumented Monitoring Platform (CRIMP) moored buoy.

Water clarity—determined by Secchi disk depth—was highest near PR23 (12.7 m) and lowest at PR34 (5.0 m). Macroalgae with high loads of trapped sediment was observed overgrowing most of the coral on PR34 and no *M. flabellata* colonies were present. Interestingly, the Secchi disk depth at PR43 of 7.7 m, where 11 *M. flabellata* colonies were counted including the largest colony surveyed, was much lower than that at PR23 where only three colonies of moderate size were found (Table 1.2). Water clarity was fairly consistent in the central lagoon patch reef area from PR14 at the southern end to PR38 at the northern end, and ranges from 9.1 to 12.7 m (Fig. 1.4).

Water Flow at PR14, PR15, and CRIMP Buoy

Water flow as determined via clod card dissolution showed similarities between PR14 and CRIMP but a significant difference between those higher flow sites and PR15 in November ($p<0.0001$) and April ($p<0.0001$). PR14 had the highest water flow of the three sites, contrary to the initial assumption that the CRIMP site would have highest flow (Table 1.3). Water temperature in Kāne'ohe Bay was virtually the same during the experimental period and at both time points (November 2016, 25.4–25.9 °C; April 2017, 25.3–25.9 °C; PacIOOS), thus differences in clod card diffusion from

temperature are minimal (Jokiel and Morrissey 1993). Clod card dissolution was higher at all three sites in November compared to April (Fig. 1.8).

Sedimentation at PR14, PR15, and CRIMP Buoy

Sedimentation at PR14 and CRIMP was highly similar and significantly different from sedimentation at PR15 (p = 0.0095) for both time points. Due to the small number of sediment traps and a consistently higher mean weight in November than in April, the means for both months at each site were pooled for comparison (Table 1.4; Fig 1.9).

Post-Bleaching Coral Recovery and Observations

Bleached coral fragments collected in late September 2015 showed substantial, visible symbiont re-pigmentation within 30 d in shaded water tables and most appeared normally pigmented by day 50 (Fig. 1.10). Purple chromoprotein pigmentation was visually prominent on several fragments and most fragments regained uniform purple polyp pigmentation within ~35 d. Purple pigmentation at growth margins were faintly visible, consistent with a growth enhancement function (D'Angelo et al. 2012). In early December 2015, small patches of sediment-smothered tissue on several fragments were noted with subsequent rapid tissue loss. This occurred on concave as well as convex areas of the fragments and became a commonly occurring problem in the water tables. Additionally, white patches of tissue loss appeared on several vibrant purple fragments. While never observed directly preying on tissue, Acotylean flatworms likely *Priosthiostomum montiporae*, were commonly found underneath the plastic bases and were removed regularly from the water tables to prevent further tissue loss. Purple fragments were almost exclusively targeted and the larger, unlabeled fragments (10–15 cm^2) remained untouched by the flatworms (Fig. 1.11).

In February 2016, the extensive loss of tissue from sediment-smothering lead to a change in methods for maintaining a subset of the fragments in the water tables. The vertical, hanging placement of several fragments on one tile served as a test of several solutions to the observed problems. By hanging the corals vertically, sediment was less likely to accumulate, the flatworms were denied access to coral tissue, and fragments were placed close enough to fuse into larger fragments. Tissue loss was not observed on these tiles for the remainder of the experiment and fusion between fragments was observed (Fig 1.11).

Water Table Temperatures

Mean temperatures in the water tables at the start of the recovery period averaged 26.9 °C and remained below 28 °C until mid-October. Seawater temperatures at HIMB (PacIOOS monitoring) peaked at 29.6 °C in early September 2015 but were decreasing by end of month. This decrease in temperature likely permitted a natural recovery process to take place despite comparatively higher temperatures in the water tables (Fig. 1.12).

Coral Fragment Growth and Mortality

Coral fragments were weighed twice, 232 days (7.62 months or 33 weeks) apart. For the purpose of growth analysis, fragments were grouped by start weight and a mean for each weight group was calculated (Table 1.5; Fig. 1.13). The 36 fragments that had been glued to the vertical tiles are not a part of this analysis because those fragments could not be individually weighed. Fragments in the 2.00–2.99 g start weight category had the highest mean percent weight gain at 57.2% with a mean 6.22 mg d^{-1} (n = 47) whereas the largest category (>7 g) had the lowest percent weight gain of 29.2% but the highest mean growth per day at 11.75 mg d^{-1}(n = 12).

The number of dead fragments was tracked since predators appeared to prefer small fragments. The percent dead was highest in the two smallest and two largest groups. Overall, 64 (28%) of 248 coral fragments died from tissue loss due to sediment-smothering or predation. The largest number of dead fragments occurred in the 1–1.99 g weight class (32.2%) whereas the highest percentage of dead fragments occurred in the smallest weight class (37.5%; <1 g). Not surprisingly, the smaller fragments were the most vulnerable to sedimentation and/or predation although all had recovered from the initial bleaching (Fig. 1.14).

Histological Characterization of Montipora flabellata *with Comparisons to* Montipora patula

Microscopically, *M. flabellata* and *M. patula* were recognizably dissimilar. Although they share the same basic body plan, a few prominent differences were observed. *Porites evermanni*, *Pocillopora meandrina*, and *Montipora capitata* were also analyzed for comparison. All specimens appeared normal with little to no pathology observed.

Surface Body Wall (SBW)

Contrary to predictions that *M. flabellata* lacked cilia, strong visual evidence of a thick terminal web denoting the presence of cilia at the apical surface, was found in all samples. Mucocytes, however, were small (mean diameter ~10 µm) and notably scarce, occurring at a rate of ~0.003 mucocytes µm^{-1}. Cilia and mucocyte observations were consistent in the epidermis of the coenenchyme and polyps. In all *M. patula* samples, mucocytes were larger with a mean diameter of ~16 µm and were found at a rate of ~0.03 mucocytes µm^{-1} (Fig. 1.15)—approximately ten times more than in *M. flabellata*.

To further test a deficiency of mucocytes more broadly in *M. flabellata*, histoslides from an additional ten colonies at two timepoints were analyzed. Consistent with the previous observations, mucocyte counts were low, and when present, were highly discreet, round, and generally intact below the terminal web. In contrast, *M. patula* mucocytes were larger than the supporting cells in width and depth, irregular in shape, and were commonly observed opening at the surface to release mucus.

Coral epidermis generally contains ciliated columnar supporting and/or epitheliomuscular cells; these cells are elongated as compared to the cuboidal cells of the gastrodermis. Some species have nematocysts arranged for discharge near the apical surface and/or clusters of granular pigment cells (containing fluorescent proteins; EC Peters pers. comm) at the basal lamina. In *M. flabellata*, the epidermal cells were attenuated, or cuboidal, in most areas of the coenenchyme (approximately 10 µm thick) but were more likely to be columnar in the polyps. Below the epidermis and the thin mesoglea, the gastrodermis was also consistently thin—approximately 9–10 µm—and was sparsely occupied by symbiont cells. Densities of symbionts varied slightly by sample and body part (coenenchyme or polyp) but was consistently lower than those in *M. patula* samples. The mean symbiont diameter was 7.3 µm in both *M. flabellata* and *M. patula*.

Additionally, symbionts in *M. flabellata* appeared dark grey with Fontana-Masson stain indicating presence of melanin in all samples whereas symbionts in *M. patula* did not (Fig. 1.16). Both species had variable amounts of melanin granules dispersed in the epidermis above the nuclei. Presence of melanin associated with the symbionts is an interesting discovery since dinoflagellates are not known to produce the pigment. It is likely that melanin is synthesized by the coral and was observed enrobing the symbionts, but this requires further investigation as it may prove to be another layer of protection. No cnidocytes in the epidermis were detected and basal granular pigment cells were not found in *M. flabellata*. In *M. patula*, cnidocytes in the epidermis were present but not abundant.

Basal Body Wall (BBW)

The BBW, comprised of gastrodermis, mesoglea, and calicodermis was consistently thin (~9 μm) in *M. flabellata* as the calicodermis is approximately one-quarter the width of the gastrodermis and the mesoglea was undetectable in most areas. Notably, the lysozyme-containing bright pink, granular gland cells were absent in all *M. flabellata* samples whereas they were observed in *M. patula* in numerous areas of the BBW and in the mesenteries (Fig. 1.17).

Mesenteries

In *M. flabellata*, mesenteries were spread out in small groupings and cnidoglandular bands were small and often flat, mushroom-top shaped (Fig. 1.18a, b). No apparent clusters of digestive granular gland cells were observed in *M. flabellata,* but these were present in *M. patula*. Large batteries of spirocysts were rarely seen in *M. flabellata* mesenteries. These encapsulated, tightly coiled tubules of adhesive microfibrillae were more common in *M. patula* mesenteries (Fig. 1.18c, d).

Chromoproteins in the Epidermis

Examination of the histoslides of ten Kāneʻohe Bay *M. flabellata* colonies stained with Masson's trichrome provided additional material and an additional method for visualizing chromoproteins. Chromoproteins were not visualized with the five staining methods used for the initial set of samples, however, in the Masson's trichrome-stained slides, a vibrant, thick and grainy band in the upper half of the epidermis was observed in all of the colonies (Fig. 1.19). This band was consistent throughout the epidermis on all slides and was clearly delineated from the nuclei of the cells. Unlike fluorescent proteins in other species that cluster below and among the nuclei, these appear to be highly concentrated above the nuclei at the apical surface. The bright red staining is consistent with chromoproteins (Fig. 1.20).

Discussion

Montipora flabellata is an endemic species and is visibly unlike any other coral in Hawaiʻi. Its purple or blue coloration is uniform across the surface of the colony rather than targeted at growing tips or margins. Colonies are found only on shallow reefs (to ~8 m) where high wave action or water flow occurs (ARD pers. obs.). Despite its visible and ecological uniqueness, there is a paucity of information available

concerning *M. flabellata:* few published accounts have gone beyond mention of this species' habitat preferences (Olson et al. 2009; Forsman et al. 2010; Franklin et al. 2013), and it remains unclear what factors control its distribution. The results of this investigation suggest that a physiological trade-off may be the key to understanding this species' ability to survive and compete in supersaturating light habitats.

The environmental dynamics were significantly different where colonies were present (CRIMP buoy and PR14) versus where they were absent (PR15). The results suggest that high concentration of particulate matter in the seawater is not a determining factor for the species' distribution despite the coral's inability to remove sediment once it has deposited on the colony surface. The combination of higher water flow and higher sedimentation rates at CRIMP and PR14, instead suggest that water flow is sufficient to prevent sedimentation or remove sediment from colony surfaces. Furthermore, these results suggest that the high suspended particulate load in Kāne'ohe Bay limits *M. flabellata* colonies to reefs where water flow is constant and vigorous enough to prevent deposition. A similar test in the north portion of the Bay could provide further evidence of these findings.

Observations from the bleaching recovery experiment suggested that small fragments (< 1.99 g) are more susceptible to sedimentation and/or predation. Fragments over 2 g had the highest percent growth suggesting that patchy fragmentation of colonies in the field may have a better chance of recovering if the isolated patches of live tissue are of adequate size. This could have important ecological implications for fragmented colonies in the field during bleaching recovery, particularly where tissue loss has occurred. Results further suggested that sedimentation could be a major driving factor for habitat selection since *M. flabellata* fragments appeared unable to rid themselves of settled particles, and smothered tissue died within 24 hours. Because both cilia and mucus are required for effective debris removal, the lack of cilia or mucocytes could result in an inability to conduct this important coral function. Histological analysis of several specimens later showed cilia were present, but the number of mucocytes was abnormally low in all specimens observed. The apparent lack of mucocytes may help explain why *M. flabellata* colonies in Kāne'ohe Bay only inhabit high water flow reefs, however, more manipulative studies are needed to assess the relationship between water flow and particulate loading in this species.

Circulation in Kāne'ohe Bay is driven by waves, currents, and tides, with one or more dominating depending on the time and location in the Bay (Lowe et al. 2009). Lowe et al. (2009) provide a particularly helpful description of water movement in the Bay with zones delineated based on water residence times. Water residence times where most *M. flabellata* colonies are found varied and were as low as approximately one day and as high as 12 days. The prevailing water-moving force was measured at different locations across the Bay with waves the dominant force at the fore reef and across the reef flat, outgoing currents were dominant in the channels and immediately inside the lagoon, and water level

(tidal forcing) was dominant in the central lagoon area (Lowe et al. 2009). Trade winds, which help drive surface currents, are likely influential in areas such as the CRIMP buoy and near the Sampan Channel where very shallow colonies are particularly numerous. In surveys of shallow reefs in Kāne'ohe Bay, colonies were found primarily near the two main outgoing channels and were also sparsely found on patch reefs in the central lagoon area with a total of four colonies found south of the Sampan Channel. Suspended particulate matter is common across the entirety of Kāne'ohe Bay and settlement increases with proximity to land, particularly in the south Bay and near freshwater outlets (Hunter and Evans 1995; Lowe et al. 2009; Bahr et al. 2015). Suspended particulate matter may be high even in the channels, as evidenced by Secchi disk water clarity measurements at PR43, but water movement appears consistent (Lowe et al. 2009).

The distribution of *Montipora flabellata* (and all other coral species) throughout Kāne'ohe Bay was last described in great detail by Maragos (1972). His team surveyed over 300 sites over two years and covered the fore, fringing, and patch reefs, channels, and outside the reef crest. They employed several surveying techniques, including belt transects and boat tows. These surveys combined quantitative and qualitative techniques and provided a comprehensive understanding of coral species distribution in Kāne'ohe Bay. Interestingly, they did not find *M. flabellata* in the central lagoon area on any of the patch reefs they surveyed. Surveys and unquantified reconnaissance trips in 2014-2018 showed that *M. flabellata* is no longer present on the southern side of the Sampan Channel towards the Marine Corps Base. Some of the discrepancy in the data could be explained by the differences in methods employed; the present surveys covered the entire patch reef area and counted every colony. Water quality improvements since the 1979 diversion of the sewage outfall (Smith 1981; Hunter and Evans 1995; Bahr et al. 2015) have likely had a net positive effect on the reef habitability for this species and colonies on many of the patch reefs are in the small size class bins suggesting they are young. The very large colony on PR43, however, was likely present in the 1970s but there is no overlap between surveys on that reef. It is believed that the current *M. flabellata* population suffered moderate mortality after the warming event from 2014-2016. This likely explains the loss of colonies in the Sampan Channel since reconnaissance in this area was conducted in 2017. The survey sites visited in 2014 and 2015 have not been reassessed since the event and a recount would be an important follow-up step towards understanding the effect the event had on this species throughout the Bay.

An intriguing attribute of this coral species is its uniform purple coloration. The bright or dull purple color is highly visible among all other species on the reef. When *M. flabellata* bleaches, the colony appears lilac due to the loss of the chl *a*, c_2 and peridinin-containing symbionts while the chromoproteins remain. CPs have a slow turnover rate and a half-life of approximately three weeks (Leutenegger et al. 2007; D'Angelo et al. 2012). CPs (and fluorescent proteins; FPs) contributed between 4.5–14% of the

total soluble protein in corals species measured by Leutenegger et al. (2007). They determined that the slow turnover was an indication of a low associated cost to producing the proteins and further stated a requirement for high concentrations of CPs and FPs if the function is for photoprotection. They concluded that it is "cheap to be colorful", however, Dove (2004) found that corals with high concentrations of CPs were "hypersensitive" to bleaching. Indeed, *M. flabellata* was the first coral species to bleach in Kāneʻohe Bay in early September 2014 (ARD pers. obs.), the beginning of the multi-year warming event (Bahr et al. 2017). However, it remains unclear whether the presence of high concentrations of CPs in *M. flabellata* is associated with high susceptibility to thermally-driven bleaching.

Photoprotection implies protection from damage to the photosynthetic mechanisms in the coral symbiotic zooxanthellae. The constitutive pigments of zooxanthellae include photoprotective pigments with absorbance spectra that overlap with photosynthetic pigments, whereas chromoproteins absorb light energy in the ultra-violet radiation (UVR) spectrum and yellow portion of the photosynthetically active radiation (PAR) spectrum (~560-590 nm; unpub. data). Studies on land plants have shown that the yellow portion of the PAR spectrum is second only to UVR for potential to harm photosynthetic machinery, specifically the oxygen-evolving complex of Photosystem II (Ohnishi et al. 2005; Takahashi et al. 2010; Zavafer et al. 2015). Similar studies on specific wavelength damage to coral symbionts have not yet been conducted, therefore the conceptual framework for photodamage in corals has been modeled from these available studies. Considering the likelihood that shallow water corals experience supersaturating conditions for many hours each day, pigments absorbing in the yellow PAR spectrum, complementary to the photoprotective pigments in the zooxanthellae, would provide an additional layer of protection. This is accomplished in *M. flabellata* at the cost of surface mucus. It is commonly accepted that most corals block UVR with symbiont-produced mycosporine-like amino acids (MAAs) that are translocated to the coral surface mucus. These secondary metabolites absorb UVR in the 310–365 nm range (Banaszak et al. 2000; Oren and Gunde-Cimerman 2007; Rosic and Dove 2011) and are also capable of scavenging radical oxygen species (ROS). Thus, a coral that does not produce sufficient quantities of mucus would not be as equipped with these important functions as other species. The presence of UVR-absorbing melanin enrobing the zooxanthellae, together with the epidermal layer of chromoproteins are consistent with a strong investment in photoprotection that differs in strategy from most other corals. While the presence of melanin in corals is not novel, the close association with the zooxanthellae in *M. flabellata* is interesting, particularly because the association appears to be absent in *M. patula*. The targeted presence of melanin in *M. flabellata* requires further investigation.

Conclusions

The results from this investigation support a role of photoprotection for the CPs localized in the epidermis of *M. flabellata* colonies. The comparatively low number or near lack of mucocytes in this species' epidermis suggests an energy trade-off, which benefits the putative photoprotection function of CPs over functions carried out in the mucopolysaccharide surface layer. In Kāne'ohe Bay, suspended particulate matter is a common characteristic of the seawater and *M. flabellata* colonies were observed inhabiting only areas of high water flow where continuous flushing of the colony surface obviates the need for mucus production. Next steps towards understanding this unique species should include histology of colonies from more oligotrophic waters where pigmentation tends to be blue rather than purple, and more quantitative water flow measurements throughout and outside the species' range. It is possible the physiological characteristics of this endemic species are consistent regardless of location and water clarity.

References

Bahr KD, Jokiel PL, Toonen RJ (2015) The unnatural history of Kāneʻohe Bay: coral reef resilience in the face of centuries of anthropogenic impacts. PeerJ 3:e950. doi: 10.7717/peerj.950

Bahr KD, Rodgers KS, Jokiel PL (2017) Impact of three bleaching events on the reef resiliency of Kāneʻohe Bay, Hawaiʻi. Front. Mar. Sci. 4: 398. doi: 10.3389/fmars.2017.00398

Banaszak A, LaJeunesse T, Trench R (2000) The synthesis of mycosporine-like amino acids (MAAs) by cultured, symbiotic dinoflagellates. J. Exp. Mar. Bio. Ecol. 249:219–233

D'Angelo C, Smith EG, Oswald F, Burt J, Tchernov D, Wiedenmann J (2012) Locally accelerated growth is part of the innate immune response and repair mechanisms in reef-building corals as detected by green fluorescent protein (GFP)-like pigments. Coral Reefs 31:1045–1056

Darling ES, Alvarez-Filip L, Oliver TA, McClanahan TR, Côté IM (2012) Evaluating life-history strategies of reef corals from species traits. Ecol. Lett. 15:1378–86

Doty MS (1971) Measurement of water movement in reference to benthic algal growth. Bot. Mar. 14:32–35

Dove S (2004) Scleractinian corals with photoprotective host pigments are hypersensitive to thermal bleaching. Mar. Ecol. Prog. Ser. 272:99–116

Enrıquez S, Méndez E, Iglesias-Prieto R (2005) Multiple scattering on coral skeletons enhances light absorption by symbiotic algae. Limnol. Oceanogr. 50:1025–1032

Forsman ZH, Concepcion GT, Haverkort RD, Shaw RW, Maragos JE, Toonen RJ (2010) Ecomorph or endangered coral? DNA and microstructure reveal Hawaiian species complexes: *Montipora dilatata/flabellata/turgescens* & *M. patula/verrilli*. PLoS One 5:e15021 doi: 10.1371/journal.pone.0015021

Franklin EC, Jokiel PL, Donahue MJ (2013) Predictive modeling of coral distribution and abundance in the Hawaiian Islands. Mar. Ecol. Prog. Ser. 481:121–132

Hunter CL, Evans CW (1995) Coral reefs in Kaneohe Bay, Hawaii: Two centuries of western influence and two decades of data. Bull. Mar. Sci. 57:501–515

Jokiel PL, Maragos JE, Franzisket L (1978) Coral growth: buoyant weight technique. In: Stoddart DR and Johannes RE (eds) Coral reefs: research methods. UNESCO, Paris, France. pp 529–541

Jokiel PL, Brown EK (2004) Global warming, regional trends and inshore environmental conditions influence coral bleaching in Hawaii. Glob. Chang. Biol. 10:1627–1641

Jokiel PL, Morrissey JI (1993) Water motion on coral reefs: evaluation of the 'clod card' technique. Mar. Ecol. Prog. Ser. 93:175–181

Leutenegger A, D'Angelo C, Matz MV, Denzel A, Oswald F, Salih A, Nienhaus GU, Wiedenmann J (2007) It's cheap to be colorful: Anthozoans show a slow turnover of GFP-like proteins. FEBS J. 274:2496–2505

Lowe RJ, Falter JL, Monismith SG, Atkinson MJ (2009) A numerical study of circulation in a coastal reef-lagoon system. J. Geophys. Res. Ocean. 114:1–18

Maragos JE (1972) A study of the ecology of Hawaiian reef corals. Doctoral Dissertation. University of Hawaii. Honolulu, USA

Marcelino LA, Westneat MW, Stoyneva V, Henss J, Rogers JD, Radosevich A, Turzhitsky V, Siple M, Fang A, Swain TD, Fung J, Backman V (2013) Modulation of light-enhancement to symbiotic algae by light-scattering in corals and evolutionary trends in bleaching. PLoS One 8:e61492

Nakamura T, Van Woesik R (2001) Water-flow rates and passive diffusion partially explain differential survival of corals during the 1998 bleaching event. Mar. Ecol. Prog. Ser. 212:301–304

Nakamura T, Yamasaki H, Van Woesik R (2003) Water flow facilitates recovery from bleaching in the coral *Stylophora pistillata*. Mar. Ecol. Prog. Ser. 256:287–291

Ohnishi N, Allakhverdiev SI, Takahashi S, Higashi S, Watanabe M, Nishiyama Y, Murata N (2005) Two-step mechanism of photodamage to photosystem II: Step 1 occurs at the oxygen-evolving complex and step 2 occurs at the photochemical reaction center. Biochemistry 44:8494–

Olson ND, Ainsworth TD, Gates RD, Takabayashi M (2009) Diazotrophic bacteria associated with Hawaiian *Montipora* corals: Diversity and abundance in correlation with symbiotic dinoflagellates. J. Exp. Mar. Bio. Ecol. 371:140–146

Oren A, Gunde-Cimerman N (2007) Mycosporines and mycosporine-like amino acids: UV protectants or multipurpose secondary metabolites? FEMS Microbiol. Lett. 269:1–10

Palmer CV, Roth MS, Gates RD (2009) Red fluorescent protein responsible for pigmentation in trematode-infected *Porites compressa* tissues. Biol. Bull. 216:68–74

Peters EC, Price KL, Horowitz DB (2005) Histological preparation of invertebrates for evaluating contaminant effects. In: G Ostrander (ed) Techniques in Aquatic Toxicology. CRC Press. pp 654–688

Preisendorfer R (1986) Secchi disk science: Visual optics of natural waters. Limnol. Oceanogr. 3:909–926

Rodgers KS, Jokiel PL, Brown EK, Hau S, Sparks R (2015) Over a decade of change in spatial and temporal dynamics of Hawaiian coral reef communities. Pac. Sci. 69:1–13

Rosic NN, Dove S (2011) Mycosporine-like amino acids from coral dinoflagellates. Appl. Environ. Microbiol. 77:8478–86

Smith SV (1981) Kaneohe Bay sewage diversion experiment: Perspectives on ecosystem response to nutritional perturbation. Pac. Sci. 35:279–402

Takahashi S, Milward SE, Yamori W, Evans JR, Hillier W, Badger MR (2010) The solar action spectrum of photosystem II damage. Plant Physiol. 153:988–93

Veron JEN, Stafford-Smith M (2000) Corals of the World. Australian Institute of Marine Science, Townsville MC, Qld, Australia

Zavafer A, Cheah MH, Hillier W, Chow WS, Takahashi S (2015) Photodamage to the oxygen evolving complex of photosystem II by visible light. Sci. Rep. 5:16363

Tables and figures

Figure 1.1. *Montipora flabellata* colonies with deep purple pigmentation, Kāneʻohe Bay. Photos by Fred Farrell.
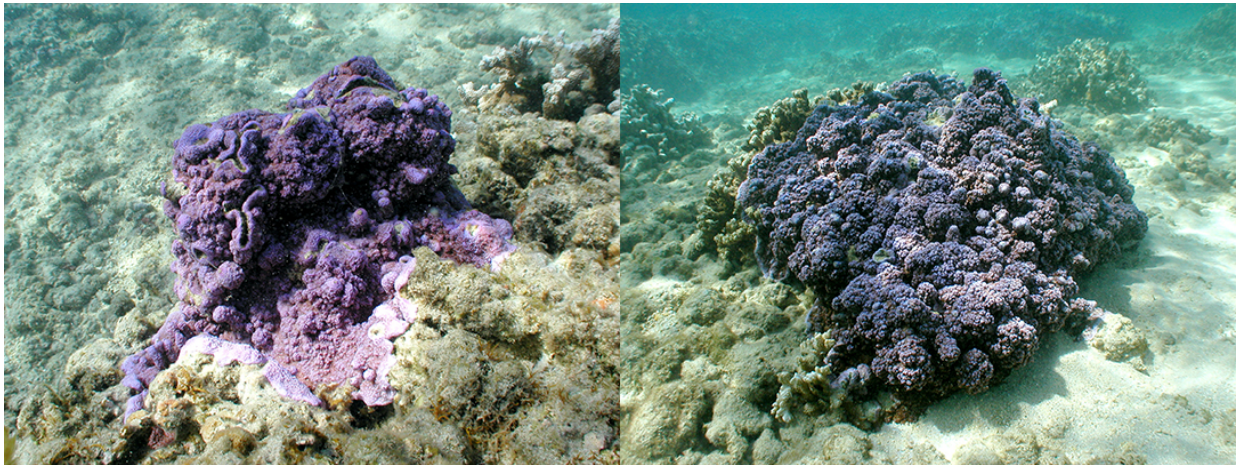
Figure 1.2. Bleached *Montipora flabellata* colonies in September 2014 (left, center). Bleached *M. flabellata* in October 2014 (right; Z. Forsman). All photos taken in Kāneʻohe Bay. Some purple pigment remaining in colonies in September but mostly absent by October.

Figure 1.3. *Montipora patula* (left) with purple in polyps only (inset), and *M. flabellata* (right) with uniform coloration.
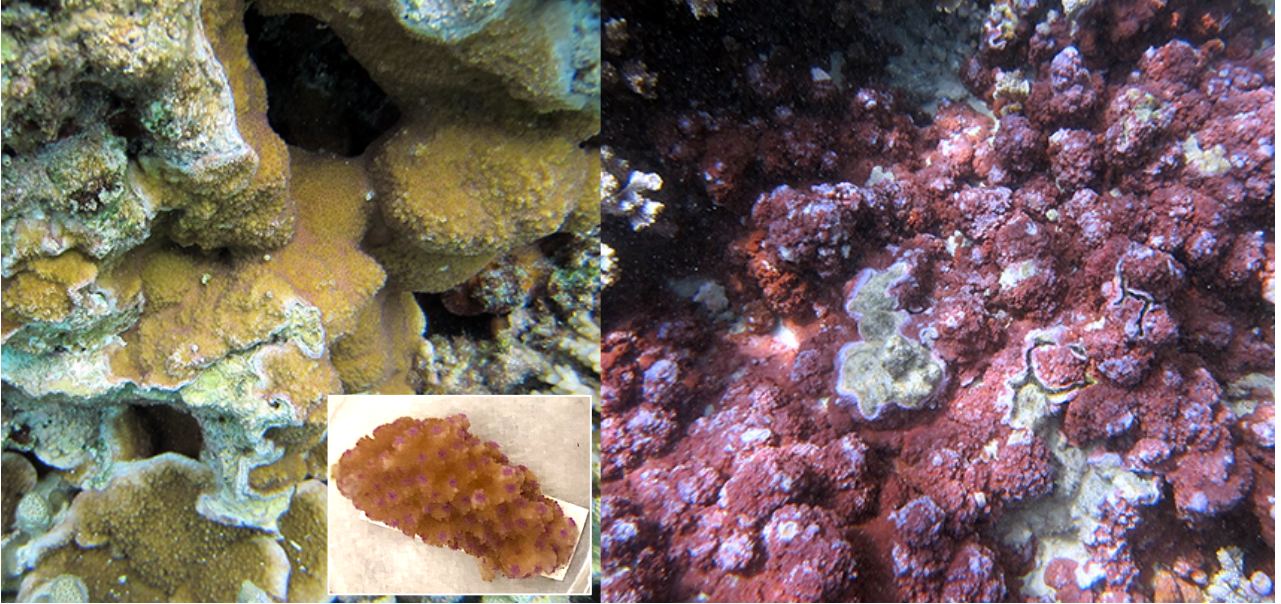
Figure 1.4. Map of Kāneʻohe Bay survey sites. Filled purple circles denote presence of *M. flabellata* colonies. Empty purple-rimmed circles denote sites where colonies were absent. Dark purple circles denote sites where *M. flabellata* colonies were present in 1972. Purple stars denoting presence of *M. flabellata* (unquantified). Green numbers = Secchi disk depths (m). MP = *Montipora flabellata*. Circle size refers to number of colonies counted at each reef.
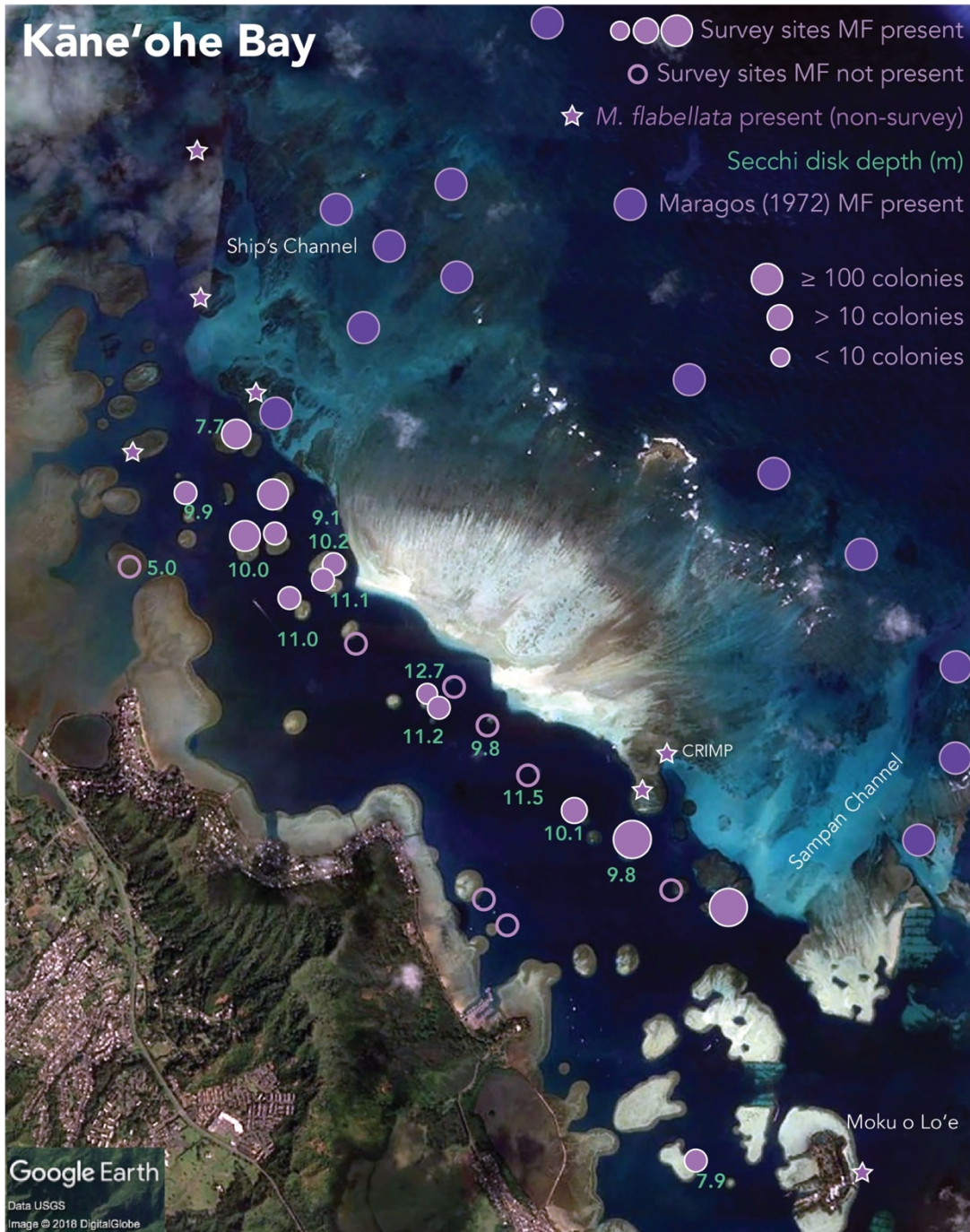
Figure 1.5. Illustration of example survey path. Entire reefs were surveyed in this manner to locate, measure, and record the presence of *Montipora flabellata* colonies.
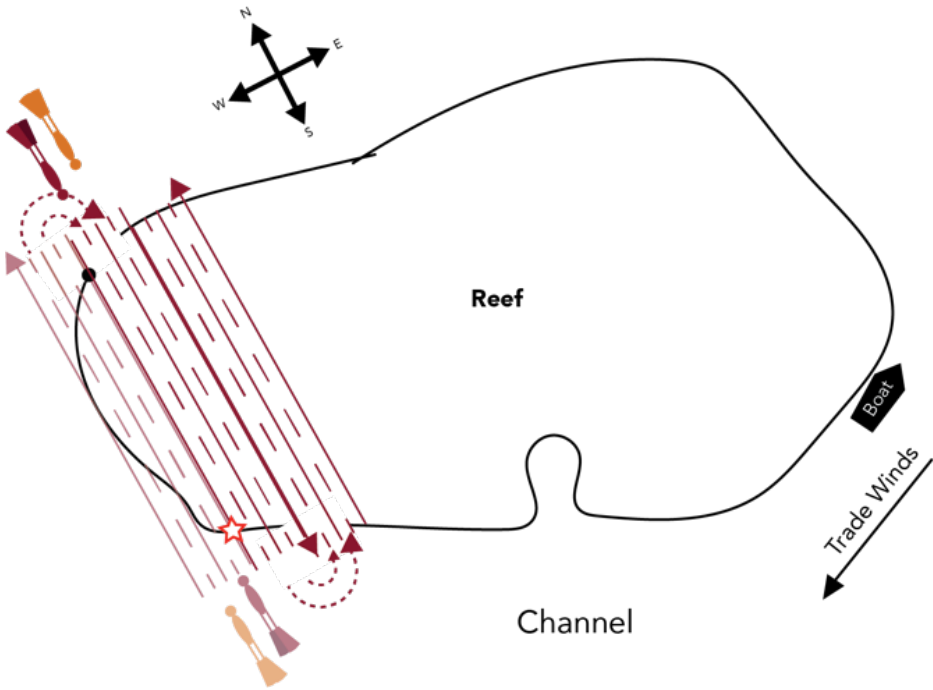
Table 1.1. Staining technique, stain uses, and description of colors and corresponding structures, substance, and tissue types employed for this investigation.

Staining Technique	Primary Uses	Colors
Hematoxylin & Eosin (H&E)	Common stain for nuclei, mucins, protein	purple = nuclei light purple = mucus, bright pink = cnidae, granular gland cells, zooxanthellae pink = cytoplasm, muscle, mesoglea, protein
Periodic acid-Schiff reagent/ alcian blue	PAS: glycoproteins, connective tissue, mucus, basement membrane. AB: mucopolysaccharides	bright purple = membranes, mesoglea, zooxanthellae blue = mucocytes, mucus
Cason's trichrome	Visualize mesoglea and other connective tissue	red = nuclei orange = cnidae blue = mesoglea, muscle, connective tissue
Fontana-Masson	Visualize pigment melanin	black = melanin, argentaffin substances red = nuclei pink = cytoplasm
Movat's modified pentachrome	Visualize collagen and mucopolysaccharides in same sample	black = nuclei yellow = collagen blue = mucocytes, mucus bright red = cnidae red = muscle
Masson's trichrome	Visualize mesoglea and other connective tissue	red = protein, muscle, chromoproteins, i.e., hemoglobin black = nuclei blue = mesoglea

Figure 1.6. Survey results for presence of *M. flabellata* colonies on all reefs by colony size class. Total of 359 colonies recorded with largest number of colonies in the 10–20 cm size class.
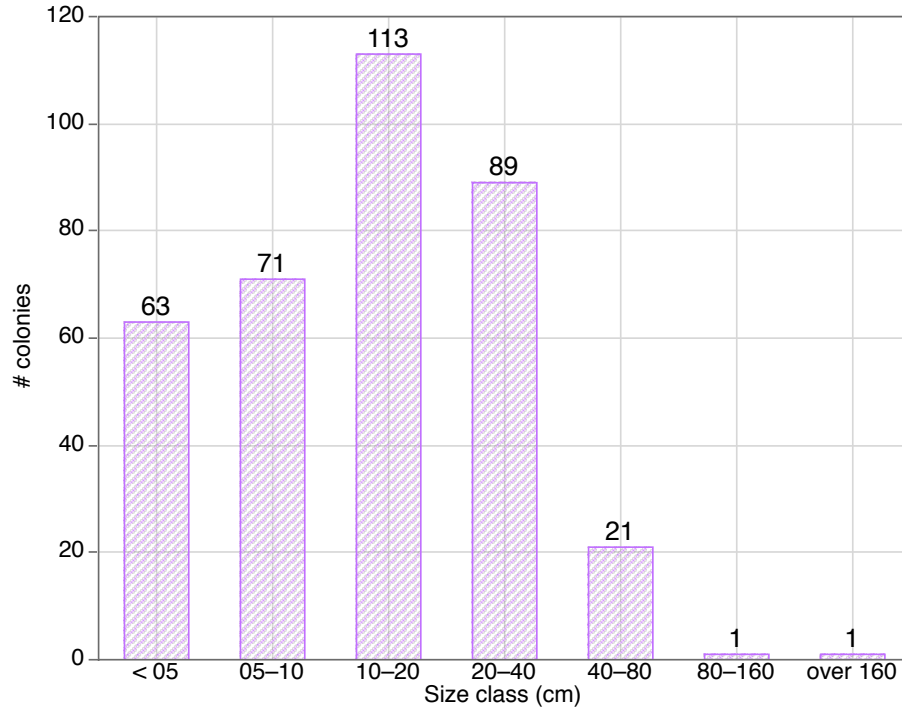
Figure 1.7. Largest *Montipora flabellata* colony observed in Kāneʻohe Bay during surveys in 2014. Located on PR43, this is the only colony categorized in the >160 cm size class. Purple pigmentation not visible in photo. Photo by David Slater.

Table 1.2 Patch reefs surveyed for presence of *M. flabellata* in Kāneʻohe Bay with colonies listed by colony size class. Asterisks on patch reefs denote overlap with Maragos (1972) surveys. Secchi disk depth measurements in meters and seawater residence time zones (RZ; Lowe et al. 2009) over number of days for water exchange.

Patch Reef	Location	Secchi depth (m)	RZ/ days	< 5	5-10	10-20	20-40	40-80	80-160	> 160	Total colonies
4*	South	7.9	6/36	0	2	0	1	0	0	0	3
11	Sampan	--	3/4	11	15	35	31	8	0	0	100
12*	Sampan	--	3/4	8	11	8	5	4	1	0	37
14*	Central	9.8	5/12	24	23	44	42	7	0	0	140
16	Central	10.1	5/12	7	7	7	2	0	0	0	23
17	Central	--	5/12	0	0	0	0	0	0	0	0
18	Central	--	5/12	0	0	0	0	0	0	0	0
19*	Central	11.5	5/12	0	0	0	0	0	0	0	0
20*	Central	9.8	5/12	0	0	0	0	0	0	0	0
21*	Central	--	5/12	0	0	0	0	0	0	0	0
22*	Central	11.2	5/12	0	1	0	0	0	0	0	1
23*	Central	12.7	5/12	0	0	3	0	0	0	0	3
26*	Central	--	5/12	0	0	0	0	0	0	0	0
27*	Central	11.0	5/12	1	4	4	0	0	0	0	9
28*	Central	11.1	5/12	0	1	4	1	0	0	0	6
29*	Central	10.2	5/12	0	0	1	0	0	0	0	1
30*	Central	10.0	5/12	0	0	2	0	0	0	0	2
31*	Central	10.0	5/12	4	3	4	3	0	0	0	14
34	North	5.0	4/1	0	0	0	0	0	0	0	0
38*	Central	9.9	5/12	3	4	0	1	0	0	0	8
40*	Central	9.1	5/12	1	0	0	0	0	0	0	1
43	North	7.7	4/1	4	0	1	3	2	0	1	11
				63	71	113	89	21	1	1	359

Table 1.3. Summary statistics of One-way ANOVA for clod card dissolution as proxy for water flow comparison between sites in November 2016 (N) and April 2017 (A) with summary statistics of Welch's ANOVA Test for testing means equal, allowing standard deviations are not equal (below).

Location	Month	N	R^2	Response Mean	Site Mean	Std. Error	p-value	DF
CRIMP	N	6			0.8038	0.0118		
PR14	N	5			0.8834	0.0130		
PR15	N	6			0.6545	0.0118		
		17	0.927778	0.774529			<0.0001	2
CRIMP	A	5			0.5740	0.0099		
PR14	A	6			0.5922	0.0090		
PR15	A	6			0.4965	0.0090		
		17	0.816681	0.553059			<0.0001	2

Welch's ANOVA Test

Location	Month	N	F Ratio	DF Num	DF Den	Prob > F
ALL	N	17	101.4024	2	7.9947	<0.0001
ALL	A	17	43.3674	2	8.0408	<0.0001

Figure 1.8. One-way ANOVA plots for clod card dissolution (g hr^{-1}) at three sites in November 2016 (left) and April 2017 (right).
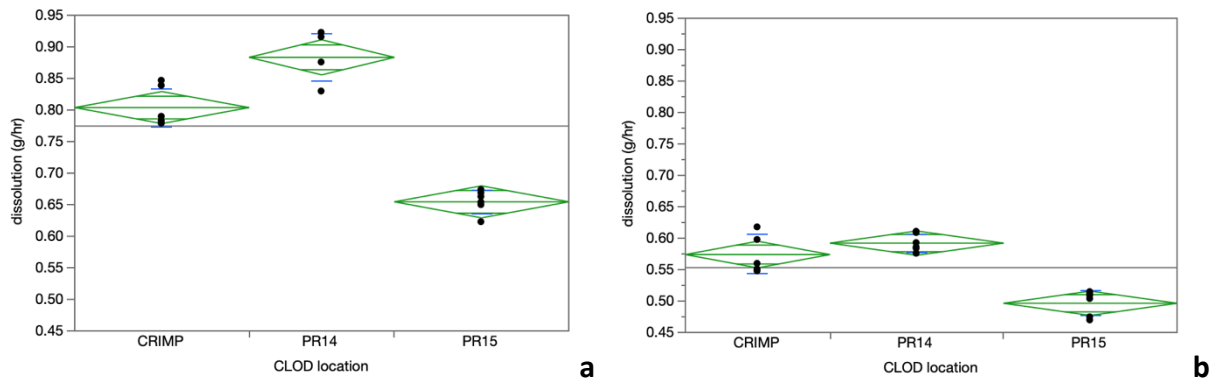
Table 1.4. Summary statistics for One-way ANOVA of weight in grams of two sediment traps per time point with Welch's ANOVA statistics (below).

Location	Month	N	R^2	Mean (g)	Site Mean (g)	Std. Error	p-value	DF
CRIMP	N	2		0.64	0.58	0.0268		
	A	2		0.53				
PR14	N	2		0.59	0.55	0.0268		
	A	2		0.52				
PR15	N	2		0.21	0.20	0.0268		
	A	2		0.20				
All Sites		12	0.9329	0.45			<0.0001	2

Welch's ANOVA Test

Location	Month	N	F Ratio	DF Num	DF Den	Prob > F
ALL	N&A	12	116.4596	2	4.3524	0.0002

Figure 1.9. One-way ANOVA plot for weight in grams of recovered sediment at three sites in November 2016 and April 2017.
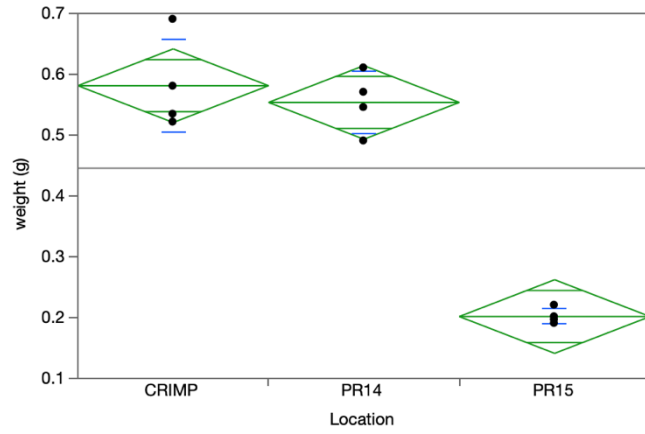
Figure 1.10. Fragments from bleached colony at time of collection (left) and 37 days later (right). Visible re-establishment of symbiotic algae in recovering fragments and lightly host-pigmented growing margins visible on several fragments (right).
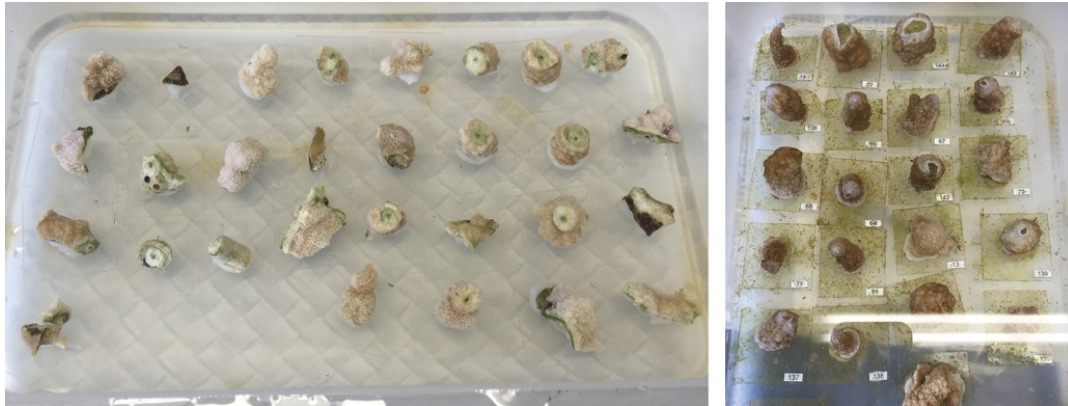
Figure 1.11. New vertical hanging method for maintaining *M. flabellata* in water tables to avoid sediment-smothering and *Priosthiostomum montiporae* predation (left, center). Fragment status prior to return to reef with some fusion occurring (right).
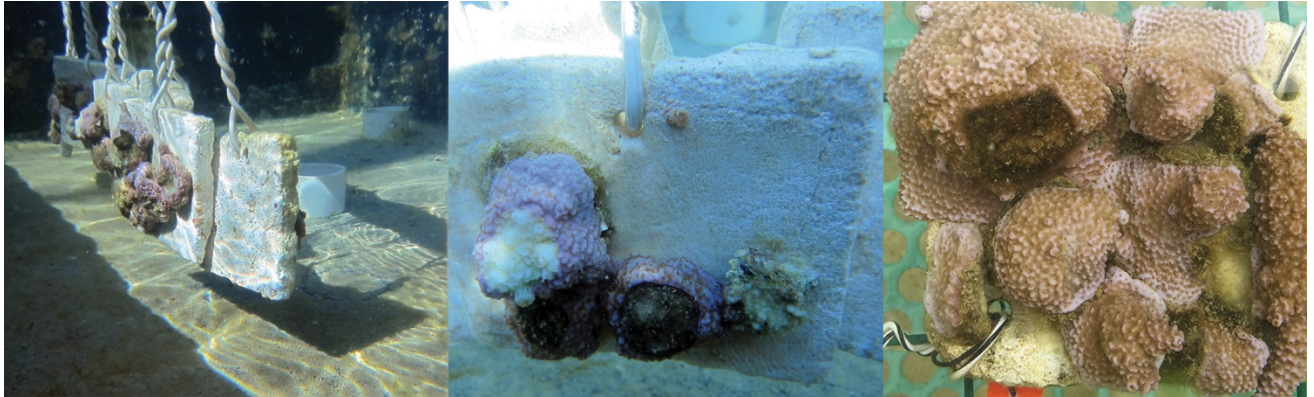
Figure 1.12. Maximum seawater temperatures at HIMB (PacIOOS) showing period from beginning of 2014 warming event to August 2016 (black line). Water table temperatures as measured separately (red dots).
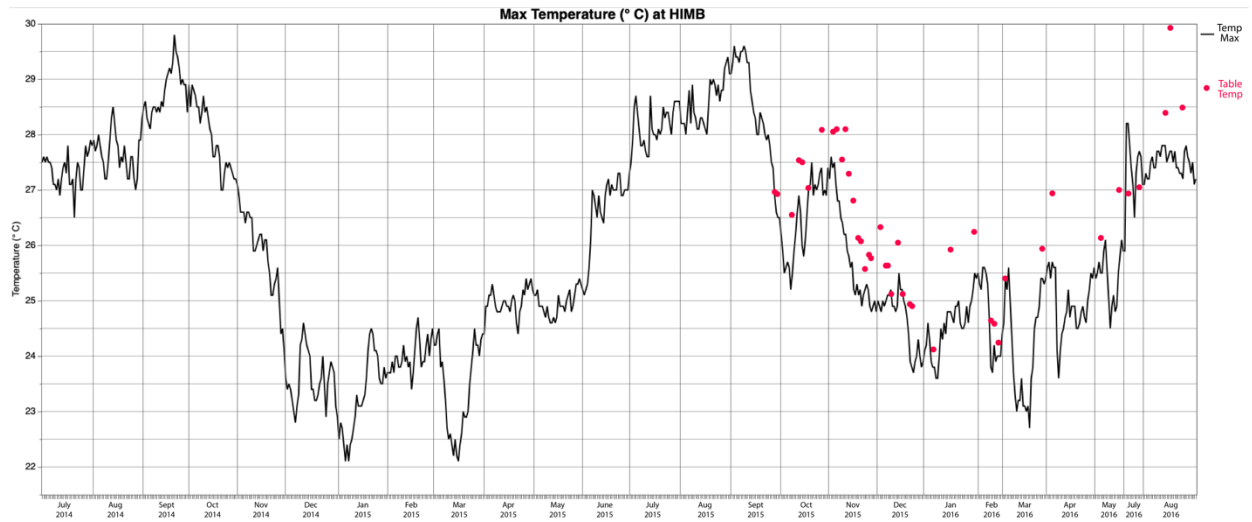
Table 1.5. Buoyant weighing results for 248 *M. flabellata* fragments of varying sizes grouped by start weight in grams. Total time period: 232 days.

Weight category (g)	Mean start weight (g)	Mean growth/day (mg)	Mean weight gain (g)	% Mean weight gain	Total count	Dead count	% Dead
<1	0.68	1.50	0.35	50.9	8	3	37.5
1-1.99	1.61	3.36	0.85	52.6	59	19	32.2
2-2.99	2.49	6.22	1.44	57.2	57	10	17.5
3-3.99	3.39	6.26	1.45	42.9	53	13	24.5
4-4.99	4.48	7.98	1.85	42.4	22	4	18.2
5-5.99	5.48	9.99	2.32	43.0	19	4	21.1
6-6.99	6.57	9.34	2.17	33.6	11	4	36.4
>7	9.19	11.75	2.73	29.2	19	7	36.8
					248	64	26.0

Figure 1.13. *Montipora flabellata* fragment growth binned by beginning weight in grams. Mean growth rate (purple bars) in mg d^{-1}. Mean percentage gain (%; black bars)
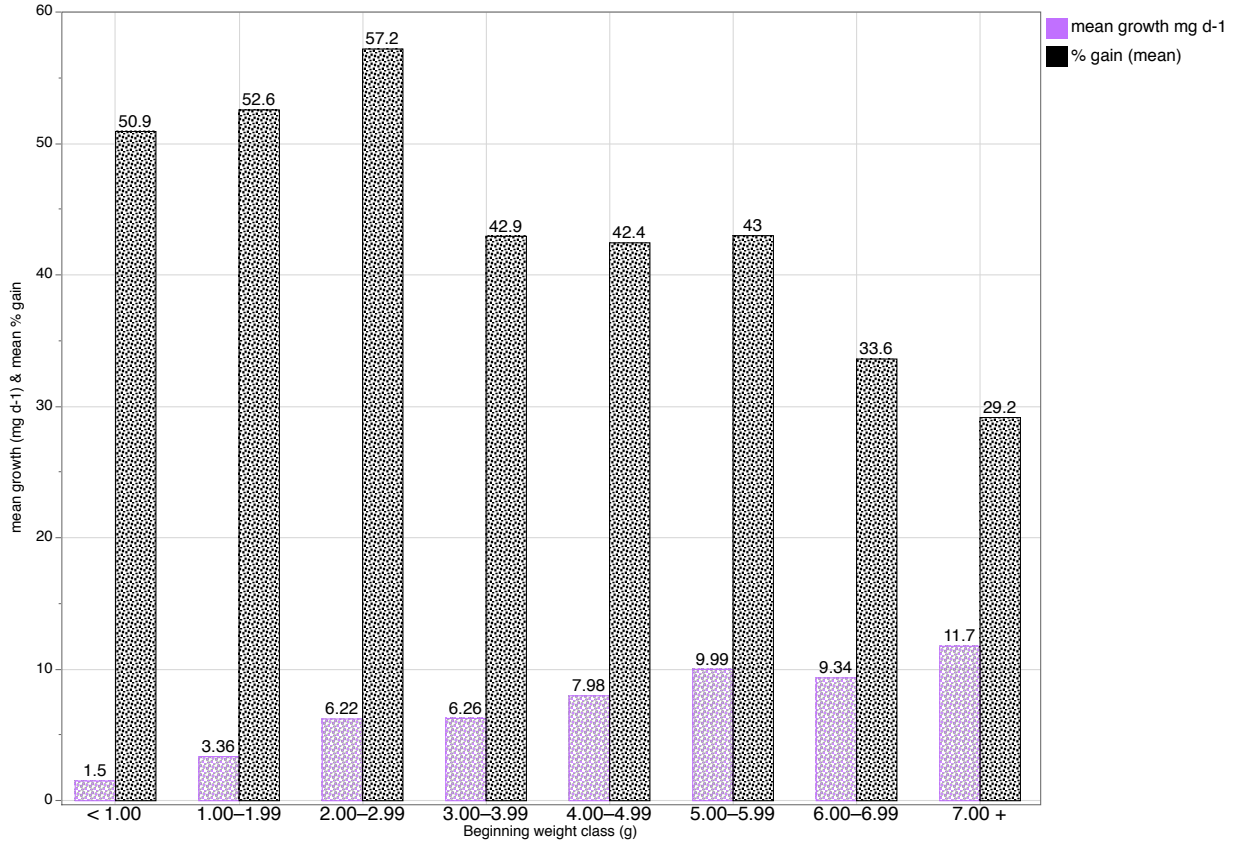
Figure 1.14. Total number of fragments by beginning weight class in grams (purple bars) and total number of dead fragments per weight class (nested black bars) at end of experiment.
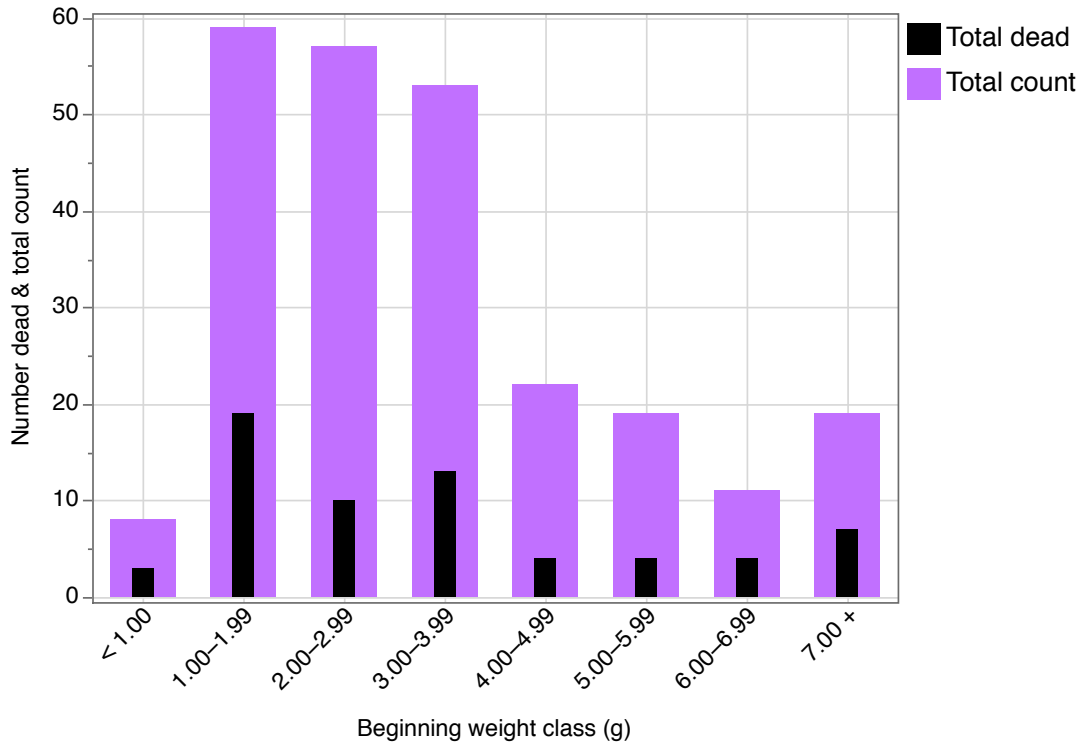
Figure 1.15. Photomicrographs of sections of epidermis in *M. flabellata* (top) and *M. patula* (bottom) stained with H&E at 20x. Lack of mucocytes in epidermis of polyp and coenenchyme notable in *M. flabellata* as compared to *M. patula*. Ep=epidermis, Coen=coenenchyme, Mu=mucocyte, Ci=cilia, Cn=cnidae, BBW=basal body wall, SBW=surface body wall, GA=gastrodermis, Sy=symbiont.
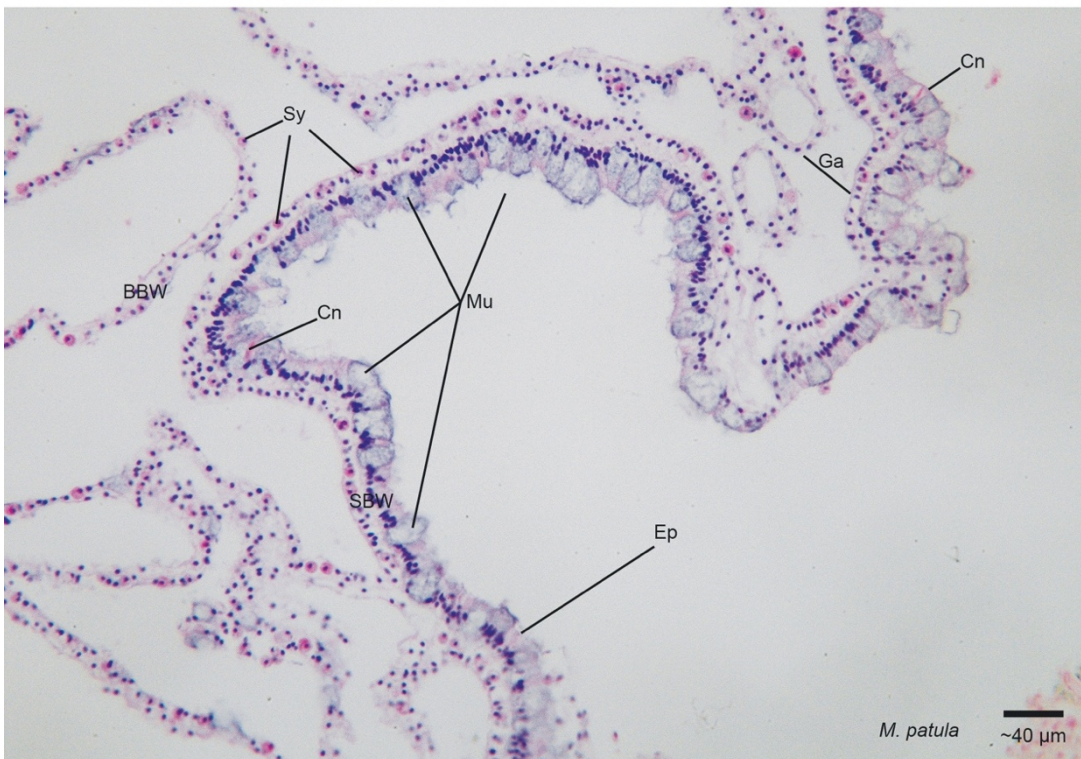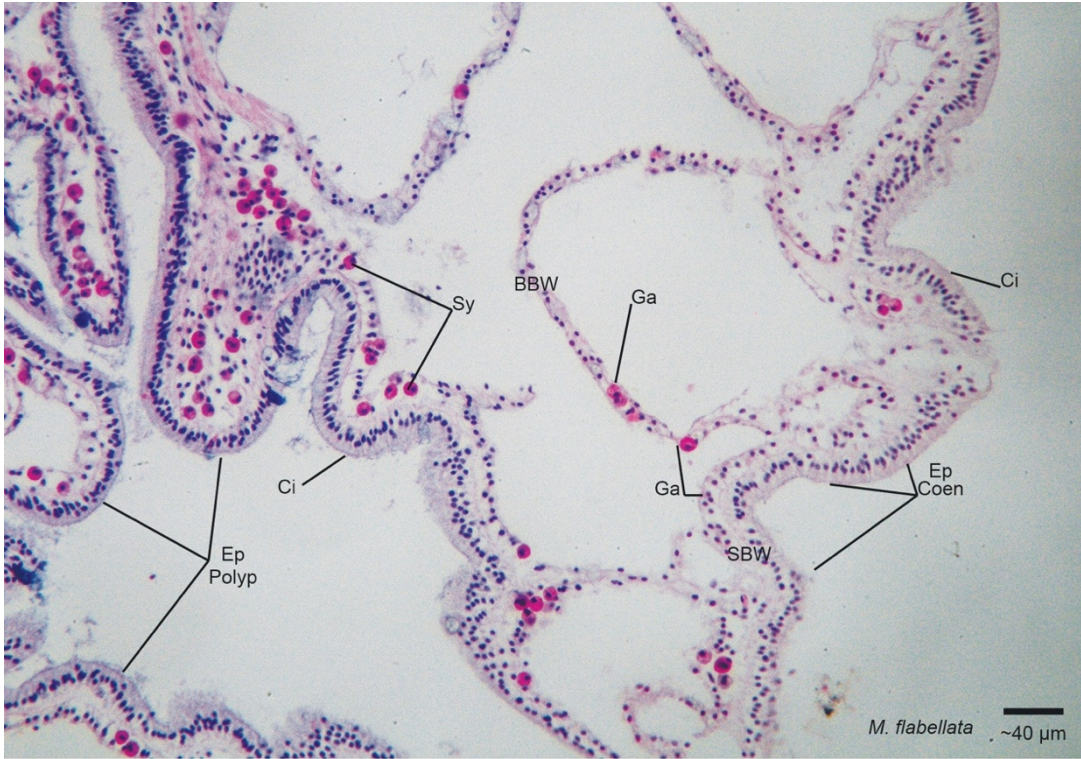
Figure 1.16. Photomicrographs of polyp details in *M. flabellata* (top) and *M. patula* (bottom) stained with Fontana-Masson staining for melanin at 40x. Note darkly stained symbionts in *M. flabellata* and pale or no staining in *M. patula*. Nu = nuclei, Sy = symbiont, Me = melanin granules.
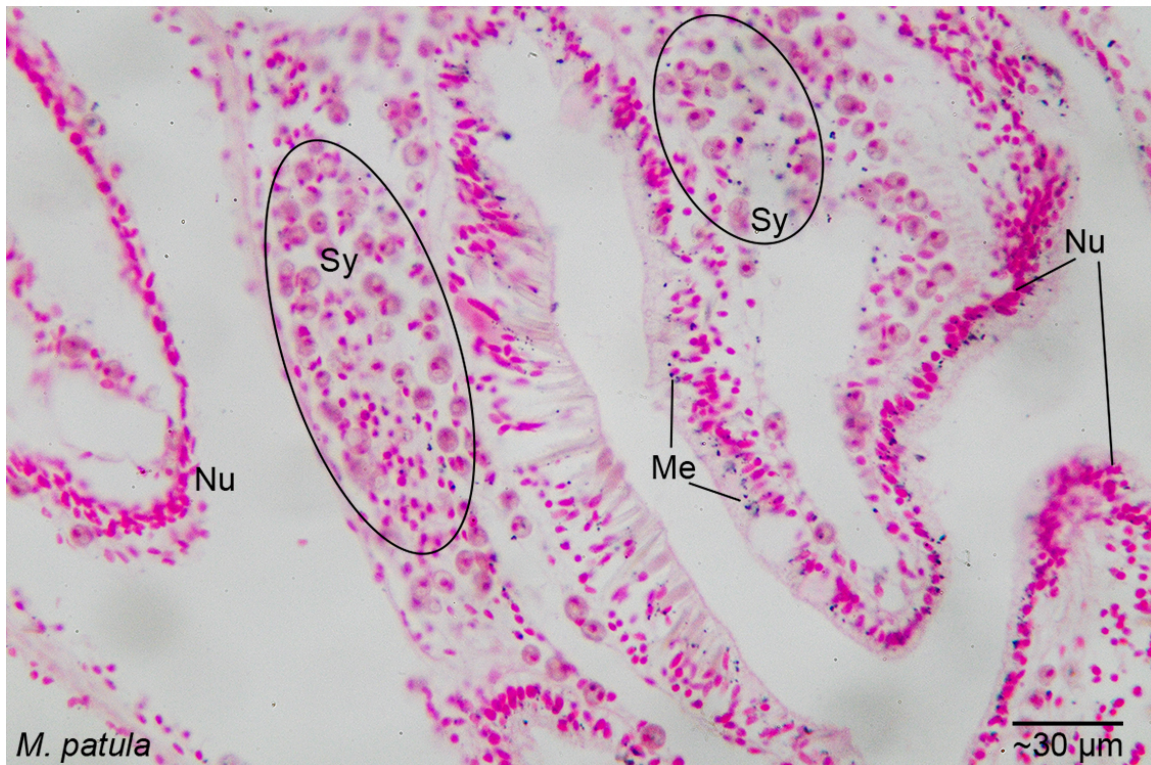
Figure 1.17. Photomicrograph of granular gland cells (GGC) in basal body wall of *M. patula* at 10x and inset enlarged view (40x).
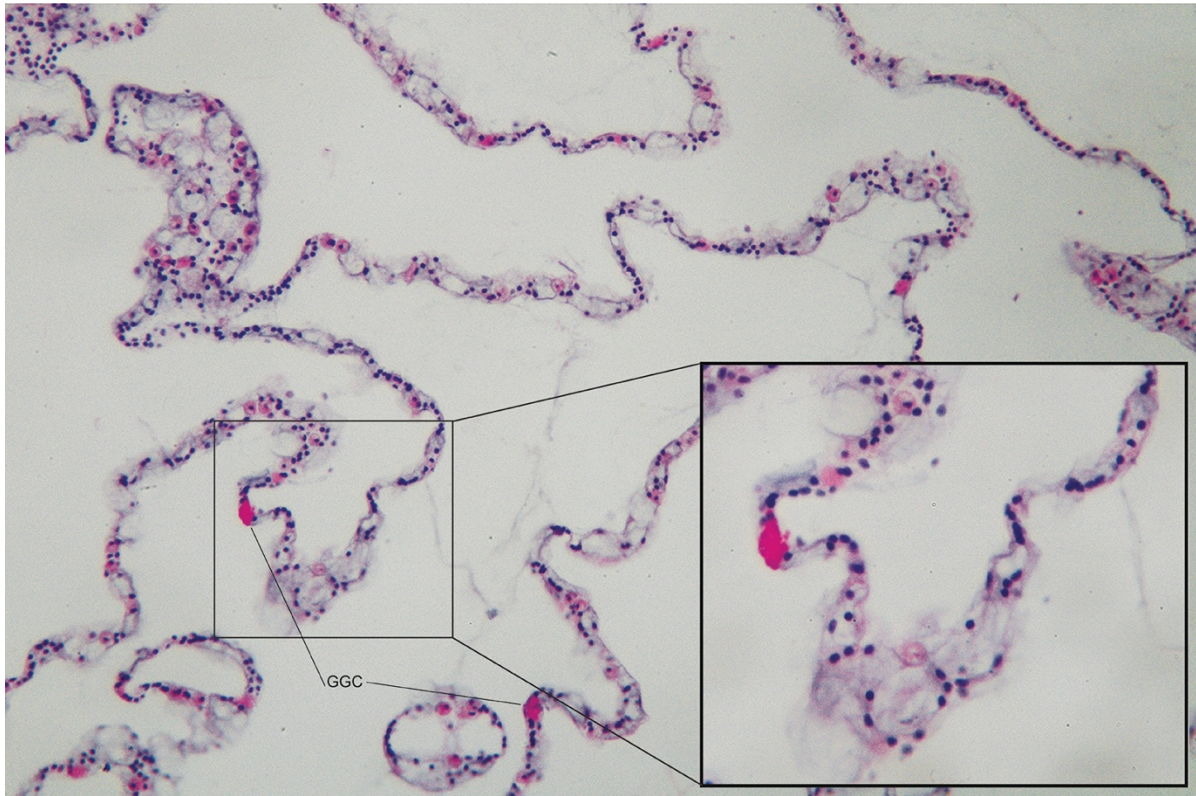
Figure 1.18. Photomicrographs of mesenteries in *M. flabellata* (a, b) and *M. patula* (c, d) stained with H&E at 20x. CGB=cnidoglandular band, Cn=cnidae, Sp=spirocyte, Mu=mucocytes, GGC=granular gland cell.
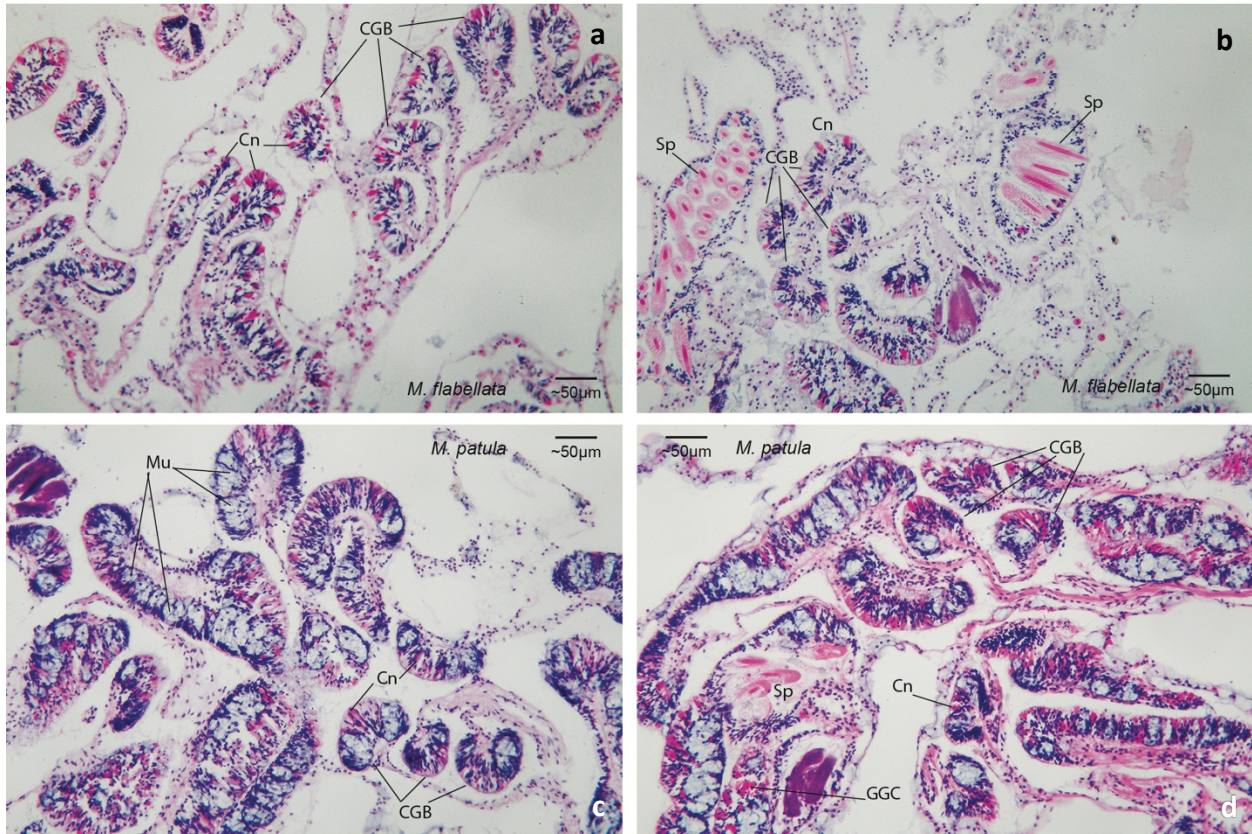
Figure 1.19. Photomicrographs of *M. flabellata* colonies stained with Masson's trichrome at 20x. Chromoproteins are thickly stained at the apical surface of the epidermis in the SBW. Small numbers of mucocytes throughout epidermis. SBW=surface body wall, CP=chromoproteins, Mu=mucocytes, Nu=nuclei, Sy=symbionts.

Figure 1.20. Photomicrograph of *Montipora flabellata* specimen stained with Masson's trichrome at 40x with brightly red-stained chromoproteins filling apical region of epidermis and low mucocyte count. SBW=surface body wall, CP=chromoproteins, Mg=mesoglea, Mu=mucocyte, Sy=symbiont.

DETERMINING THE LOCATION OF FLUORESCENT AND NON-FLUORESCENT PIGMENTS IN HAWAIIAN CORAL EPITHELIA

Angela Richards Donà

Abstract

The locations of host pigments in coral epithelia provide insight into their function(s). Persuasive evidence suggests that fluorescent proteins (pigments; FPs) and similarly structured non-fluorescent pigments (chromoproteins; CPs) provide photoprotection for the coral symbionts. Evidence also exists that suggests these pigments serve an immunity function and assist in the growth of new coral tissue. Intriguing studies on the surface patterning of FPs also raise the possibility of communication with or "sensing" of external environments via visual or phototaxis functions, although it is unclear whether CPs can be perceived in similar fashion. The goals of this investigation were threefold: (1) to describe the host pigment distribution within the coral epithelia, (2) to specifically determine whether fluorescent pigments are in the epidermis and/or polyp tentacles, and (3) to describe fluorescent pigment surface patterns in four species of Hawaiian corals (*Montipora flabellata*, *Montipora patula*, *Porites compressa*, *Leptastrea purpurea*) from Kāneʻohe Bay, Oʻahu. This investigation employed laser scanning confocal microscopy to achieve the stated goals. Results showed that FPs are found in the epidermis of the polyps and coenenchyme to varying degrees in all four species but in *M. flabellata* cyan, green, and red fluorescent proteins were found only in the epidermis consistent with a photoprotective function. Novel cyan fluorescent rod-like structures were found extending from the epidermis into deeper regions of the coral epithelia in all species, but their origin and function are unclear. Discrete surface patterning occurred in only one of the species (*L. purpurea*) and appeared highly targeted around the oral disk and the septo-costae. Discovery of FPs exclusively in the epidermis of *M. flabellata* adds to the evidence supporting a photoprotective function for these coral host pigments.

Introduction

The coral/algal symbiosis imparts a mostly uniform brown appearance to many coral colonies. The brown color is a characteristic of dinoflagellates (zooxanthellae) from the family Symbiodiniaceae and all other colors are believed to be produced by the coral. Most coral-host pigments are fluorescent proteins (FPs) and may appear cyan, green, red, orange, and/or yellow (Verkhusha and Lukyanov 2004; Alieva et al. 2008) to the human eye. Chromoproteins (CPs), which may also be present, are non-fluorescent pigments that appear pink, purple, or blue (Dove et al. 1995; Prescott et al. 2003; Alieva et al. 2008). These host pigments can be intensely visible, even in daylight, or invisible until excited with violet or blue high-energy wavelengths. Beyond the obvious aesthetic value of a colorful coral reef, these pigments have several important proposed functions that include protection for the photosynthetic machinery of the symbionts (Kawaguti 1969; Salih et al. 1997, 2000; Smith et al. 2013), assistance in the immune response (Palmer et al. 2008, 2009), quenching of superoxide radicals (Bou-Abdallah et al. 2006), and a light enhancement function in low light conditions (Schlichter et al. 1988; Roth et al. 2015a). Despite supporting evidence of these proposed functions, the photoprotection and photo-enhancement roles remain a matter under dispute because the functional mechanisms have not been identified (Mazel et al. 2003; Smith et al. 2013).

Photoprotection and Photo-enhancement

Light energy in the PAR spectrum incident upon a substance or matter, interacts with the pigments present in that matter and may be absorbed, transmitted, and/or reflected, depending on wavelength. Some pigments are also able to fluoresce; emitting absorbed light at a longer wavelength with a loss of energy. Mazel et al. (2003) reported that in 19 species of Caribbean coral, green fluorescent protein (GFP) absorption, emission, and reflection are trivial in the context of the internal coral light environment and that solar radiation is neither reduced nor enhanced by their presence. Gruber et al. (2008) found that on average, only 60.9% of symbiont and FP surface area co-occurred. In another study, red FPs (RFPs) were found in conjunction with a greatly reduced concentration of symbionts in diseased sections of *Porites compressa*, suggesting that RFPs are either poor at photoprotection or not associated with photoprotection at all (Palmer et al. 2009). More recent work, however, looked specifically at CP ability to protect algal symbionts *in vitro* from excess light and found that Chl *a* excitation at peak CP absorbance is reduced up to 55% in the presence of the CPs (Smith et al. 2013). Since FPs and CPs are not exclusive in their presence in coral epithelia, and since these pigments have several possible functions, it is conceivable that FP and CP functions vary among different distantly related and/or

ecologically distinct coral species. Determining the location of these pigments in the coral epithelia may thus provide more clues about their functions.

Constitutive photoprotective pigments (diadinoxanthin/dinoxanthin; β,β-carotene) of the zooxanthellae prevent excess light energy from reaching the chlorophyll a (Chl a) reaction centers where it may cause damage to Photosystem II (PSII). These pigments absorb light energy at the same wavelengths as the photosynthetic pigments they protect. Coral host pigments may supplement that protection by absorbing light energy before it reaches the zooxanthellae. The absorbance spectra for green and cyan FPs, like diadinoxanthin, coincide with Chl a absorbance—particularly in the violet and blue regions of the photosynthetically active radiation (PAR) spectrum—but RFP and CP spectra do not overlap with Chl a; rather, they are complementary (Dove et al. 1995). RFPs and CPs absorb maximally in the ~560–590 nm range (yellow), which coincides with the part of the PAR spectrum where Chl a absorbance is minimal. RFP and CP absorbance range is also out of sync with Peridinin, the high-efficiency accessory pigment that transfers light energy to Chl a reaction centers. Peridinin absorbs maximally at ~480 nm with a broad shoulder to ~540 nm (Johnsen et al. 2011).

Under light saturating conditions, photosynthetic machinery commonly becomes damaged and photosynthetic performance drops (Takahashi et al. 2010; Takahashi and Badger 2011; Karim et al. 2014). Throughout the course of the day, a varying fraction of photosystems will be functional while others may be under repair. Like photosynthesis, repair occurs continuously and is strongly induced by blue light with induction weakening with increasing light wavelengths (blue to green to red; Nixon et al. 2010; Valle et al. 2014). Photodamage may be caused by excess light energy from all wavelengths of the PAR spectrum but ultraviolet (UV) and yellow light have the highest potential to cause damage (Takahashi et al. 2010). Damage first occurs in the oxygen evolving complex of PSII and subsequently results in the breakdown of the large D1 protein subunit, which requires *de novo* synthesis (Ohnishi et al. 2005; Hakala et al. 2006; Zavafer et al. 2015). This requires time and energy that could otherwise be used for photochemistry.

Under low light conditions, i.e., in the mesophotic zone, shaded regions of colonies, or colonies growing under overhangs, FPs are believed to aid coral by absorbing more of the sparsely available light energy and transferring it to the Chl a reaction center (Salih et al. 2000). Similar to antenna pigments, this could occur via resonance energy transfer (Taiz and Zeiger 2010). Resonance transfer of light energy requires pigments to be at distances relative to the Ångström scale (0.1 nanometers) and held in stable harvesting complexes. To accomplish this, coral host pigments would necessarily reside in the gastrodermis with the zooxanthellae but this is not likely close enough. Furthermore, Roth et al. (2015b) found that corals with and without FPs had similar photosynthetic outputs making it unlikely that FPs contribute to photosynthesis in a significant manner.

FP and CP Location

For FPs and CPs to function as photoprotectors and/or photo-enhancers, they must be present in sufficient quantities and be strategically located relative to the location of the zooxanthellae. Theoretically, for FPs and/or CPs to "screen" zooxanthellae from harmful excess solar radiation, the pigments must be physically located between the source of light energy and the symbionts, i.e., such as in the coral epidermis, to intercept select wavelengths. To enhance light energy in low light conditions through lower wavelength energy transfer to zooxanthellae, they must be in exceptionally close proximity. In several studies, the location of FPs has been reported to be above, below, and among the zooxanthellae and in densely packed aggregates in anatomical structures (Salih et al. 1997). They have been reported in the epidermis of the Caribbean coral *Montastraea cavernosa* (Mazel et al. 2003), and in the epidermis of diseased sections of *P. compressa* (Palmer et al. 2009). Gruber et al. (2008) found strong targeting of FPs in body parts, i.e., oral disc, tentacles, and along septa or septo-costae, resulting in highly patterned morphologies. The reported locations of FPs support the likelihood that they may function as photoprotectors or photo-enhancers despite some of the photo-physical evidence arguing against these functions. Notably, the location of CPs in coral epidermis has not been definitively determined.

FPs and CPs in Hawaiian Corals

Hawaiian reefs have low coral diversity compared to other areas of the Pacific but have a relatively large number of coral species with visible pink, blue, or purple pigmentation. Host pigment fluorescence is assumed to be present in Hawaiian species, but little information is available on this topic. This section of the investigation aims to elucidate the general type (color) and location of constituent host fluorescent and non-fluorescent proteins in local Hawaiian corals from Kāneʻohe Bay. The corals chosen for this investigation are common in the bay, range in polyp size from minute to small (<1 mm^2) and reside in areas of reef with variable water flow regimes. All were collected from shallow reefs no deeper than five meters.

Porites compressa Dana is the most common species in Kāneʻohe Bay (Maragos 1972; Jokiel 1991; Veron and Stafford-Smith 2000). It forms large thickets that dominate many of the patch reefs. Colonies grow large with tissue-covered individual "fingers" that often fuse. *P. compressa* polyps are very small (~ 0.6 mm^2 in diameter) and are tightly spaced with shared walls and a well-defined columella. This species expresses RFPs during infection or during stress (Palmer et al. 2009) but it is unknown if they produce other host pigments as part of their inventory.

Montipora flabellata Studer is an encrusting coral that commonly forms long, thin protrusions around shrimp tubes that extend upwards from the colony. Colony sizes in Kāneʻohe Bay range from a few centimeters to a few meters in any given direction and can form plates and whorls (ARD pers. obs.) It is the fifth most common coral in the state of Hawaiʻi (Coral Reef Assessment and Monitoring Project) and is found in shallow water with high wave motion and water flow and/or surge. Polyps are minute (~ 0.3mm^2 diameter) and may be sparsely or densely placed along the surface, and randomly interspersed with bumpy to smooth papillae that may fuse to form ridges. *M. flabellata* host pigments are grossly visible and range in color from purple to blue depending on location. In Kāneʻohe Bay, *M. flabellata* tends to have a uniform purple appearance that becomes more intense in the warmer months (ARD pers. obs.).

Montipora patula Verrill is an encrusting coral that is morphologically similar to *M. flabellata* with the exception of the polyp/papillae structure. Unlike *M. flabellata*, papillae tend to form around the polyps providing higher definition for the polyps that often appear as a raised column. Polyps are minute (~ 0.4 mm^2 diameter) and may be brown and indistinguishable from the papillae and tissue-covered coenosteum, the area between polyps. In other individuals, the polyps may be purple and in contrast to the rest of the brown-colored colony. This purple polyp patterning makes it easily distinguishable from *M. flabellata* and is the only local species known to possess CPs in discreet clusters. *M. patula* is fairly common at sites with medium to high water flow and, like *M. flabellata*, has been observed in Kāneʻohe Bay with similar plating morphology and growth around shrimp tubes (ARD pers. obs.).

Leptastrea purpurea Dana is an encrusting coral that tends to thrive in more eutrophic conditions with lower water flow than *P. compressa* and the Montiporid corals previously described. Often found growing on rubble in sand, colonies are generally small and rounded, approximately 5–7 cm^2, and polyps are considerably larger than those of the other species (~1–2 mm^2). Colonies have well-defined septo-costae that appear white or pale brown with darker tones within the calices. Green fluorescence is often visible inside and around the polyp even in high ambient light.

The functions of FPs and CPs are likely constrained by their locations within the coral epithelia. To determine the probability of certain previously proposed functions, I employed the use of laser scanning confocal microscopy to locate cyan, red, and green fluorescent proteins. The location of Chl *a* fluorescence was also identified to provide a visual map of the coral epithelia since Chl *a* is present in the zooxanthellae and symbiont position in the coral is known.

It was hypothesized that to serve a photoprotective role, the FPs and CPs would necessarily reside in the coral epidermis, which is physically situated above the zooxanthellae-filled gastrodermis. Confocal microscopy was used to characterize the FP constituents and locations. Z-stack scans provided 3-D recreations of small regions of the coral that could be viewed from all planes and could be clipped at any

slice within the plane. In this manner, depth measurements could be taken and location of the FPs relative to the location of known physical coral structures (e.g., polyps, septo-costae, oral disc) could be determined. Importantly, it was possible to determine whether the FPs were stacked above, below, or within other FPs or Chl *a* (zooxanthellae). The Chl *a* was used as a known locator to better understand the structure of the coral. Because zooxanthellae reside in the gastrodermis, any visible fluorescence that stacks above the Chl *a* would be evidence of FPs in the epidermis. For the purpose of this investigation, epidermis of coenenchyme is separate from that of the polyps and tentacles. Septo-costae or any other areas where FPs were found are discussed separately (Fig. 2.1).

Methods

Coral Fragment Collection

Four species of scleractinian coral—*Montipora flabellata*, *M. patula* (preferentially, colonies with purple polyps), *Leptastrea purpurea*, and *Porites compressa*—were collected for this study (Table 2.1). Two small fragments (0.5–1.5 cm^2) were collected from separate areas of randomly chosen colonies using hammer and chisel. Samples were collected from fourteen sites in Kāne'ohe Bay ranging from as far north as patch reef (PR) 51, near the shipping channel, to PR14 near the Sampan Channel (Fig. 2.1). Every effort was made to collect specimens from each species evenly throughout the range and from similar light habitats, particularly in the 1–5 m range of reef flats. Similarly oriented, flat regions were targeted (when possible) to minimize variability in symbiont density. Because *Montipora flabellata* is only found in high water flow areas, fringing or south bay reefs were not included in the collection sites.

Once fragmented, specimens were placed in individually-labeled Whirl-paks (Nasco, Atkinson, WI) underwater and were transferred to a seawater-filled cooler on the boat. On return to the Coral Reef Ecology Lab at the Hawai'i Institute of Marine Biology (HIMB), samples were labeled with waterproof paper adhered to tissue-free undersides with reef-safe superglue (Bulk Reef Supply, MN, USA), and placed in a 660-liter, seawater flow-thru mesocosm covered with a 70% shade cloth. Three collection dates from April 30 to June 4, 2018 provided a realistically small window of time to collect comparable data for 96 fragments from 48 total colonies of corals (12 colonies per species).

Confocal Laser Scanning Microscopy

Prior to imaging the samples for data collection, a trial was conducted on several spare fragments of each species to determine the correct settings best used for all. All confocal imaging was done on a Zeiss LSM 710 laser scanning confocal microscope with LSM Zeiss Zen Black software 2011 version. First, excitation lasers and emission ranges were chosen and assigned artificial colors to provide data and visualization on the fluorescence present in each sample, including chlorophyll *a* fluorescence at room temperature. The excitation laser selections were as follows: 405 nm, covering 414–474 nm range and colored blue, 488 nm covering 494–553 nm range and colored green, and 561 nm covering 568–702 nm range and colored red. These artificial colors were chosen to represent emitted fluorescence in those ranges for intuitive visualization since cyan fluorescence tends to have maximum emission between 485-495 nm, green fluorescence max emission ranges from 500 to 524 nm, and red fluorescence has max emission ranging from 576-600 nm (Alieva et al. 2008). Chlorophyll *a* fluorescence in corals has a maximum emission around 685–690 nm (Mazel and Fuchs 2003; Mazel et al. 2003). Optimal values for master gain and laser power (for each laser), zoom, number of pixels (1024 x 1024), and pinhole were selected so that all samples could be visualized without excessive photobleaching while also minimizing noise. Master gain, which amplifies the signal without photobleaching, also amplifies the signal-to-noise ratio while laser power adds brightness for visualization but can bleach the sample. During the trial it was clear that not all coral species were able to be exposed to the same values of master gain and laser power without cellular damage, so the optimized values least likely to harm the most sensitive samples were determined and applied for all. The 405 nm laser was set to 28.0 power and 450 master gain, the 488 nm laser was set to 1.4 power and 350 master gain, and the 561 nm laser was set to 28.1 and 500 master gain. The pinhole was set to 1 Airy Unit (AU). These settings are denoted as Set1.

On day two, corals were transported in two buckets with approximately 3 gallons of seawater to the confocal laser scanning microscopy (LSM) facility at HIMB. Each fragment was inverted and placed into a 35-mm diameter glass bottom petri dish with a 14-mm diameter microwell of 0.17-mm glass thickness (MatTek Corp, Ashland MA) for optimal imaging. The dish was then placed on the stage in the climate-controlled environmental chamber of the microscope. The fluorescence in the sample was illuminated by selecting the Locate tab in the software, configured for fluorescence with the APO Calibration LSM (5x) objective and the green Long Pass (LP) filter for the mercury halide lamp. The flattest or most convex area of the sample was chosen for imaging to minimize excessive laser scanning time. Once in focus, the Live function button under the Acquisition tab was activated for a continuous scan of the sample. To collect data for the entire coral's epithelia, a z-stack was performed, which scans the sample in thin layers from the oral to the aboral surface. The Best Fit option was used for maximal

visualization, however this needed to be reset before beginning the z-stack scan. Scans were taken at intervals of 17.34 μm for all samples, but the number of slices depended on the thickness of the tissue and the rugosity of the fragment. While actively scanning the sample, the first and last slices of the z-stack were set by turning the focus knob until fluorescence could no longer be detected on the oral surface. The last slice was set by reversing the focus knob through the sample until the lowest layer of fluorescing tissue was no longer visible. Finally, in the Optimize Sectioning and Step panel, Optimal was selected for a 50% section overlap, and the Live scan was stopped. This procedure was followed for each coral fragment with z-stack scanning times ranging from three to ten minutes.

Post-Scanning Image Processing and Analysis

The output from z-stack scans visually reconstructs the coral epithelia in thin slices from oral surface to skeleton. It is a visual framework of the coral assembled by the location of the pre-selected fluorescence emission ranges and the colors assigned to represent them. Only those tissue structures with fluorescence appear in the z-stack visual representation of the scanned coral. All healthy, hermatypic corals have zooxanthellae in the gastrodermis of the surface and basal body walls. The known location of zooxanthellate Chl *a* fluorescence provides a structural framework to better understand the unknown location of coral host pigments. The first scanned slice captured any fluorescence present at the oral surface and the last slice captured fluorescence at the tissue interface with the skeleton. Image processing in Zeiss Zen Black software allowed z-stack scans to be viewed optimally. Several settings were first determined and repeated for all files (fragments), particularly, Threshold, the setting that balances the noise in the sample and pixel visualization. Threshold was set to a low 1.5, which allowed some noise in order to view detailed areas of fluorescence. Triangulation of files were set to the highest level of precision, which resulted in long image-mounting times but provided a more precise, pixel-by-pixel view of the file. Once mounted, 3-D representations were oriented to top (surface) view and compared to 2-D versions to measure polyp size. The flattest, most well-defined polyps were chosen for length and width measurements. The image was then rotated to view the coral cross section for tissue depth measurements. A minimal and maximal depth measurement was recorded. Image capture was done for surface view and half view (halfway through the X-Y plane), a side view with all colors represented, a side view with red fluorescence blocked, and a clipped internal view on the X-Z or Y-Z plane. Presence of cyan and green fluorescence was recorded, and an attempt was made to define their locations within the visible structure. When fluorescence was found in strongly defined color blocks, measurements of their minimal and maximal depth (Z-plane) were recorded as well as measurements of depth within the structure (as

determined by red fluorescence). It was not possible to measure scattered pixels. Finally, a photographic representation of the 2-D scan was archived (Fig. 2.2).

During image analysis, it was noted that while impossible to tease out the different locations of red host (575–609 nm; Alieva et al. 2008) and Chl *a* fluorescence (~688 nm), it was potentially important. To address this concern a small subsample (8 fragments, 2 from each species, 8.3% of total) from the second- and third-collection dates were re-scanned with most of the original settings but with different laser excitation wavelengths; 488 nm, 561 nm, and 633 nm. The 488 nm laser was colored green and detected an emission range from 493–556 nm, the 561 nm laser (pink) detected emission in the 563–631 nm range, and the 633 nm laser (red) detected emission in the 639–701 nm range. These settings are denoted as Set2. Detection of cyan fluorescence was necessarily omitted (only three lasers possible at a given time), the green fluorescence range remained nearly identical to the previously described scans, but the red and the Chl *a* fluorescence were separated to provide distinct visualization of both. Analysis on these samples was conducted as outlined above. All data were imported into JMP Pro 13 and graphs were created using a binary choice for presence (=1) or absence (=0).

Results

Fluorescent Proteins (FPs) in the Epidermis

With the exception of one fragment each of *Montipora patula and M. flabellata*, none of the specimens exhibited FPs in the epidermis when lasers were in initial settings (Set1) to emit cyan (CFP), green (GFP), and red/chl *a* fluorescence (n=24 per species). CFPs were found sparsely dispersed throughout the epidermis of *M. patula*, and GFPs sparsely dispersed in *M. flabellata* epidermis. When the lasers were changed to separate out the red FPs from Chl *a* emission (Set2), three of the four species appeared to have RFPs in the epidermis (n=2 per species); *M. flabellata*, *M. patula*, and *P. compressa*. Only *L. purpurea* did not have RFPs in the epidermis, although it should be noted that they were present in the septo-costae of *L. purpurea*, which is likely in the epidermis, but the lack of zooxanthellate Chl *a* in that region makes it difficult to determine definitively (Fig. 2.3). Additionally, CFP rod-like structures extended above the Chl *a* clusters in ~70% of samples and will be discussed further. It is unclear what these structures are.

FPs in Septo-costae

Leptastrea purpurea is unique among the four species investigated because it has relatively large polyps and well-defined ridges between the shared walls, thus the term septo-costae is here used. These so-called septo-costae are highly visible between the polyps because they appear unpigmented and are well organized. *Porites compressa* has shared, well-defined walls that are less broad than those of *L. purpurea* (Fig 2.2a).

In *M. flabellata*, the septo-costae are neither uniform nor well-defined. In *M. patula*, the papillae directly surrounding the polyps take a form similar to a corallite but septo-costae in this species are also not well-defined. The term septo-costae as it refers to these two montiporids is less rigid in definition, referring simply to the skeletal structure directly surrounding the polyp (Fig. 2.2b).

CFPs were not found in the septo-costae of any of the species but GFPs were prominent in 18 of the 24 samples of *L. purpurea* (Fig. 2.4). As expected, Chl *a* fluorescence was ubiquitous in the montiporids and *P. compressa*, whereas only *L. purpurea* (n=2) and *P. compressa* (n=1) had RFPs as visualized from Set2 scans. Notably, the one *P. compressa* fragment with RFPs had a *Trematodiasis* lesion (Palmer et al. 2009) with copious RFPs visible during the LOCATE phase of the confocal scan process. The lesion was avoided to the extent possible for the z-stack scan, but it was apparent that the RFPs extended in all directions several millimeters beyond the edges of the lesion (Fig. 2.5).

FPs in Tentacles

Zooxanthellate Chl *a* was present in all of the species' tentacles as shown in the 2-D images (Fig. 2.2) as well as in the z-stack scans. CFPs were present in the tentacles of three species; *L. purpurea*, *M. flabellata*, and *M. patula*, while GFPs were present only in the montiporids, and only one *M. patula* sample, in particular. RFPs from the Set2 scan were found in *L. purpurea* and *M. flabellata* tentacles only (Fig. 2.6).

The type of image that is produced from the z-stack scan does not show high definition of the structures that are artificially colored, however, with knowledge of coral physiology and a view of FPs as they relate to the Chl *a* structures, it is possible to make an educated guess. That is the case with the FPs that are found around the oral disc, the tentacles, and the mesenteries/gastrovascular cavity. Tentacles may be retracted and thus in some cases it is difficult to determine with great confidence whether FPs are in the tentacles, the highly infolded mesenteries, mesenterial filaments, or surrounding the gastrovascular cavity. It is clear that most of the FPs in the four species tend to cluster around the polyps, and in *L.*

purpurea in particular, patterns form around the oral disk, the peristome, and mesenteries/gastrovascular cavity. These patterns suggest a highly targeted function in these areas only, which is not entirely consistent with a photoprotective role.

FPs in Mesenteries/Gastrovascular Cavity

Leptastrea purpurea and *Montipora patula* were the only species that had FPs in what appeared to be the mesenteries or gastrovascular cavity (Fig. 2.7). In *L. purpurea*, GFPs were visible from the surface and from within when clipped in the x-y plane (Fig. 2.8a). Moving through the clipped plane, it was possible to see that the CFPs and GFPs lined the cavity (Fig. 2.8d). In a 2-D run through the slices of one of the *L. purpurea* specimens, mesenterial filaments were viewed extruded out of the mouth. No coral host FPs were present but the cnidoglandular band was heavily covered in Chl *a* fluorescence. In *M. patula*, none of the mesentery FPs were visible from the surface (Fig. 2.9a,b). CFPs and GFPs were present in the cavity area, but unlike in *L. purpurea* (Fig. 2.8d), they did not line the cavity and appeared to be densely dispersed throughout the mesenterial folds or in invaginated polyps (Fig. 2.9c, d).

Rod-like Structure CFPs

A feature of nearly all samples examined from all four species was the presence of CFPs in rod-like structures of unknown origin (Fig. 2.10). These generally extended towards the surface from the top of the Chl *a*/RFP layer in what appeared to be the epidermis. They may extend beyond the epidermis, but this was not clear since there was no structure that delineated the oral surface. In many cases these rod-like structures also embedded into the Chl *a*/RFP structures (gastrodermis) and in other instances may also have extended below. CFP rods appeared to be randomly placed and not associated with any particular skeletal or tissue structures. These structures were generally rod-straight and thin and are believed to be different from other CFP structures that were wavy or broken and sometimes found among the rod-like structures (Fig. 2.9b, d). These wavy CFP structures appeared to be external organisms or debris because when viewed in the 2D run, they were seen changing position and were captured by the scans at different horizontal and vertical positions. The appearance of these potentially exogenous objects or organisms was a common occurrence in all species, however, in *L. purpurea* they occurred less frequently than in all others and absence of these was more common than presence (Fig. 2.10). Given their ubiquitous nature, these structures may have an important influence on the corals and further investigation into their origin and function is warranted.

Discussion

If FPs and/or CPs are photoprotective, then they likely reside in the epidermis, above the zooxanthellae that they protect. The theory that these protein pigment complexes act as screens between solar radiation and the photosynthetic machinery of the coral's symbiotic algae formed the basis for the current investigation. The z-stack scans provided compelling evidence of FP location in the epidermis of the coenenchyme and polyps, particularly in *M. flabellata.*

The strongest signal of GFPs among the species was in *L. purpurea*. The GFPs in the broad ridges of the septacostae were prominent and likely located in the epidermis. The type of widespread, thick cover is consistent with a screening effect, however, there are no underlying zooxanthellae in the septo-costae along the ridges. Thinning at these ridges is consistent with histological sections where zooxanthellae are generally in lower concentrations but screening here would be limited to blocking light from reaching the highly reflective skeleton, potentially to minimize wavelength-specific multiple scattering (Enrıquez et al. 2005; Marcelino et al. 2013; Swain et al. 2016). This could benefit the algal symbionts, but the mechanism needs to be further investigated. Thick clusters of GFPs are also found around the peristome, and sometimes alternating with Chl *a*/RFPs in patches surrounding the oral disk. While interesting, this patterning does not specifically support nor counter the screening/photoprotection hypothesis.

Presence of the Novel CFP Rod-like Structures

Presence of the rod-like CFPs in the majority of the samples is intriguing yet inconclusive since their identification and function are unknown. They do not appear to associate reliably with the same skeletal or tissue structures but appear to be located in the epidermis and often extend deeper into the tissue. As observed during several 2D runs, they do not appear to be ingested food, nor do they seem to be mesenterial filaments. If these structures are endogenous, there still remains the issue of the highly-pigmented, straight, tubular structure. Randomly placed, rod-like structures are not consistent with the ability to screen zooxanthellae from solar radiation, although the wavelengths would be compatible with this task. Further investigation of these structures should be conducted to identify their origin and function(s), and whether they are unique to certain species or ubiquitous in corals. To that end, more targeted use of the confocal microscope and other spectral techniques, i.e., hyperspectral imaging, could be employed to produce a more complete visualization of the structures. Once we understand their origin, we can better determine their function.

The limitation of employing a maximum of three simultaneous lasers, combined with the need to visualize the symbiont's Chl *a* fluorescence for structural context, resulted in an incomplete view of the FPs present in a given sample. Testing two samples per species with a different laser configuration resulted in the understanding that RFPs are important and should be investigated further. Also important to better understand are the densities required to adequately carry out the proposed functions. The apparently low density of RFPs in the epidermis of *M. flabellata* did not seem adequate to screen the underlying zooxanthellae (Fig. 2.11) but thick clusters in the polyps may be more than adequate although they appear to be among the zooxanthellae, not above. Another possible explanation for the presence of RFPs in the epidermis is the CP ability to kindle—a photoactivation of the pigment that converts the non-fluorescent chemical structure to a fluorescent conformation (Chudakov et al. 2003; Verkhusha and Lukyanov 2004; Alieva et al. 2008). The second scan, Set2 (approximately three weeks post collection), yielded very strong RFP and stronger more widespread GFP signals for one particular specimen of *L. purpurea*, illustrating the high variability of FP expression in these corals (Fig. 2.12).

Conclusions

Fluorescent proteins were found in the epidermis in several species but not consistently, uniformly or in a way that would strongly support a conclusion that all FPs serve a photoprotective role in these Hawaiian species. They are, however, found in the tentacles and in other areas of the polyps where they could serve to protect these important structures. RFPs from Set2 scans were present at the tips of *L. purpurea* tentacles (Fig. 2.13b, d, f), which is consistent with a screening function, assuming the tentacles are fully extended. Oddly, and counter to the photoprotective theory, the tentacles folded inwards during the high-powered laser scans leaving the Chl *a*-packed undersides of tentacles exposed. If the tentacles retract entirely, the GFPs surrounding the peristome may in fact protect the zooxanthellae in the retracted tentacles. RFPs were also present in *M. flabellata* Set2 scan but the patterning is unclear. Given the information gathered from the confocal scans, it appears that photoprotection could be a function of FPs but is not likely the only function. The patterning found in *L. purpurea* is more consistent with an external communication function proposed by Gruber et al. (2008). The functions of FPs likely vary by species, light environment, and stress circumstances. It is clear that some FPs can absorb light energy that would otherwise be funneled to the Chl *a* reaction center of PSII, but whether they do that to the benefit of the zooxanthellae in corals is still a matter of debate.

Acknowledgments

References

Alieva NO, Konzen KA, Field SF, Meleshkevitch EA, Hunt ME, Beltran-Ramirez V, Miller DJ, Wiedenmann J, Salih A, Matz M V (2008) Diversity and evolution of coral fluorescent proteins. PLoS One 3:e2680

Bou-Abdallah F, Chasteen ND, Lesser MP (2006) Quenching of superoxide radicals by green fluorescent protein. Biochim. Biophys. Acta - Gen. Subj. 1760:1690–1695

Chudakov DM, Feofanov AV, Mudrik NN, Lukyanov S, Lukyanov KA (2003) Chromophore environment provides clue to "kindling fluorescent protein" riddle. J. Biol. Chem. 278:7215–7219

Dove S, Takabayashi M, Hoegh-Guldberg O (1995) Isolation and partial characterization of the pink and blue pigments of Pocilloporid and Acroporid corals. Biol. Bull. 189:288–297

Enríquez S, Méndez E, Iglesias-Prieto R (2005) Multiple scattering on coral skeletons enhances light absorption by symbiotic algae. Limnol. Ocean. 50:1025–1032

Gruber DF, Kao H-T, Janoschka S, Tsai J, Pieribone VA (2008) Patterns of fluorescent protein expression in Scleractinian corals. Biol. Bull. 215:143–154

Hakala M, Rantamäki S, Puputti EM, Tyystjärvi T, Tyystjärvi E (2006) Photoinhibition of manganese enzymes: Insights into the mechanism of photosystem II photoinhibition. J. Exp. Bot. 57:1809–1816

Johnsen G, Bricaud A, Nelson N, Prézelin BB, Bidigare RR (2011) In vivo bio-optical properties of phytoplankton pigments. In: Roy S., Llewellyn C.A., Egeland E.S., Johnsen G. (eds) Phytoplankton Pigments: Characterization, Chemotaxonomy and Applications in Oceanography. Cambridge University Press, New York, pp 496–537

Jokiel PL (1991) Jokiel's illustrated scientific guide to Kāneʻohe Bay. doi 10.13140/2.1.3051.9360

Karim W, Seidi A, Hill R, Chow WS, Minagawa J, Hidaka M, Takahashi S (2014) Novel characteristics of photodamage to PSII in a high-light-sensitive symbiodinium phylotype. Plant Cell Physiol. 56:1162–1171

Kawaguti S (1969) Effect of the green fluorescent pigment on the productivity of the reef corals. Micronesica 5:313

Maragos J (1972) A study of the ecology of Hawaiian reef corals. Doctoral Dissertation. University of Hawaii at Manoa

Marcelino LA, Westneat MW, Stoyneva V, Henss J, Rogers JD, Radosevich A, Turzhitsky V, Siple M, Fang A, Swain TD, Fung J, Backman V (2013) Modulation of light-enhancement to symbiotic algae by light-scattering in corals and evolutionary trends in bleaching. PLoS One 8:e61492

Mazel CH, Fuchs E (2003) Contribution of fluorescence to the spectral signature and perceived color of corals. Limnol. Oceanogr. 48:390–401

Mazel CH, Lesser MP, Gorbunov MY, Barry TM, Farrell JH, Wyman KD, Falkowski PG (2003) Green-fluorescent proteins in Caribbean corals. Limnol. Oceanogr. 48:402–411

Nixon PJ, Michoux F, Yu J, Boehm M, Komenda J (2010) Recent advances in understanding the assembly and repair of photosystem II. Ann. Bot. 106:1–16

Ohnishi N, Allakhverdiev SI, Takahashi S, Higashi S, Watanabe M, Nishiyama Y, Murata N (2005) Two-step mechanism of photodamage to photosystem II: Step 1 occurs at the oxygen-evolving complex and step 2 occurs at the photochemical reaction center. Biochemistry 44:8494–8499

Palmer C V, Mydlarz LD, Willis BL (2008) Evidence of an inflammatory-like response in non-normally pigmented tissues of two scleractinian corals. Proc. Biol. Sci. 275:2687–93

Palmer C V, Roth MS, Gates RD (2009) Red fluorescent protein responsible for pigmentation in trematode-infected *Porites compressa* tissues. Biol. Bull. 216:68–74

Prescott M, Ling M, Beddoe T, Oakley AJ, Dove S, Hoegh-Guldberg O, Devenish RJ, Rossjohn J (2003) The 2.2 A crystal structure of a pocilloporin pigment reveals a nonplanar chromophore conformation. Structure 11:275–84

Roth M, Padilla-Gamiño J, Pochon X, Bidigare R, Gates R, Smith C, Spalding H (2015a) Fluorescent proteins in dominant mesophotic reef-building corals. Mar. Ecol. Prog. Ser. 521:63–79

Salih A, Hoegh-Guldberg O, Cox G (1997) Photoprotection of symbiotic dinoflagellates by fluorescent pigments in reef corals. 217–230

Salih A, Larkum A, Cox G, Kühl M, Hoegh-Guldberg O (2000) Fluorescent pigments in corals are photoprotective. Nature 408:850–3

Schlichter D, Fricke HW, Weber W (1988) Evidence for PAR-enhancement by reflection, scattering and fluorescence in the symbiotic deep water coral *Leptoseris fragilis* (PAR=Photosynthetically Active Radiation). Endocytobiosis Cell Res. 5:83–94

Smith E, D'Angelo C, Salih A, Wiedenmann J (2013) Screening by coral green fluorescent protein (GFP)-like chromoproteins supports a role in photoprotection of zooxanthellae. Coral Reefs 32:463–474

Swain TD, DuBois E, Gomes A, Stoyneva VP, Radosevich AJ, Henss J, Wagner ME, Derbas J, Grooms HW, Velazquez EM, Traub J, Kennedy BJ, Grigorescu AA, Westneat MW, Sanborn K, Levine S, Schick M, Parsons G, Biggs BC, Rogers JD, Backman V, Marcelino LA (2016) Skeletal light-scattering accelerates bleaching response in reef-building corals. BMC Ecol. 16:10

Taiz L, Zeiger E (2010) Plant Physiology. 5th Edition. Sinauer, Massachusetts

Takahashi S, Badger MR (2011) Photoprotection in plants: a new light on Photosystem II damage. Trends Plant Sci. 16:53–60

Takahashi S, Milward SE, Yamori W, Evans JR, Hillier W, Badger MR (2010) The solar action spectrum of Photosystem II damage. Plant Physiol. 153:988–93

Valle KC, Nymark M, Aamot I, Hancke K, Winge P, Andresen K, Johnsen G, Brembu T, Bones AM (2014) System responses to equal doses of photosynthetically usable radiation of blue, green, and

red light in the marine diatom phaeodactylum tricornutum. PLoS One 9:1–37

Verkhusha V, Lukyanov KA (2004) The molecular properties and applications of Anthozoa fluorescent proteins and chromoproteins. Nat. Biotechnol. 22:289–96

Veron JEN, Stafford-Smith M (2000) Corals of the World. Australian Institute of Marine Science, Townsville MC, Qld, Australia

Zavafer A, Cheah MH, Hillier W, Chow WS, Takahashi S (2015) Photodamage to the oxygen evolving complex of photosystem II by visible light. Sci. Rep. 5:16363

Tables and figures

Table 2.1. Coral species collected by location with number of fragments in ( ). Patch reef numbers in top row in order by collection time (left to right). CRN = CRIMP Buoy North, CRW = CRIMP Buoy West, SBE = Sand bar East, SBS = Sand bar South. LP = *Leptastrea purpurea*, MF = *Montipora flabellata*, MP = *Montipora patula*, PC = *Porites compressa*.

Reef	51	50	43	35	42	30	29	26	23	CRN	CRW	SBE	SBS	14
	PC	MF (4)	MF(2)	LP(3)	MP	LP(2)	LP	LP(2)	PC	MP	MP	MP	MF(2)	MF
	MP	MP	MP			PC	PC	PC(2)	MP(3)	PC(2)	MF	PC	LP	MP
		PC	PC			MF	MP	MF				LP(2)		LP
														PC

Figure 2.1. Satellite map of Kāneʻohe Bay, Oʻahu from Google Earth. Collection sites marked with orange stars. Patch reef numbers and site codes in white. CRN = CRIMP Buoy North, CRW = CRIMP Buoy West, SBE = Sand bar East, SBS = Sand bar South.
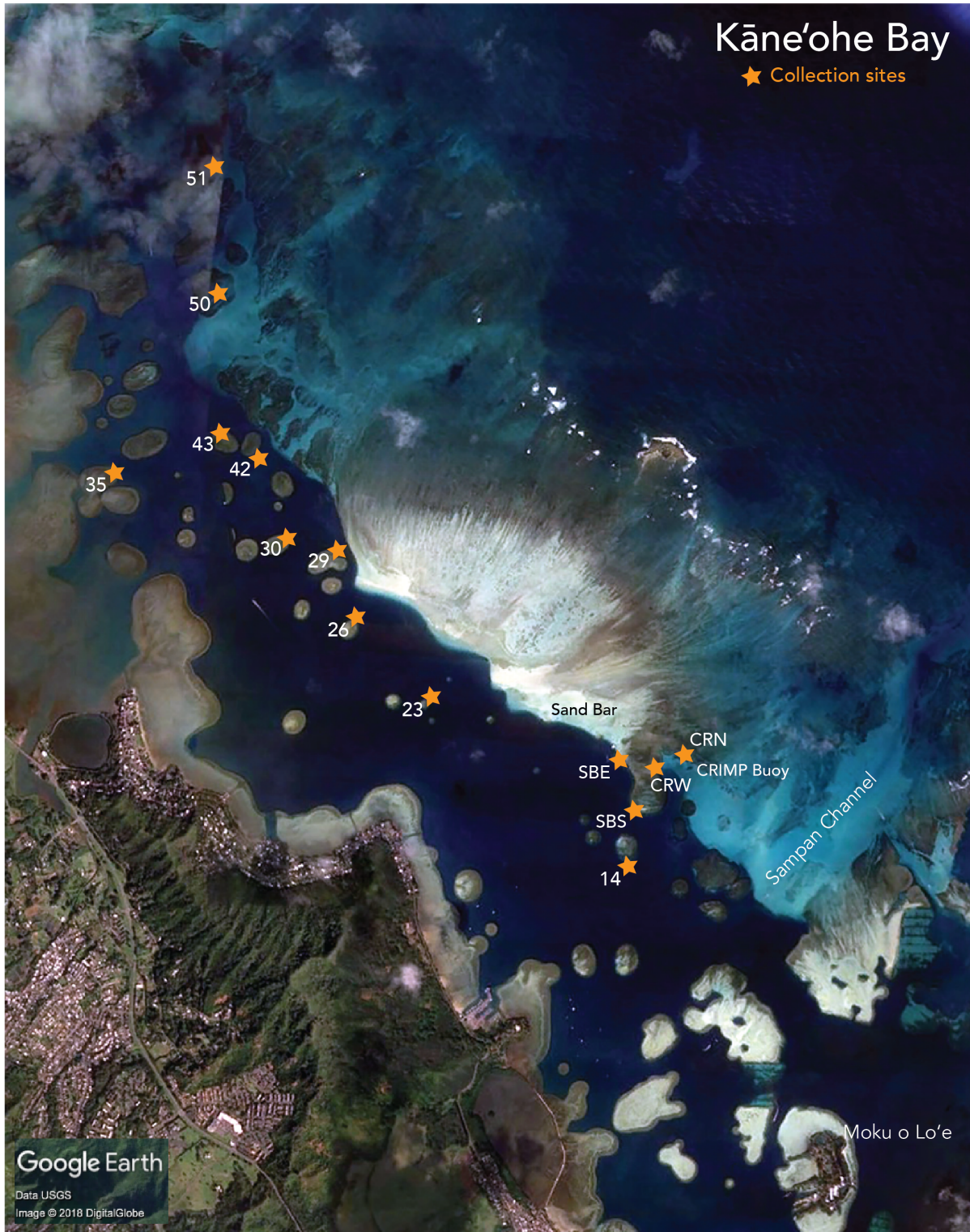
Figure 2.2. Confocal 2-D fluorescence image of four species of coral: (a) one large polyp of *Leptastrea purpurea* with in-folded tentacles, (b) several polyps of *Montipora flabellata* with tentacles well-defined in two, (c) numerous papillae of *Montipora patula* with tentacles visible in three polyps, (d) well-defined polyps of *Porites compressa* with many visible oral discs. Note overall red appearance representing Chl *a* fluorescence.
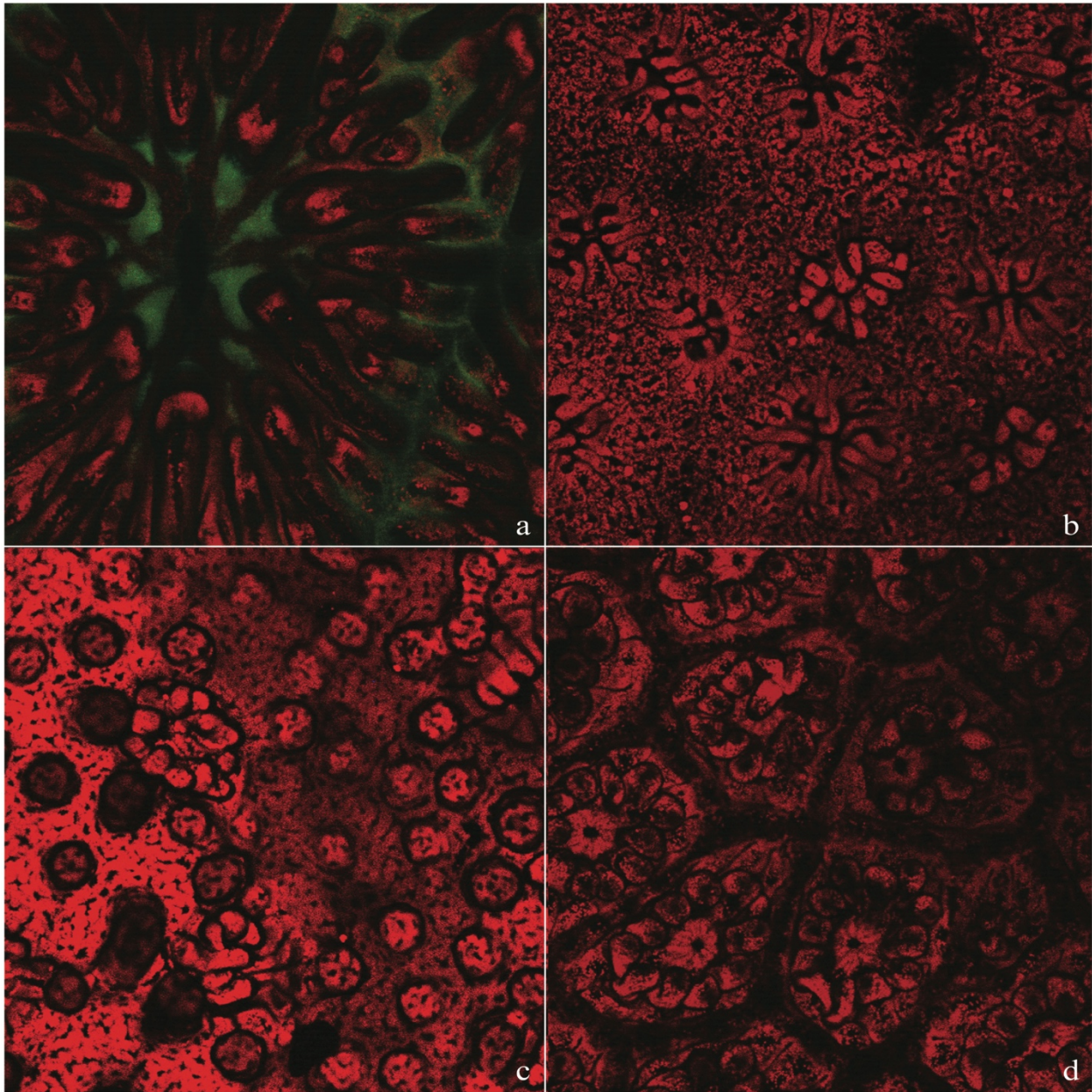
Figure 2.3. FPs in the epidermis of four coral species. LP=*Leptastrea purpurea*, MF=*Montipora flabellata*, MP=*Montipora patula*, PC=*Porites compressa*. CFP=cyan fluorescent protein, GFP=green fluorescent protein, Chl *a*/RFP=chlorophyll a/red fluorescent protein, RFP=red fluorescent protein. 1 = present, 0 = not present
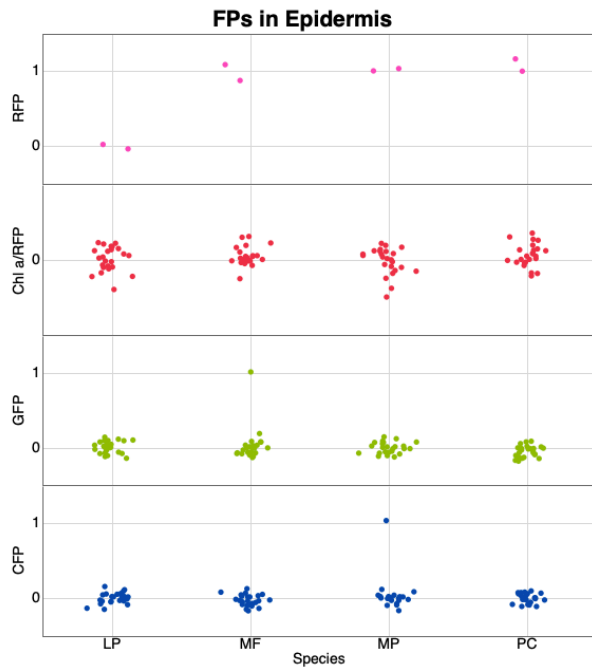
Figure 2.4. FPs in the septo-costae of four coral species. LP=*Leptastrea purpurea*, MF=*Montipora flabellata*, MP=*Montipora patula*, PC=*Porites compressa*. CFP=cyan fluorescent protein, GFP=green fluorescent protein, Chl *a*/RFP=chlorophyll a/red fluorescent protein, RFP=red fluorescent protein. 1 = present, 0 = not present
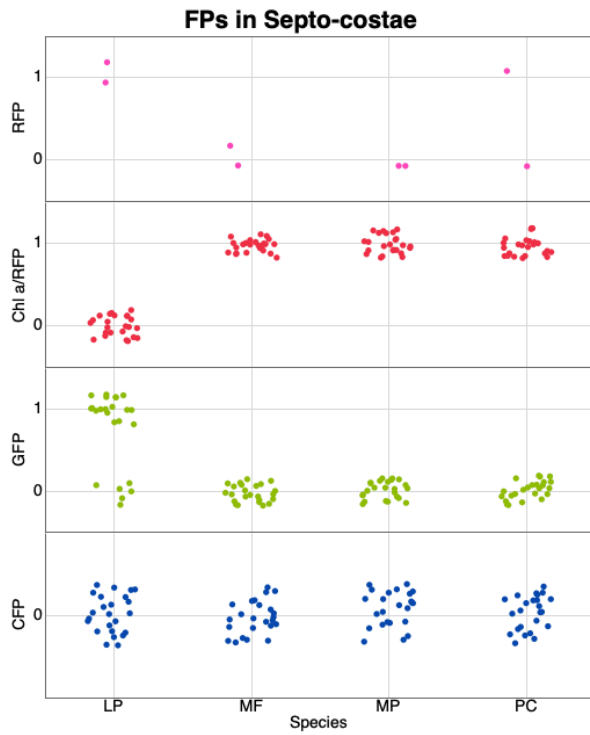
Figure 2.5. *Porites compressa* from Set2 scan with Chl *a* and RFPs separated. In (a) RFPs are pink in color on left side of 2-D image. Same view in image (b) top view of z-stack scan with pink pixels denoting where RFPs are located.
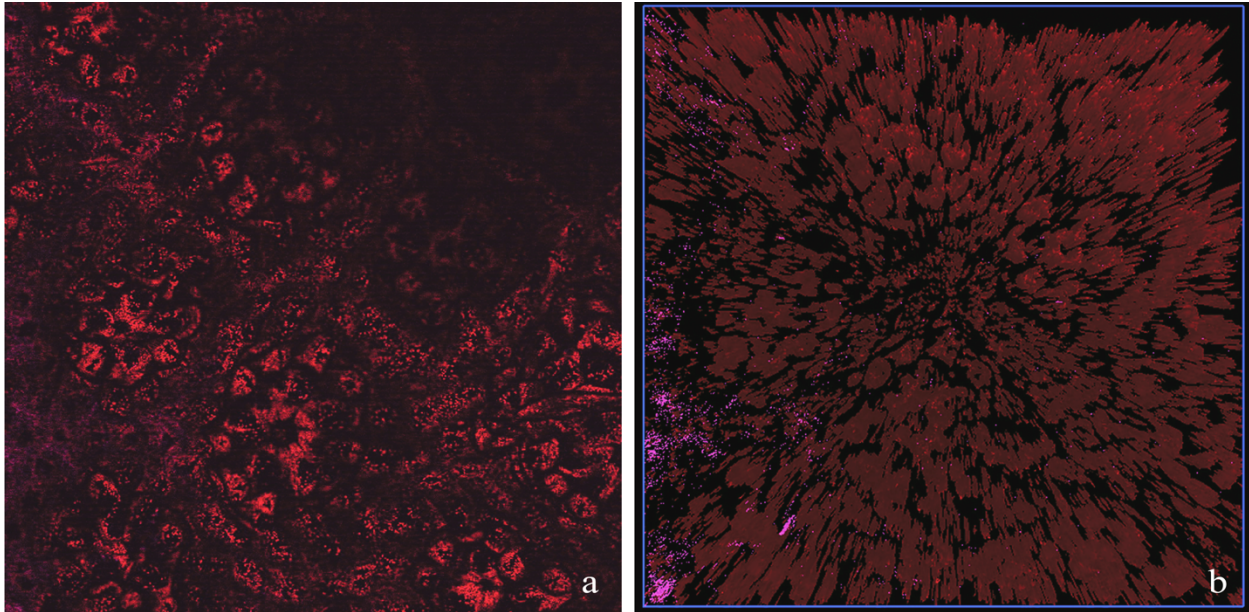
Figure 2.6. FPs in the tentacles of four coral species. LP=*Leptastrea purpurea*, MF=*Montipora flabellata*, MP=*Montipora patula*, PC=*Porites compressa*. CFP=cyan fluorescent protein, GFP=green fluorescent protein, Chl *a*/RFP=chlorophyll a/red fluorescent protein, RFP=red fluorescent protein. 1 = present, 0 = not present
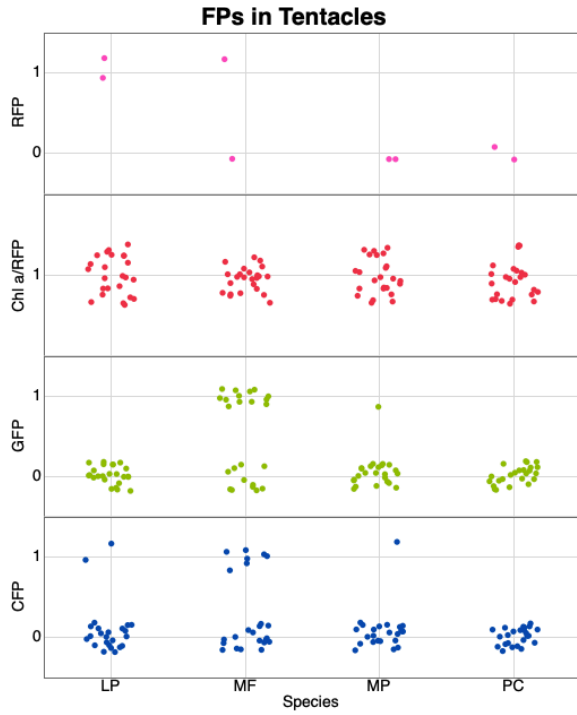
Figure 2.7. FPs in the mesenteries or gastrovascular cavity of four coral species. LP=*Leptastrea purpurea*, MF=*Montipora flabellata*, MP=*Montipora patula*, PC=*Porites compressa*. CFP=cyan fluorescent protein, GFP=green fluorescent protein, Chl *a*/RFP=chlorophyll a/red fluorescent protein, RFP=red fluorescent protein. 1 = present, 0 = not present
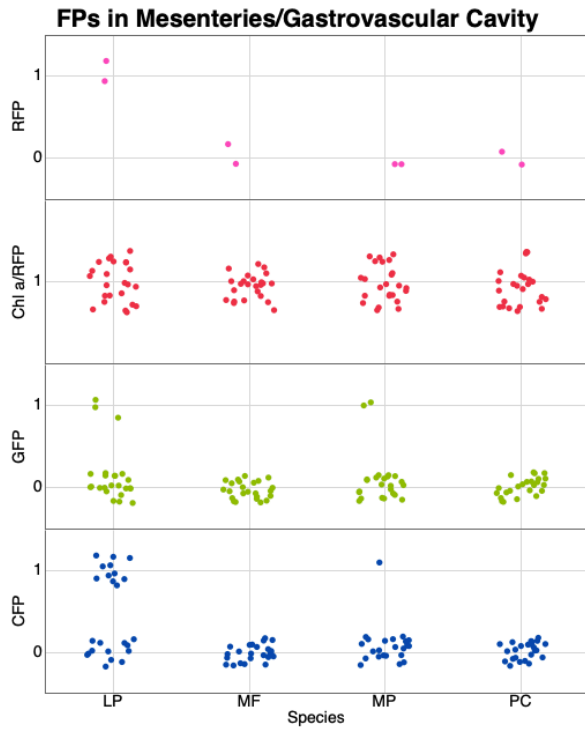
Figure 2.8. (a) 2-D scan of *L. purpurea* fragment showing details of polyp. (b) Z-stack top view scan, (c) z-stack view of X-Y plane, (d) z-stack view of clipped X-Y plane. Note blue rod-like structures extending from proposed oral surface.
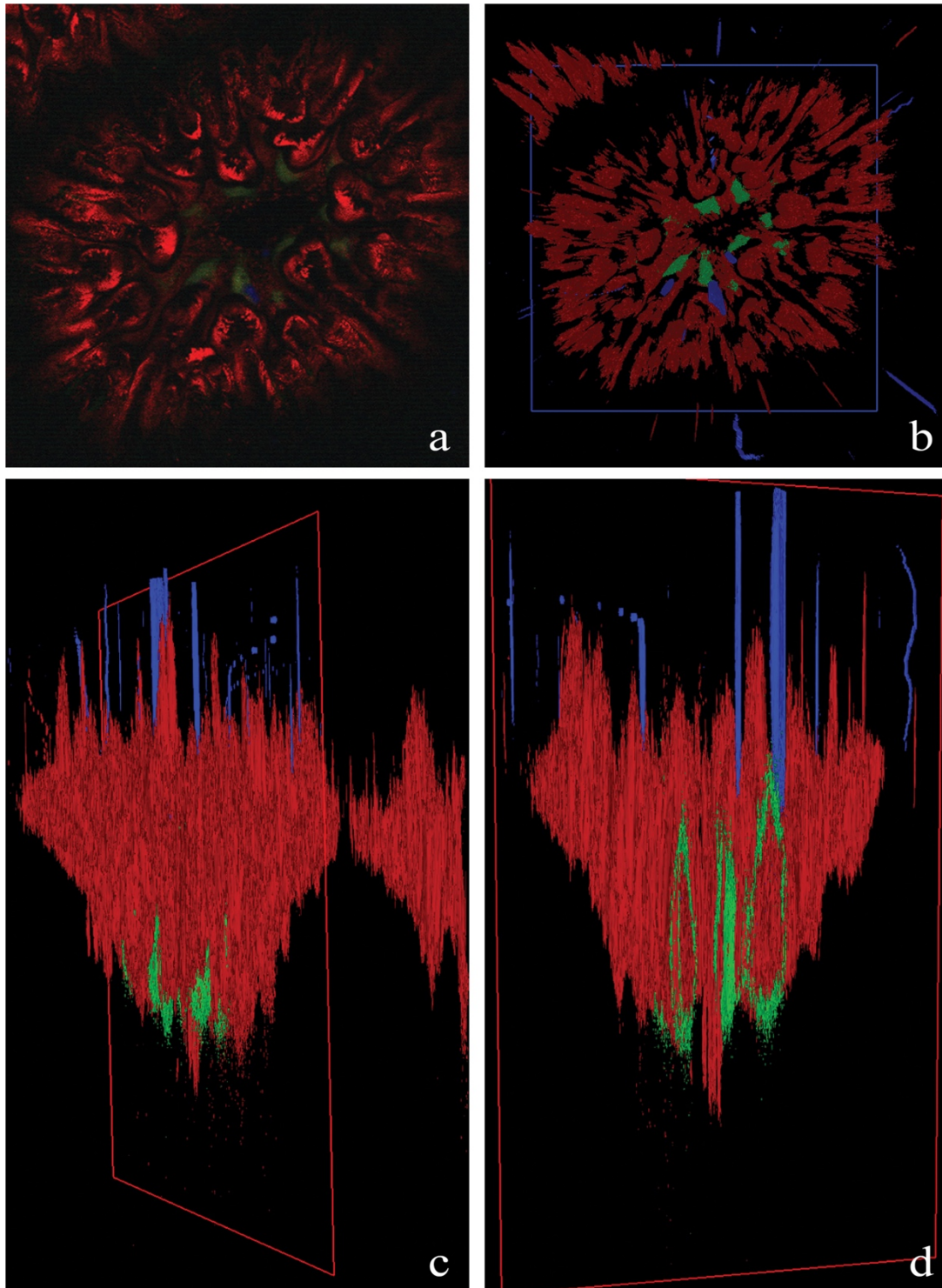
Figure 2.9. (a) 2-D scan of *M. patula* fragment showing surface details with one visibly outward polyp. (b) z-stack top view scan, (c) z-stack view of clipped X-Y plane with visible cavities, (d) z-stack view of X-Y plane with the Chl *a*/RFPs channel removed for visualization.
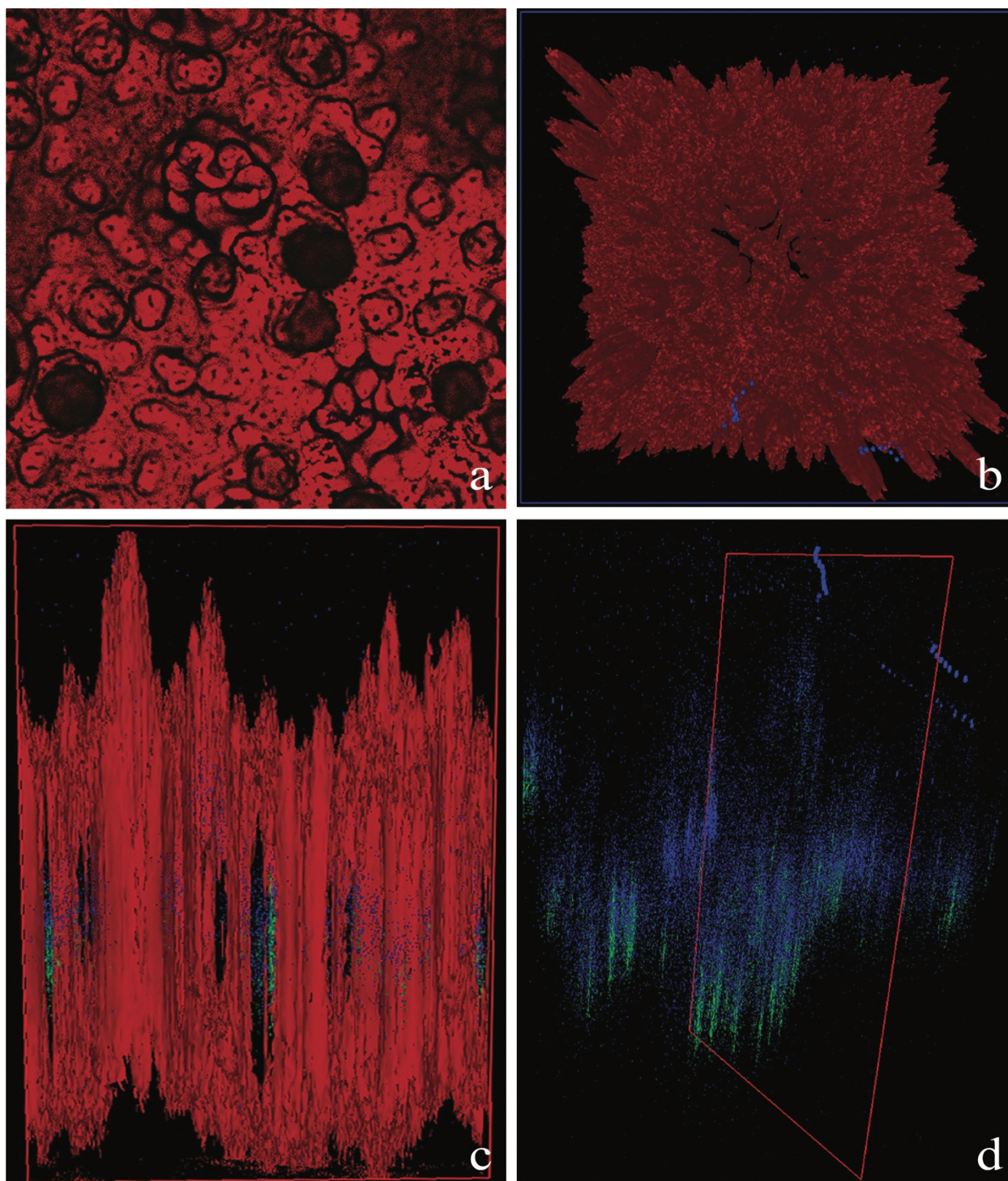
Figure 2.10. (a) Presence (= 1) and absence (= 0) of CFP rod-like structures in all species. (b) Distribution of structures by presence/absence. LP=*Leptastrea purpurea*, MF=*Montipora flabellata*, MP=*Montipora patula*, PC=*Porites compressa*. CFP=cyan fluorescent protein.
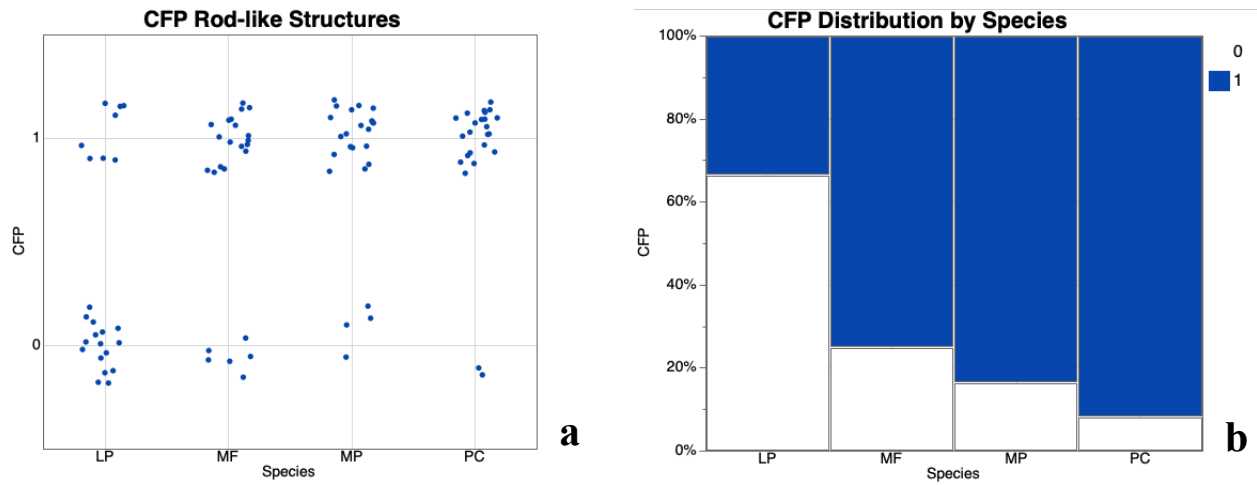
Figure 2.11. *Montipora flabellata* Set2 scan with differentiation between zooxanthellar Chl *a* and coral host red fluorescence. (a) 2-D image with visible red fluorescence (pink coloration) in the tentacles, (b) top view of z-stack scan, (c) z-stack scan of X-Y plane, (d) same scan with Chl *a* fluorescence emission hidden.
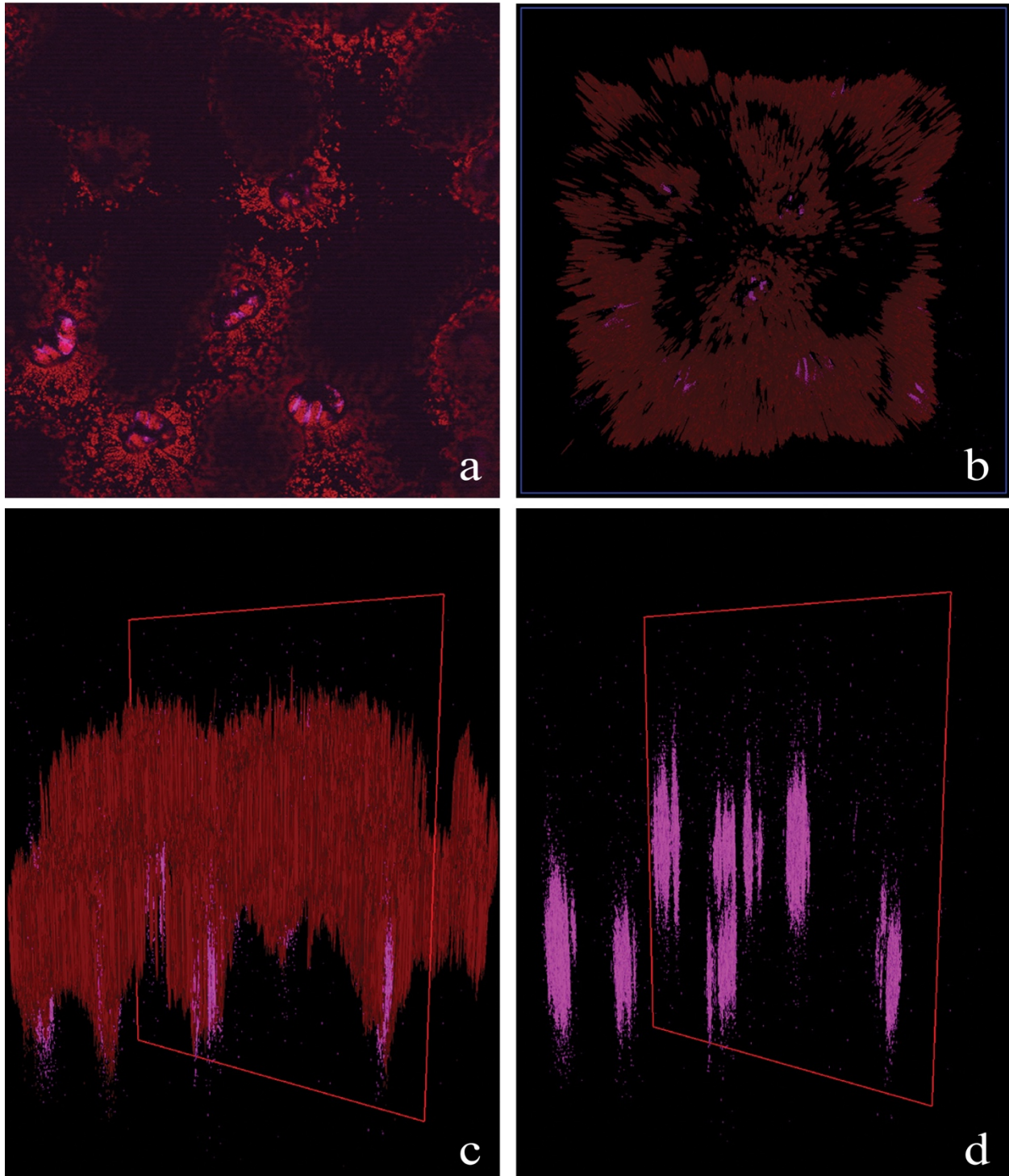
Figure 2.12. Scan of same *L. purpurea* fragment three weeks apart. (a) Set1 2-D image, (b) Set2 2-D image, (c) Set1 z-stack scan top view, (d) Set2 z-stack scan top view, (e) Set1 z-stack mid-way through cross section, (f) Set2 z-stack mid-way through cross section.
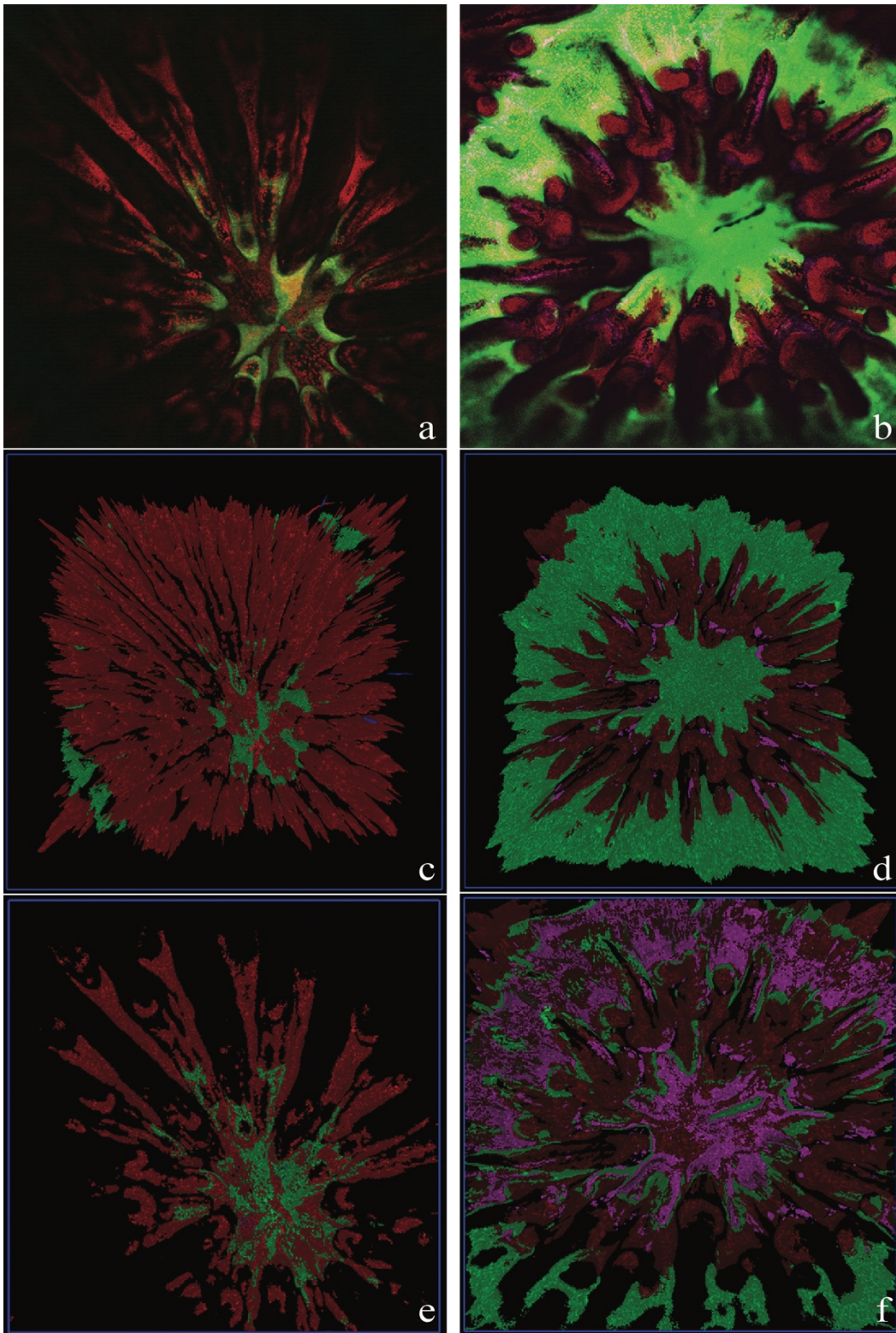
CHAPTER THREE

INVESTIGATING THE POTENTIALLY PHOTOPROTECTIVE ROLE OF CORAL HOST PIGMENTS IN THE PHOTOSYNTHETIC EFFICIENCY OF DINOFLAGELLATE SYMBIONTS

Angela Richards Donà

Abstract

The encrusting stony coral *Montipora flabellata* Studer is visually unique in Kāneʻohe Bay due to its striking, uniform purple coloration. Chromoproteins (CPs) are non-fluorescent coral host pigments responsible for the purple hue and are physically and functionally separate from pigments in the photosynthetic apparatus of their symbiotic algae (zooxanthellae). Dinoflagellate photosynthetic pigment functions have been well-characterized but the role(s) of CPs (or other similar fluorescent pigments) in host epithelia of Hawaiian corals have not yet been explored. It was determined in Chapter One of this dissertation that CPs are present in *M. flabellata* in thick sheaths at the surface of the epidermis where they have the potential to block harmful yellow light and minimize damage to the oxygen-evolving complex. This investigation sought to determine whether CPs have a direct effect on the photosynthetic efficiency of the coral endosymbionts in *M. flabellata* and three other common species in the Bay. The method was designed to be simple, pairing measurements from rapid light curves with spectral absorptance at the exact same location on the coral to determine whether there is a connection between pigment systems. A minimally invasive approach was undertaken to avoid destructive experiments on the numerous replicates needed for strong inference, and to allow further analyses with confocal microscopy. The precise and near simultaneous pairing of the photosynthetic and absorptance measurements aimed to decrease the variability in coral morphological structures and host and zooxanthellae pigment concentrations, thus allowing direct comparisons of the data. The hypothesis that CPs and/or FPs have a measurable effect on the photosynthetic efficiency of the symbiotic algal cells was tested in the four species using relative absorption at 574 nm paired with photosynthetic parameters F_v/F_m, ΔNPQ, ETR_{max}, and E_k in least squares regression with linear and polynomial fits. Results showed that all species had high absorption at 574 nm relative to the same wavelength in dinoflagellates alone, but this had no effect on any of the photosynthetic parameters in any of the species. These results do not support the hypothesis that CPs affect photosynthetic efficiency, however, the lack of correlation does not exclude the possibility that CPs are photoprotective. While inconclusive regarding the question of photoprotection, the method did provide a better understanding of the photosynthetic capabilities of the different coral species. *Montipora flabellata* colonies had some of the highest absorption values at 574 nm, and interestingly, low E_k (231.2 µmols photons m^{-2} s^{-1}) indicating this shallow water species reaches saturating irradiance early in the day and likely experiences the longest daily super-saturating photon flux densities of all species tested. This has great implications for the photophysiological health of this coral during bleaching events and helps to explain why *M. flabellata* is particularly vulnerable to increasing seawater temperatures due to global climate change.

Introduction

Hermatypic corals in the order Scleractinia are tropical, sessile animals that harbor microscopic algal cells for nutrient cycling and aid in calcium carbonate deposition. The coral tissue, specifically the gastrodermal layers of the surface and basal body walls, provides a highly efficient light-capturing environment for the algae. The algae—dinoflagellates from the order Symbiodiniaceae—fix inorganic carbon (primarily HCO_3^-) from the surrounding seawater through oxygenic photosynthesis. The mutualistic symbiotic relationship provides the coral host with up to 100% of its nutritional requirements (Muscatine et al. 1981, 1984) through the translocation of up to 95% of the photosynthate produced by the dinoflagellates (Falkowski et al. 1984; Muscatine et al. 1984; Davy et al. 2012). The importance of the symbionts (also termed "zooxanthellae") to the coral host cannot be overstated and several decades-worth of published research on the topic provide details of this multi-faceted relationship (Pearse and Muscatine 1971; Trench 1993; Wakefield et al. 2000, to name only a few). Separate from the symbionts, coral hosts produce colorful protein-pigment complexes that have drawn increased interest recently due to their prominence during bleaching events. In 2014, the uniformly-purple coral *Montipora flabellata* Studer was the first coral species to bleach in Kāneʻohe Bay. The extent of the bleaching (personally observed) was severe for this species and although unquantified, it was clear that a number of colonies were lost as a result of the event. The overarching theme of this investigation focuses on characterizing the functional role of the coral host pigments and in particular, chromoproteins (CPs) found in the coral species *M. flabellata* and *M. patula* Verrill. Several potential functions have been documented for these (and fluorescent pigments) in Indo-Pacific corals including immunity functions, colony growth enhancement, and photoprotection (Salih et al. 1997a; Palmer et al. 2009a, 2009b; D'Angelo et al. 2012; Smith et al. 2013). The vulnerability to bleaching *M. flabellata* has demonstrated has made the study of this coral species more imperative and challenging. As a result of tightened permitting for this species, small sample sizes and an effort to return as many samples to the reef as feasible, were part of the overall study design. For this reason, a non-invasive, minimally destructive approach to determining CP function was sought. This study employed the first instance of near simultaneous, paired spectral reflectance and photosynthetic performance measurements on corals to answer the basic question of whether CPs have an impact on the algal symbionts *in hospite*. The study was expanded to include a total of four common species (*M. flabellata*, *M. patula*, *Leptastrea purpurea* Dana, and *Porites compressa* Dana) in Kāneʻohe Bay for comparison as only two of the corals are known to produce CPs (*M. flabellata* and *M. patula*). The fragments used for these analyses were secondarily used for confocal microscopy and pigment location determination (described in Chapter Two of this dissertation). This pairing of physiological function in the zooxanthellae with the unknown coral pigment function may also shed light on the

potential for a photoprotective role. Implicit in the term *photo*protective is the concept that the coral pigments protect the algal cells. The primary goal for this protocol was to test the hypothesis that chromoproteins have a photobiological role in the coral holobiont and their presence in coral epidermis has a measurable effect on algal photosynthetic efficiency. The protocol was to be carried out with minimally invasive, non-destructive instrumentation and provide characterization of whole coral absorbance and photosynthetic performance parameters for correlation analysis in the four common Hawaiian coral species.

Coral Host Pigments – Chromoproteins and Fluorescent Proteins

Chromoproteins (CPs) are tetrameric proteins that envelope a non-coplanar chromophore (Prescott et al. 2003; Verkhusha and Lukyanov 2004) and are responsible for the uniform purple pigmentation of the Hawaiian coral *M. flabellata* and the purple polyps in *M. patula*. Red fluorescent proteins (RFPs) are highly similar with small conformation and sequence differences in the amino acid sequence motif (Prescott et al. 2003). Both have maximal absorbance peaks in the yellow region (560–590 nm) of the photosynthetically active radiation (PAR) spectrum. CPs also show absorbance in the ultraviolet radiation (UV-R) portion of the solar irradiance spectrum with maximum absorbance peaks at ~320–330 nm (Dove et al. 1995; Alieva et al. 2008). Efforts to characterize the pigments and determine their functions have yielded some important yet contradictory results. For instance, several investigators (Salih et al. 1997b, 2000; Dove 2004; Smith et al. 2013) have reported evidence in support of a photoprotective role for pigments that absorb maximally in this range. Others provide evidence against or reasons to question the putative photoprotective role (Dove et al. 1995; Mazel et al. 2003; Dove 2004; D'Angelo et al. 2008). For instance, Mazel et al. (2003) stated that evidence of photoprotection would entail a lowering of the chlorophyll *a* (Chl *a*) excitation at the corresponding range of CP absorption. Smith et al. (2013) tested this hypothesis and found up to 18% reduction in Chl *a* excitation in the CP absorption range. Considering that Chl *a* absorbs weakly in that region, a reduction in absorption may be trivial. D'Angelo et al (2008) found that CPs were not upregulated in response to increasing intensity in photon flux density (PFD), particularly when PFDs were higher than 400 μmols photons m^{-2} s^{-1}. Upregulation of photoprotective pigments would be a realistic response to high intensity, damaging PFD. Smith et al. (2013) provide the most compelling evidence to date for CP's photoprotective role, showing less photodamage in CP-pigmented corals than in those without CPs. They exposed two color morphs to orange light (595 nm maximum) for 12 hours each day for two days at 1000 μmols photons m^{-2} s^{-1} in addition to the 200 μmols photons m^{-2} s^{-1} under which they were grown. This acute treatment caused notable photodamage as measured by reduction in effective quantum yield ($\Delta F'/F_m'$). These

92

photophysiological measurements of quantum yield demonstrate a relationship between the presence of the pigments and photosynthetic performance but the approach was intentionally destructive and involved an unclear number of highly-stressed corals. The current study did not follow this destructive approach, rather, it was based on finding relationships between pigments and photosynthetic parameters in presumed-healthy corals. It is unclear whether a destructive approach is necessary to determine the validity of a photoprotective role in Hawaiian CPs.

Photosynthetic Pigments in Dinoflagellates

The dinoflagellate photosynthetic apparatus within chloroplasts contains various pigments that absorb light energy from the sun (in discrete packets called quanta or photons) and uses them to carry out photochemistry or photoprotection. The concentrations of these pigments vary depending on numerous factors, i.e., changes in irradiance due to season, depth, and water clarity; and salinity (Stimson 1997; Kuffner 2005; Apprill et al. 2007). Super-saturating solar irradiance conditions are common on reefs, particularly at shallow depth where PFD (number of photons per unit area) can range from ~300–1800 µmols photons m^{-2} s^{-1}. Zooxanthellae are adapted to the light fields associated with the depth of the host coral colony and their position within that colony (Iglesias-Prieto et al. 2004) and may acclimate to transient changes in the light field by increasing or decreasing pigment concentrations (Iglesias-Prieto and Trench 1994; Johnsen et al. 1994). The ability and time associated with acclimation varies by species, but light regimes at a given depth are relatively stable under normal conditions (Iglesias-Prieto and Trench 1994).

Chlorophyll *a* is ubiquitous in photosynthetic organisms and serves as both light-harvesting and special reaction center pigments. In dinoflagellates, Chl *a* peaks (and shoulders) of maximum absorbance are located at 440 and 420 nm, respectively, in the blue range of the PAR spectrum and shares peaks at 590, 625, and 635 nm with Chl c_2 in the red region (Fig. 3.1a, b). The photosystem II (PSII) reaction center Chl *a* has maximal absorbance in dinoflagellates at 675 nm (Johnsen et al. 1994; Johnsen et al. 2011). Chlorophyll c_2 and peridinin are both light-harvesting (antenna) pigments with the ability to pass light energy excitation via resonance transfer to other light-harvesting pigments and the Chl *a* reaction center pigments. Chlorophyll c_2 also shares a maximum absorbance peak at 460 nm with peridinin and diadinoxanthin (Fig. 3.1b; Johnsen et al 1994). Peridinin has broad absorbance with a maximum peak at 540 nm, which allows it to be highly efficient at absorption of excitation energy and transfer to the Chl *a* reaction centers. Peridinin concentration and light-harvesting pigment concentration in general, increases with decrease in light to maximize photon capture and photochemistry in low light conditions. Under high light conditions, photoprotective pigments increase with a concurrent decrease in light-harvesting

pigments (Johnsen et al. 1994). β, β-carotene is present in low concentration relative to the other pigments yet serves the important functions of photoprotection and radical oxygen species (ROS) scavenger (Johnsen et al. 1994; Apprill et al. 2007). Its broad absorption has dual peaks at ~450 and 480 nm, which coincide with most of the other pigment constituents. Xanthophylls Diadinoxanthin (DD) and dinoxanthin (DN) are photoprotective pigments and residents in protein complexes on the lumenal side of the thylakoid membrane involved in nonradiative dissipation of excess excitation energy or NPQ (Jeffrey and Haxo 1968; Iglesias-Prieto and Trench 1997; Brown et al. 1999). The relative concentrations of DD and DN are determined by the presence or absence of light. DD concentration is highest in dark-acclimated cells and is activated upon buildup of protons in the thylakoid lumen. The xanthophyll cycle (XC) entails the conversion of monoepoxide DD to the di-epoxide DN with the aid of associated enzymes within seconds upon application of light. Thus, the relative concentrations of these photoprotective pigments are in constant flux. Diadinoxanthin/dinoxanthin have broad absorbance in the blue portion of the PAR spectrum with peaks at ~450 and ~480 nm (Roy et al. 2013).

In photochemistry, the basic mechanistic function of antenna pigments in light-harvesting complexes of photosystem II (LHCII) is to absorb photons and transfer the energy to the Chl *a* reaction centers. To transfer energy, the range of absorption of the donor pigment must overlap with the absorption potential of the acceptor pigment. This fundamental physical requirement explains why absorbance spectra (Fig. 3.1b) have numerous overlapping peaks and shoulders in the blue to green regions of the PAR spectrum. Energy is transferred, from higher to lower energy wavelengths, to the Chl *a* special pair, which absorbs maximally at 675 nm in dinoflagellates and is clearly recognizable as a solitary peak in the far-red portion of the PAR spectrum. Light energy decreases with increase in wavelength, thus absorbance in the blue portion of the PAR spectrum (~420–480 nm) is optimized by antenna as well as photoprotective pigments allowing greater flexibility for transfer or heat dissipation.

Although zooxanthellae are adapted to the light regime associated with their host colony's position on the reef, PFD can nevertheless be supersaturating and damage to PSII commonly occurs. Damage to the photosynthetic apparatus in plants and algae manifests first in the breakdown of the manganese cluster of the oxygen-evolving complex (OEC) from direct photoexcitation of manganese. (Hakala et al. 2005; Ohnishi et al. 2005; Tyystjärvi 2008; Takahashi et al. 2010; Takahashi and Badger 2011; Karim et al. 2014). The OEC is responsible for supplying replacement electrons to RCs in PSII. When the OEC is damaged, PSII RCs are left devoid of electrons, shutting down electron transport, while promoting long-lived excited states of Chl *a,* which further promote the creation of ROS. Eventually, the very large D1 protein in PSII breaks down and must undergo *de novo* synthesis. Overall effects of this damage to photosynthesis depend on the balance of damage and ROS vs. ongoing repair (Takahashi and Badger 2011). Until recently it was believed that excess light energy reaching RCs (via antenna pigments)

caused photodamage, however, it is now clear that light *intensity*, specifically, light in the UV and yellow region (~550–600 nm) of the PAR spectrum are responsible and reduction in overall light energy will actually slow repair and hinder ROS scavenging (Tyystjärvi 2008; Takahashi et al. 2010; Takahashi and Badger 2011). Given that chromoproteins absorb light energy in the UV and yellow region of the PAR spectrum, these pigments could function as a screen to protect OECs from these wavelengths and avoid direct photoexcitation and subsequent damage to PSII D1 protein.

Photosynthetic Parameters from Pulse Amplitude-Modulated Fluorometry (PAM)

PAM fluorometry is a commonly used method for measuring parameters of photosynthesis in land and aquatic plants and algae. The use of PAM for corals is less common and more complicated due to heterogeneous surface and internal skeletal morphologies, inherent tissue absorbance, and varying thicknesses of the coral epithelia. The effects of these complications can be minimized through replication, careful choice of measuring light intensity, proper choice of PAR values during RLCs that work for all species involved, and consistency throughout the experiment in system parameters and method of data capture. The value of the data derived from PAM fluorometry instruments exceeds the pitfalls of working with difficult corals.

Three processes compete for incoming photons within chloroplasts: photochemistry (P), fluorescence (F), and non-photochemical quenching (NPQ) where P + F + NPQ = 1. In general, 70-75% of photons are used in NPQ, 25-30% are used in photochemistry, and 0–0.5% are emitted at lower wavelengths (fluorescence) with the release of heat (Maxwell and Johnson 2000). It is this competitive nature between the processes that allows measurement of photosynthetic efficiency via PAM and the non-destructive and portable nature of the Diving-PAM in particular, made this instrument the preferred method for this investigation. Fluorescence is a relatively small portion of the overall activity taking place within chloroplasts, but it is easily measured. Each measurement involves the full saturation of reaction centers (RCs) during rapid light curves (RLCs) so that the contribution of P = 0 with each saturating pulse of light. During that very brief time, fluorescence is measured and the contribution of NPQ is derived so that P(=0) +F + NPQ = 1. In a dark-acclimated sample, the **optimal quantum yield (F_v/F_m**; defined as maximum fluorescence (F_m) minus baseline fluorescence (F_0) or F_v divided by F_m is calculated. F_v/F_m is a robust and commonly-used photosynthetic parameter to understand photosynthetic efficiency in corals (Brown et al. 1999; Gorbunov and Kolber 2001; Levy et al. 2003; Scheufen et al. 2017). Higher values of F_v/F_m indicate higher photosynthetic efficiency. A more thorough description of the theory behind the use of PAM fluorometry can be found in chapter four of this dissertation and in Govindjee (2004) and Schreiber (2004).

Electron transport is the result of excitation energy reaching and oxidizing the reaction center Chl *a* and the subsequent replacement of that electron by the oxygen-evolving complex. Relative electron transport rate (ETR; in µmols electrons m^{-2} s^{-1}) is calculated as quantum yield (F_v/F_m) x photon flux density (PFD) x 0.84 (assumed light absorbance) x 0.5 (based on the requirement of 2 photons for transport of 1 electron). Due to the highly dependent nature of this variable to F_v/F_m and the imperative to choose a value along the course of the nine saturation pulses, ETR_{max}, derived from the acquired data in the equation by Platt et al. (1980), was chosen to represent this photosynthetic parameter. ETR_{max} describes the organisms' maximum capacity for electron flow. Higher values of ETR_{max} represent higher capacity.

RLCs are similar to photosynthesis vs. irradiance or P vs. E curves in graphically depicting increases (and decreases) in ETR with increasing PFD (Fig. 3.2). With increasing PFD, ETR is considered light-limited until it reaches a maximum value and becomes biochemistry limited (i.e., by Rubisco for the Calvin-Benson Cycle or ADP; Taiz and Zeiger 2010). ETR plateaus at saturating PFD or may decrease as a result of photoinhibition from excess light intensity. The slope (α) of the increase in ETR with increasing PFD, intersects ETR_{max} at E_k, the light saturation index. E_k is reported in units of µmols photons m^{-2} s^{-1} and represents an important parameter of photosynthesis (Sakshaug et al. 1997). Highly efficient photosynthetic organisms have low E_k values, i.e., cells grown in low light, indicating the need for less light to reach maximum ETR.

NPQ is a highly dynamic process that begins with the xanthophyll cycle (Demers et al. 1991; Demmig-Adams and Adams III 1992; Maxwell and Johnson 2000). Close correlation between NPQ and the relative content of photoprotective xanthophylls has been reported in plants and dinoflagellates (Bilger and Björkman 1990; Demers et al. 1991; Demmig-Adams and Adams III 1992). Within seconds of the application of the first RLC saturating pulse, proton buildup in the thylakoid lumen is detected and the XC is activated. NPQ values are first recorded at the second saturating pulse and are highly variable. NPQ increases with increase in PFD as fluorescence yield decreases. Steep increases in NPQ are particularly noticeable when ETR begins to decrease with saturation. The range of NPQ values from the beginning to the end of the RLC is highly variable and each value is dependent on the initial P + F + NPQ = 1 equation. The range of increase in NPQ is more informative than any of the single values of NPQ recorded during the RLC, thus the range (ΔNPQ; calculated as the final value minus the first) was used in the analyses. Keeping in mind that CP light absorption originates from a separate process in a different part of the coral at at different wavelengths than DD and DN, correlation between the two processes would not likely be directly linked, however, evidence of indirect linkage would be consistent with a photoprotective role for CPs.

The majority of investigations into fluorescent pigment and chromoprotein function have been conducted in the Caribbean and Indo-Pacific leaving an interesting opportunity to investigate the status of these pigments in Hawaiian coral species. The first step in the investigation was to determine which FPs and CPs were present in four common species in Kāneʻohe Bay and satisfy the assumption that they were located in the epithelia in a manner relative to the zooxanthellae where they could screen the algal cells. These questions were answered in Chapters One and Two of this dissertation. The second step involved developing a non-invasive method to measure pigment absorbance and photosynthetic performance in near simultaneous fashion. The simple approach taken here paired RLC and reflectance measurements of dark-acclimated whole coral samples with a Diving-PAM and subsequently with a modular spectrometer. The four coral species chosen for this investigation were meant to represent common species with varying polyp sizes and from diverse reef environments. Chromoproteins are visible in *Montipora flabellata* (uniformly across the colony) and in *M. patula* (in polyps only) and the two species have many common attributes while inhabiting different reef environments. Both can be found at shallow depths, but *M. patula* tolerates mid to low water flow, whereas *M. flabellata* is not found in these environments. *Leptastrea purpurea* is known to thrive in high sediment, low water flow environments. Its polyp size is the largest among the species in Kāneʻohe Bay and green fluorescence is often visible in ambient light. *Porites compressa* is the most abundant species in the bay and known to employ RFPs for wounds caused by trematodes in Trematodiasis (Palmer et al. 2009a; Aeby et al. 2011). Additionally, data was available from a previous experiment involving CP extraction and RLCs from *M. flabellata* colonies. These data were analyzed similarly to provide supplementary support to the findings.

Methods

Coral Collection and Processing

Analysis was completed on two datasets from two separate coral collections from Kāneʻohe Bay in 2017 and 2018. The first dataset (1) was comprised of rapid light curve (RLC) measurements and reflectance measurements on whole coral fragments from four species. The second dataset (2) was comprised of RLCs on whole coral fragments of one species (*M. flabellata*) and absorbance spectra from pigment extracts in solution. Collection protocols for both sets were similar: each required removal from the reef with hammer and chisel, direct transfer into pre-labeled 55 oz. Whirl-Pak sample bags (Nasco Inc. Wisconsin, USA), placement onboard the research boat into covered seawater-filled coolers, and immediate acclimation in ~70% shaded, 660-liter mesocosms upon return to the Coral Reef Ecology

Laboratory at Hawaiʻi Institute of Marine Biology (HIMB). The mesocosms were furnished with seawater pumps for circulation and porous stone bubblers for oxygenation. Individual colonies were kept separate in large ~96 oz, labeled bowls until individual fragments were processed and labeled.

Dataset (1) Four Species

Ninety-six fragments from four species—*Montipora flabellata*, purple-polyp *M. patula* morphs, *Porites compressa*, and *Leptastrea purpurea*—were collected from various patch reefs in Kāneʻohe Bay ranging from Ship's Channel to the Sampan Channel (Fig. 2.1). The collection process for these corals is detailed in Chapter Two of this dissertation. Two replicate fragments from each colony from a total of 12 colonies (n = 24) per species were subjected to PAM and spectral reflectance measurements in rapid succession.

Supplemental Dataset (2) Montipora flabellata

Twenty-two unique *M. flabellata* colonies were collected from the large patch reef #50 (Fig. 2.1). Each fragment was approximately 15 cm^2 and all were fragmented with a Dremel tool into nine smaller replicates, labeled, and attached to 5 cm^2 tiles three days after collection. One replicate from each colony was submerged in 50 mL of potassium phosphate buffer solution and immediately placed in a dark, 4 °C refrigerator for water-soluble pigment extraction (Fig. 3.3 a). The remaining replicates were randomly placed into a flume. All replicates experienced the same light and water flow conditions during acclimation. Four replicates per colony (4 x 22 colonies; n = 88) were randomly subsampled for PAM measurements three days after processing. These data, collected prior to the above planned experiment, were used for additional analyses.

Measurements of Photochemistry and Specular Reflectance (R)

For dataset (1) measurements of four coral species, a Diving-PAM (Heinz Walz GmbH, Germany) and the Flame-S-UV-VIS-ES modular spectrometer (Ocean Optics, Dunedin Fl, USA) were set up in a darkroom for RLCs and specular reflectance (R) measurements on dark-acclimated corals. The Diving-PAM was fitted with a 5 mm diameter blue light probe and connected to a PC laptop with WinControl version 3.25 software (Heinz Walz GmBH, Germany). The Flame spectrometer and the DH-2000 UV-VIS-NIR deuterium/halogen light source were connected via a bifurcated R400-7-SR reflectance probe. The Flame was also connected by USB to a MacBook Air running OceanView

Spectroscopy Software version 1.6.3. Corals were acclimated in the darkroom for a minimum of 20 minutes before commencing measurements. All values of PAR, gain, damp, and other PAM parameters, as well as boxcar width, scans to average and other spectrometer parameters were chosen during a testing session previous to the day of coral collection. PAR values were calibrated to attain an inflection point in ETR at or about the sixth saturating pulse with a subsequent reduction in ETR for all species during the light curve measurements. The consecutive and increasing PAR values were: 0, 55, 165, 225, 385, 475, 500, 550, and 585 µmol photons m^{-2} s^{-1}. The spectrometer was calibrated for reflectance measurements using the WS-1 reflectance standard (PTFE optical diffuser; Ocean Optics) providing >98% reflectivity from 250-1500 nm.

Two ring stands with clamp holders were set up facing one another to support the PAM and spectrometer probes and provide accuracy when changing probes during successive measurements on the same coral fragment. In this manner, the precise area measured by the PAM was also measured by the spectrometer. At times it was necessary to hold the coral in place to achieve this precision. The PAM probe was fitted with a surgical rubber tube that extended 2 mm beyond the surface of the probe to protect the fiber optics and coral surfaces from damage. It also allowed the probe to be placed directly on the coral surface at a 90° angle and thus always at a consistent distance for each fragment. Within seconds following the last saturating pulse of the light curve measurements, reflectance measurements were recorded. The 6.35 mm diameter reflectance probe was fitted with an opaque black rubber tube that extended 2 mm beyond the surface of the probe, which allowed the probe to be placed at a 90° angle to and at a precise distance from the coral surface (as with the PAM probe) for specular reflectance measurements. Stray light was effectively blocked by the black tubing and coral reflectance measurements were taken in the 180 nm – 800 nm range of the UV and visible light spectrum.

Measurements of optimal quantum yield require samples to be dark-acclimated, thus RLCs for each coral were run before reflectance measurements. One precise location per fragment was measured by both PAM and spectrometer and the time to complete the paired measurements was minimized in an effort to avoid variability in the data due to diel changes in the algal photochemistry. Each "session" (x3) resulted in measurements for 32 coral fragments and took under three hours to complete. Coral fragment size and reflectance measurements constrained measurements to only one RLC per fragment. A thorough description of the RLC protocol can be found in Chapter Four of this dissertation.

Pigment Extractions and Spectral Absorbance (D) Measurements

For dataset (2), several liters of 0.6 M K_2HPO_4, 0.6 M KH_2PO_4 (6.65 pH) potassium phosphate buffer solution were prepared as per protocols described in Dove et al. (1995). After 48 hours refrigerated

in this solution, the coral fragments were removed, and the "whole" extracts were poured into individual 50 mL Falcon tubes. The whole extract was homogenized with a Maxi Mix II vortex mixer for approximately 10 s and 1000 µL was pipetted into a plastic cuvette for spectral absorbance (D) measurements with a Flame-S-UV-VIS-ES modular spectrometer (Ocean Optics, Dunedin Fl, USA). Each cuvette was placed in a 1 cm-path cuvette holder (200-2000 nm) attached at opposite ends to two P400-1-SR 400 µm fibers, which were themselves attached to the Flame spectrometer at one end and the DH-2000 UV-VIS-NIR deuterium/halogen light source at the other. The Flame was also attached via USB cable to a MacBook Air (2013) running OceanView Spectroscopy Software, version 1.6.3 (Ocean Optics). Measurement settings (scans to average = 10, boxcar width = 2) were selected and background reference spectra (light and dark) were collected for the phosphate buffer following steps in the OceanView Absorbance Wizard. Blocking ambient light with a black box placed over the cuvette holder, an absorbance spectrum for each whole extract sample was recorded. Whole extracts were then placed in an International Portable Refrigerated Centrifuge, Model PR-2 (International Equipment Company, MA, USA) for 15 min at 19,000 rpm to separate large particle debris from the working solution. With pigments still in solution, ~5 mL of "raw" extract was transferred to a 15 mL Falcon tube (Fig 3.3b.) as the raw working solution. Absorbance spectra were collected for each raw extract sample, as described previously. It was determined that no loss of pigment absorbance occurred during extract centrifuge thus raw extract values were used for this analysis. Photos of individual fragments were uploaded to ImageJ to determine a rough estimate of tissue area. Absorbance at various wavelengths of interest were adjusted by the estimated area for statistical analysis.

Data Analysis –Dataset (1) Four Species

The number of colonies sampled per species was based on a power analysis done in JMP Statistical software (SAS version 12) from one-way analysis of quantum yield (F_v/F_m) measurements collected previously for two of the species—*M. flabellata* and *P. compressa*—used in the current study. The least significant number (LSN) given with significance (α) equal to 0.05 was consistently less than 11, therefore 12 colonies from each species were sampled from across Kāneʻohe Bay.

Data from WinControl (Diving-PAM) and OceanView (Flame Spectrometer) was downloaded and saved as .txt files after each set of 32 corals was measured. Each measurement time was recorded within both software programs as well as manually on a spreadsheet with the coral fragment ID. Data was imported into Microsoft Excel and each measurement was cross-referenced and assigned to the correct coral fragment based on the recorded times. Values for E_k and ETR_{max} were derived by the REG1 function (Platt et al. 1980) in the WinControl software. Reflectance (R) data was collected (%) and was

first converted from 0-100 scale to 0-1 scale by dividing each value by 100. Next, values were converted to absorptance (A) using the simple equation: A = 1 – R (Enrıquez et al. 2005; Scheufen et al. 2017; Vásquez-Elizondo et al. 2017) and normalized to zero at 750 nm and additionally at 700 nm, providing two sets of normalized data. Absorptance spectra normalized to 750 nm for each fragment were graphed for visualization and peaks of maximum absorbance in the 550–600 nm range were determined for each species (Figs. 3.4–3.7 a). Mean values for each colony were calculated and spectra normalized to 700 nm were graphed by species (Figs. 3.4–3.7 b). All data prep was done in Microsoft Excel and R Studio.

To estimate the contribution of photosynthetic dinoflagellates in the whole coral reflectance measurements, a comparison model was developed using data provided by G. Johnsen from *in vivo* absorption spectra from whole cell suspensions of the dinoflagellate *Prorocentrum minimum* (Johnsen et al. 1994). Like *Symbiodinium* spp. dinoflagellates, *P. minimum* utilizes the pigments Chl *a*, Chl c_2, peridinin, diadinoxanthin, and dinoxanthin for photosynthesis. The dataset represented cells grown under white light with scalar irradiances (400–700 nm) of 35 µmol photons m^{-2} s^{-1} for low light (LL) cultures and 500 µmol photons m^{-2} s^{-1} for high light (HL) and absorption at each wavelength had been converted to *a**—a Chl a-specific absorption coefficient (Nelson and Prézelin 1993; Fig. 3.1). To render the data applicable for comparison, a ratio of all wavelengths to the value at 675 nm (red Chl *a* maximum) was calculated (Fig 3.8). The same was done for all whole coral absorptance spectra resulting in dimensionless ratios with values at 675 nm equaling one. The coral ratio at each wavelength was divided by the dinoflagellate ratio at that wavelength for a ratio of ratios (coral:dino) that describes the difference in absorption between the two spectra. In this manner, values for coral host pigments from the whole coral could be compared to the dinoflagellates in the region of the spectrum where photosynthetic dinoflagellates absorb minimally (550–600 nm). The coral:dino ratio spectra were graphed (Figs. 3.9–3.12) and absorbance peaks in the 550–600 nm range were recorded and used for statistical analysis. The bivariate fit function in JMP Pro version 14.0 was used to determine whether correlation existed between photosynthetic parameter (F_v/F_m, ΔNPQ, ETR_{max}, E_k) values at maximum peaks of absorptance (574 nm, 597 nm) within and among the species. One-way Analysis of Variance (ANOVA) was also done for all parameters by species. Only one reference peak (574 nm) was ultimately used since it was the only peak without absorbance by photosynthetic pigments. To avoid uncertainty in the results, 597 nm was eliminated from the analysis.

Data Analysis – Dataset (2) One Species

RLC and absorbance spectrum data files were imported into Microsoft Excel as .txt files. Mean colony values (four replicates per colony, two measurements per replicate) for each photosynthetic

parameter (F_v/F_m, ΔNPQ, ETR_{max}, E_k) were derived from individual fragment measurements. Values for ΔNPQ were calculated as previously described. ETR_{max} and E_k were calculated values provided for each RLC by the WinControl software according to the underlying REG1 equations by Platt et al. (1980). All absorbance values were normalized to zero at 750 nm as is standard practice for photosynthetic organisms since light energy absorbance at wavelengths beyond 720-750 nm does not occur (Enrıquez et al. 2005; Scheufen et al. 2017; Vásquez-Elizondo et al. 2017). Using the bivariate fit function, regression analysis of photosynthetic efficiency (using each of the aforementioned parameters as response variables) and absorbance at 330 nm and 583 nm wavelengths was done using JMP Pro statistical software (SAS version 14). Absorbance values were used since no conversions or ratios were necessary.

Results

The purpose of this investigation was to test the hypothesis that chromoproteins have a photobiological role in the coral holobiont and their presence in coral epithelia has a measurable effect on algal photosynthetic efficiency. Two separate methods were employed to make the determination whether the coral host pigments and photosynthetic efficiency are positively correlated. Whereas both methods involve similar protocols for measurements of photosynthetic efficiency, the first method involves live coral reflectance (R) measurements (%) converted to absorptance (A; %) for four coral species taken immediately after RLCs and the second involves analysis of absorbance (D) spectra of raw chromoprotein extracts (one coral species) and same colony RLCs run separately.

Photosynthetic Parameter Distributions by Coral Species

The photosynthetic parameters measured during RLCs, (F_v/F_m, ETR_{max}, E_k, and ΔNPQ) were chosen to represent a range of potential effects RFPs and/or CPs may have on photosynthetic efficiency. The distributions of these parameters show important differences between species as demonstrated in histograms (Fig. 3.13–3.15). All distributions satisfied the basic requirement of normality as seen in normal quantile plots above each histogram.

ΔNPQ – Nonphotochemical Quenching of Fluorescence

One-way analysis of variance (ANOVA) showed that ΔNPQ values are significantly different between species (p<0.0001; Fig. 3.16 a). ΔNPQ minimum values started low with a small range for *L.*

purpurea colonies (0.103–0.283), whereas values for *M. patula* colonies began at the highest value (0.417) and also reached the highest value (0.953) among all four species. *Montipora flabellata* and *P. compressa* had similar minima (0.205 and 0.295 respectively) but *P. compressa* maximum ΔNPQ was higher than *M. flabellata*. These results indicate that *L. purpurea* employs the least DD and DN consistent with their lower light habitat on reefs closer to shore. The ΔNPQ is highest in *Montipora patula* suggesting habitual light stress is common, relative to the other species.

F_v/F_m – Optimal Quantum Yield

One-way ANOVA results show that there is no significant difference between colony means of F_v/F_m between species (p = 0.9373; Fig 3.16 b). The distributions of F_v/F_m by species show similarities in minima, maxima and range although notably, most *P. compressa* colonies tend toward the higher end of the range while the other species are more evenly distributed across the range. The smallest minimum value (0.332) and highest maximum (0.669) both occurred in *L. purpurea* colonies. Mean F_v/F_m values for all species were highly similar.

ETR_{max} – Electron Transport Rate Maximum

One-way ANOVA results show that colony mean ETR_{max} is significantly different between species (p<0.0001; Fig. 3.17 a). This result is driven by a large difference between *L. purpurea* and all other species, while the differences between the other three species is not significant (p = 0.2118). Greater than half of the *L. purpurea* colonies had mean ETR_{max} values higher than any of the mean colony values for the other three species (> 100 µmols electrons m^{-2} s^{-1}). *Leptastrea purpurea* ETR_{max} ranged from 55.1 to 141.6, in *M. flabellata* the range was 46.3 to 82.9, in *M. patula* 35.5 to 93.5, and in *P. compressa* 33.9 to 84.3 µmols electrons m^{-2} s^{-1}. High ETR_{max} values for *L. purpurea* are consistent with the maximization of light-harvesting pigments in the low light environment from which this species was collected.

E_k – Minimum Saturating Irradiance

One-way ANOVA results show that colony mean E_k is significantly different between species (p<0.0001; Fig. 3.17 b). Similar to ETR_{max} the result is driven by the large difference of one species to the rest, while the difference between the three remaining species is not significant (p = 0.1003). Low values of E_k signify an efficiency in reaching a light-saturated state and an advantage on light-limited reefs. *Leptastrea purpurea* colony mean was 409.4 µmols photons m^{-2} s^{-1}, whereas the next highest mean was

271.4 μmols photons m^{-2} s^{-1} in *P. compressa*—a 1.5 x decrease in minimum saturating irradiance. The lowest mean (most efficient) was found in *M. flabellata* at 231.2 μmols photons m^{-2} s^{-1}, and *M. patula* was similar at 250.8 μmols photons m^{-2} s^{-1}.

Whole Coral Absorptance

Whole coral fragments from this experiment underwent RLCs, reflectance measurements, and subsequently were used for confocal microscopy. Because whole coral measurements include the entire holobiont, the specific portion of absorptance attributed to the photosynthetic pigments of the symbiotic dinoflagellates, was unknown. Consequently, it was necessary to use the dinoflagellate *in vivo* absorption data from Johnsen et al. (1994) as a proxy to modify the whole coral datasets for comparison. Spectral graphs of coral:dino absorbance ratios (dimensionless) were produced to allow visualization of major differences in absorbance between the strictly photosynthetic pigments in the dinoflagellates and the coral host pigments from 550–600 nm. Two major peaks— varying in magnitude and range between the species— representing large positive differences in absorbance compared to dinoflagellates were found. The peak wavelength at 574 nm represented the greatest ratio value and the best choice to tease out the contribution of the coral host pigments. The second peak at 597 nm is known to contain a mixture of absorbance bands from Chl *a* and Chl c$_2$ (Johnsen et al. 1994) thus rendering this wavelength unsuitable for comparison.

The ratio at 440 nm to 675 nm for dinoflagellates only was 1.912, showing nearly double the amount of absorbance in the blue region of the spectrum as compared to the red. At 574 nm, the dinoflagellate absorbance ratio was 0.094, the lowest value throughout the spectrum. *Montipora flabellata* colonies had the highest and most variable absorbance ratios at 574 nm compared to the dinoflagellates. These ratios ranged from 3.80 to 9.66 times higher at 574 nm than the 0.094 value in dinoflagellates (Table 3.1). *M. patula* ratios ranged from 3.7–6.5 times higher, *L. purpurea* ratios were 3.9–8.6 times higher, and *P. compressa* ratios were 2.0–5.9 times higher in absorbance at 574 nm than dinoflagellate ratios at that same wavelength. The ratios for all species at 574 nm are normally distributed with *M. flabellata* and *L. purpurea* ratios comprising most values at the higher side of the distribution, and *M. patula* and *P. compressa* making up most of the lower values (Fig. 3.18). These ratios suggest that each of the four species has a coral pigment constituent that absorbs light at this wavelength.

In the photosynthetic regions of the spectrum, i.e., 400–500 nm, coral ratio values are below 1 for most fragments (all species) with the exception of one *P. compressa* and three *L. purpurea* fragments. The overall trend suggests the possibility that strong self-shading (among algal cells), coral tissue absorbance, and/or an intracellular package-effect (within the symbiotic cells) altered the whole coral *in*

vivo absorbance, lowering the values in the photosynthetic range as expected (Duysens 1956; Morel and Bricaud 1981; Kirk 2010). Coral:dino ratios at 420 nm (Chl *a*), 440 nm (Chl *a*, peridinin, diadinoxanthin), 460 nm (Chl c2, peridinin, diadinoxanthin) 540 nm (peridinin), 574 nm (coral pigment only) 578 and 588 nm (potentially coral pigment only), and 597 nm (coral pigment, Chl *a*, Chl c_2) are listed in Table 3.1 for reference. Distributions of coral:dino ratios by species show *M. flabellata* had the highest and widest range of values and *L. purpurea* with second highest values. One-way ANOVA of the coral:dino ratio at 574 nm by species shows they were significantly different ($p<0.0001$). The ratios for 574 nm were used for further analysis (Fig 3.19 a, b).

Testing Linear Relationships Between Photosynthetic Parameters and Absorption at 574 nm

A first pass at testing the potential of a linear relationship between the photosynthetic parameters and coral absorbance at 574 nm, involved using the absorptance (A) values prior to taking ratios. These regression tests showed no linear relationship exists for any of the parameters in any of the coral species. This was followed by the use of ratios to better characterize the absorbance at 574 nm and how it differed from the dinoflagellates. Least squares regression results from a bivariate fit of the mean ratio for each colony and species to each photosynthetic parameter yielded very weak/no linear relationships (Table 3.2). R-squared values for linear fit were highest for E_k in *P. compressa* (0.4479), although not strong enough to characterize the relationship as linear. Subsequently, a two-degree polynomial fit was tested for each parameter/species comparison with similar or slightly stronger fit (Table 3.2; Fig. 3.20). R-squared values were highest for E_k, particularly for *L. purpurea* (0.6431), whereas the polynomial fit only slightly increased for *P. compressa* (0.4914). The signs (+ or -) for the weak linear and polynomial relationships are not consistent between the species for any given response variable. This further indicates linear regression is a poor fit for the characterization of coral host pigment absorbance at 574 nm and photosynthesis relationship. Residual normal quantile plots for all regressions satisfied the required assumptions for the tests.

Raw Pigment Extract Absorbance and One Coral Species Photosynthetic Parameters

Graphs of absorbance spectra of extracted water-soluble pigments from the 22 *Montipora flabellata* colonies were produced for visual analysis (Fig. 3.21 a, b). These graphs indicated very high absorbance peaks in the UV-B (280–315 nm) and UV-A (315–400 nm) regions, steep declines in absorbance from ~350–400 nm, a flatter, more steady decline to 500 nm, and small, broad peaks at ~583 nm. Small shifts in absorbance maxima are common when pigments are isolated from living organisms

and this red-shifted maximum differs from the *in hospite* whole coral maximum at 574 nm as a result of the extraction from the coral in potassium phosphate buffer.

Once the data assumptions for least squares regression analysis were verified, mean absorbance (D) values at 583 nm as the explanatory variable and mean values for ΔNPQ, F_v/F_m, ETR_{max}, and E_k as the response variables, were tested and showed very weak correlation (Fig. 3.22; Table 3.3) for all parameters with the highest r^2 values at 0.11 for ETR_{max}, and E_k. The high absorbance in the UV portion of the spectrum is likely from a mixture of chromoproteins and mycosporine-like amino acids (MAAs), although the presence of MAAs was not verified. The role of MAAs as photoprotectants is well-supported in the literature (Jokiel 1980; Banaszak et al. 2000; Kuffner 2005). For this reason, another regression analysis was run on the data with absorbance values at 330 nm as the explanatory variable for all fragments. Similarly, correlation was very weak with the highest r^2 value at 0.12 for ΔNPQ (Fig. 3.23; Table 3.4).

Discussion

Whole coral reflectance measurements capture the effects of the photosynthetic cells (subject to the "package effect" and self-shading; Johnsen et al. 1994; Enrıquez et al. 2005), the coral tissue, and the coral host pigments. It is a value that represents the total of all constituents and presents a challenge if individual constituent effects are of interest. In testing the viability of a minimally invasive approach to determine the potential for photoprotection in coral host pigments, it was found that absorbance interference between various pigments (host and symbiont) rendered analysis too difficult to assess at most wavelengths. The only wavelengths corresponding to a minimal contribution by the dinoflagellates were found to be in the 550-590 nm (yellow) range of the PAR spectrum. This range can have tremendous photobiological impact on zooxanthellae since it corresponds to some of the most damaging wavelengths to the oxygen-evolving complex. Since this range also aligns well with maxima from RFP and CP absorbance, the analysis involved the determination of whether these two types of pigments have an effect on photosynthetic efficiency. In Chapter One of this dissertation, CPs were found forming thick layers in the epidermis as a potential screen for zooxanthellae in the gastrodermis. In Chapter Two, it was determined that of the three fluorescent proteins examined, only red FPs are located in surface structures (epidermis, polyps, tentacles), enabling them to have a direct effect on zooxanthellae. Therefore, the choice of using one wavelength (574 nm) for the entire analysis seemed robust and the most biologically relevant. Despite the challenges, whole coral reflectance measurements are informative and development of methods to separate the different constituent effects could be quite useful.

The low absorption in the blue region and the broad absorption in the green to orange range of the PAR spectrum (500–600 nm) by all coral species was consistent with the intracellular package effect and self-shading among algal cells (Enrıquez et al. 2005; Evertsen and Johnsen 2009; Kaniewska et al. 2014). Although coral skeleton reduces the effects of self-shading (Enrıquez et al. 2005) it clearly remains a major factor as evidenced by the whole coral spectra, particularly in *L. purpurea* where blue region absorption was highly depressed relative to the red region. To tease out the relative difference in absorbance in the yellow PAR spectrum between the whole coral and the dinoflagellates, a model for dinoflagellate spectral absorbance was necessary. To that end, data from family Symbiodiniaceae dinoflagellates was sought but not found. Data from *in vivo* measurements of whole cell suspensions of the dinoflagellate *Prorocentrum minimum* was obtained from Johnsen et al. (1994) instead. Since the constituent pigments in all dinoflagellates are the same and are regulated by light, *P. minimum* data was deemed appropriate for this investigation. Visual comparisons of reference spectra for three *Symbiodinium* spp. dinoflagellates (Iglesias-Prieto and Trench 1994; Fig. 3.24) showed relatively good agreement between these coral-associated dinoflagellates and *P. minimum*.

The units of measurement for *P. minimum* absorbance and whole coral absorptance were converted to a dimensionless value by standardizing all wavelengths by their ratios to the value at 675 nm for comparison. The wavelength 675 nm was chosen because it is a known Chl *a* peak in dinoflagellates and is separate from the wide band of absorbance in the blue region. The result showed large differences in absorption in the yellow range of the PAR spectrum between dinoflagellates and all four coral species, representing the likely portion of absorbance that can be attributed solely to coral host proteins. This is the first known instance in which spectral measurements in Hawaiian corals have indicated such prominent absorptance in the yellow region of the PAR spectrum.

For this investigation, an assumption was made that photoprotection provides a direct positive effect to the cells they are protecting. Currently, the only evidence of this in corals comes from acute irradiance trials designed to cause symbiont damage with subsequent measurement and comparison of the extent of damage in specimens with vs. without CPs (Smith et al. 2013). The study used F_v/F_m measurements to determine the extent of damage and found higher F_v/F_m values in corals with CPs. In contrast, the present investigation used PAM fluorometry, which provides several parameters of photosynthetic efficiency for analyses: F_v/F_m represents the direct fluorescence (F) measurement and is the most commonly reported parameter in the coral literature. ETR_{max} represents photochemical (P) efficiency, ΔNPQ is a measure of photoprotection in the algal cells, and E_k values, or minimal saturation irradiance, help to characterize the light regime the coral is adapted to. In this study, destructive treatments were not employed, instead, a minimally invasive approach was used with the added benefit of determining whether the Diving-PAM and modular spectrometer could be used together to yield useful

information. The lack of linear relationships between CP absorbance and photosynthetic parameters is not consistent with CPs being photoprotective if the assumption of a direct effect on the photosynthetic parameters in unstressed corals is true. It remains unclear however, whether stress and damage to the photosynthetic apparatus is necessary to verify the proposed photoprotective role of CPs in corals.

Viewed individually, the photosynthetic and spectral data collected do provide some useful results that increase our understanding of the four Hawaiian coral species. For instance, F_v/F_m values in all four species were statistically similar (p = 0.9375). *M. flabellata* and *M. patula* had consistent, narrow ranges whereas ranges for *L. purpurea* and *P. compressa* were broader. This is remarkable because these species are found in relatively diverse reef environments and all other parameters were significantly different (ETR$_{max}$, ΔNPQ and E_k; p<0.0001). In the context of this investigation, F_v/F_m was perhaps the least informative parameter. The parameter means for *M. flabellata* in dataset (1) are similar to those in dataset (2) showing good agreement between the data (Table 3.5) collected at different times of the year (May vs. August) and consistency in photosynthetic output.

E_k: An Informative Photosynthetic Parameter

Montipora flabellata had the lowest mean E_k (231.2 µmols photons m^{-2} s^{-1}) of the four species suggesting it is highly efficient at using low photon flux density. It also indicates that *M. flabellata* reaches saturation early in the day, well before PFD is at its daily maximum. On a south Kāneʻohe Bay fringing reef where suspended particulate matter is likely much higher than that experienced by *M. flabellata*, irradiance measured ~900 µmols photons m^{-2} s^{-1} at one-meter depth at approximately 13:00 on a cloudless day. That value is nearly four times higher than the E_k value of 231.2 µmols photons m^{-2} s^{-1}. *Montipora flabellata* is not found on the fringing reefs of the South Bay, presumably because water flow is insufficient and the potential for sediment deposition is high. Thus, it is likely *M. flabellata* experiences even higher PFD at mid-day and these saturating conditions continue until late in the day when light is again limiting. These results could have important implications for *M. flabellata* colony ability to manage light throughout the day as PFD becomes more intense, especially since these corals are generally found within the first five meters of depth. Furthermore, these results shed some light on the species' vulnerability to bleaching since zooxanthellae expulsion paired with longer days in supersaturating conditions could extend colony functional capability beyond physiological limits. Based on E_k alone, *M. flabellata* stands out as the species with the greatest requirement for photoprotection, but the mean ΔNPQ for this species is only mid-range (0.417) relative to the others. This may represent a significant output of photoprotection during the day or it may reflect the presence of another process that lessens the need for high ΔNPQ. *Montipora flabellata* had the widest range and highest maximum coral:dino ratio at 574 nm

(9.65) and a mean coral:dino ratio of 6.82. These values do not represent a particularly broad range of absorbance since the colonies collected for this experiment were chosen randomly and the purple coloration was only dominant in a few colonies. A more comprehensive look at the 574 nm absorbance in this species should include sampling throughout the Bay at several times during the year, particularly when the purple coloration is dominant.

M. patula had the highest mean ΔNPQ value (0.715; indicative of a large xanthophyll pool) of all species and low values of E_k (250.8 µmols photons m^{-2} s^{-1}) suggesting this species also reaches saturation early and commonly experiences supersaturating PFD (Fig. 3.25). This species is similar to *M. flabellata* in morphology and habitat but unlike *M. flabellata*, *M. patula* also tolerates lower water flow. Depending on location in Kāneʻohe Bay, this could mean higher suspended particulate in the surrounding water and thus less PFD. Consistent with the localization of CPs in polyps only, colonies appear to have a fairly high mean coral:dino ratio at 574 nm (5.22).

L. purpurea had the highest mean ETR$_{max}$ (97.71 µmols electrons m^{-2} s^{-1}), the highest mean E_k (409.4 µmols photons m^{-2} s^{-1}), and the lowest mean ΔNPQ (0.162). Consistent with a low light regime, these values indicate *L. purpurea* will reach saturation later in the day than *M. flabellata* but will run at almost double ETR capacity until light is again limiting. It is interesting that this species also has a fairly high mean (6.95) and broad range for coral:dino ratio at 574 nm indicating additional photoprotection may not be needed. These results are consistent with reports that this species grows rapidly, has high recruitment success, is thermally-tolerant, and is a "long-term winner" (Loya et al. 2001; Van Woesik et al. 2011) after bleaching events.

P. compressa did not stand out among the other species with highest or lowest values for any of the significant parameters and yet this is one of the most abundant, successful coral species in Kāneʻohe Bay (Table 3.5). A closer look at the mean values shows that while not significantly different from the others, mean F_v/F_m was highest in *P. compressa* (0.532), mean ΔNPQ (0.509) and mean ETR$_{max}$ (69.08 µmols electrons m^{-2} s^{-1}) were second highest among the species, and E_k (271.2 µmols photons m^{-2} s^{-1}) was in range with *M. flabellata* and *M. patula*. Furthermore, *P. compressa* had the lowest mean coral:dino ratio at 574 nm (4.12). It is known that this species utilizes RFPs for an immune response in Trematodiasis, but this appears to be highly localized and apparently function-specific.

Conclusions

CPs and/or RFPs in the four Hawaiian coral species do not appear to have an effect on photosynthetic efficiency as measured by PAM fluorometry.

Despite new evidence in support of a photoprotective role in *Montipora flabellata*, a final determination of the functional role of CPs could not be made. Photoprotection could not be directly correlated with photosynthetic efficiency thus, further investigations are warranted.

Results do show potential to explain *M. flabellata* vulnerability to thermal bleaching. The photosynthetic parameter E_k—minimum saturating irradiance—helps illustrate the extensive periods of time that the species operates under supersaturating irradiance conditions.

With better understanding of the underlying photobiological capabilities and limitations of all coral species, paired with knowledge of their habitats, we can better determine which species will survive and which will struggle to meet the challenges of rising seawater temperatures due to global climate change.

References

Aeby GS, Williams GJ, Franklin EC, Kenyon J, Cox EF, Coles S, Work TM (2011) Patterns of coral disease across the Hawaiian Archipelago: Relating disease to environment. PLoS One 6:e20370

Alieva NO, Konzen KA, Field SF, Meleshkevitch EA, Hunt ME, Beltran-Ramirez V, Miller DJ, Wiedenmann J, Salih A, Matz M V (2008) Diversity and evolution of coral fluorescent proteins. PLoS One 3:e2680

Apprill AM, Bidigare RR, Gates RD (2007) Visibly healthy corals exhibit variable pigment concentrations and symbiont phenotypes. Coral Reefs 26:387–397

Banaszak A, LaJeunesse T, Trench R (2000) The synthesis of mycosporine-like amino acids (MAAs) by cultured, symbiotic dinoflagellates. J. Exp. Mar. Bio. Ecol. 249:219–233

Bilger W, Björkman O (1990) Role of the xanthophyll cycle in photoprotection elucidated by measurements of light-induced absorbance changes, fluorescence and photosynthesis in leaves of Hedera canariensis. Photosynth. Res. 25:173–186

Brown B, Ambarsari I, Warner M, Fitt W, Dunne R, Gibb S, Cummings D (1999) Diurnal changes in photochemical efficiency and xanthophyll concentrations in shallow water reef corals: evidence for photoinhibition and photoprotection. Coral Reefs 18:99–105

D'Angelo C, Denzel A, Vogt A, Matz MV, Oswald F, Salih A, Nienhaus GU, Wiedenmann J (2008) Blue light regulation of host pigment in reef-building corals. Mar. Ecol. Prog. Ser. 364:97–106

D'Angelo C, Smith EG, Oswald F, Burt J, Tchernov D, Wiedenmann J (2012) Locally accelerated growth is part of the innate immune response and repair mechanisms in reef-building corals as detected by green fluorescent protein (GFP)-like pigments. Coral Reefs 31:1045–1056

Davy SK, Allemand D, Weis VM (2012) Cell biology of cnidarian-dinoflagellate symbiosis. Microbiol. Mol. Biol. Rev. 76:229–261

Demers S, Roy S, Gagnon R, Vignault C (1991) Rapid light-induced changes in cell fluorescence and in xanthophyll-cycle pigments of *Alexandrium excavatum* (Dinophyceae) and *Thalassiosira pseudonana* (Bacillariophyceae): a photo-protection mechanism. Mar. Ecol. Prog. Ser. 76:185–193

Demmig-Adams B, Adams III WW (1992) Photoprotection and other responses of plants to high light stress. Annu. Rev. Plant Physiol. Plant Mol. Biol. 43:599–626

Dove S (2004) Scleractinian corals with photoprotective host pigments are hypersensitive to thermal bleaching. Mar. Ecol. Prog. Ser. 272:99–116

Dove S, Takabayashi M, Hoegh-Guldberg O (1995) Isolation and partial characterization of the pink and blue pigments of pocilloporid and acroporid corals. Biol. Bull. 189:288–297

Duysens LNM (1956) The flattening of the absorption spectrum of suspensions, as compared to that of solutions. Biochem. Biophys. Acta 19:1–12

Enrıquez S, Méndez E, Iglesias-Prieto R (2005) Multiple scattering on coral skeletons enhances light absorption by symbiotic algae. Limnol. Ocean. 50:1025–1032

Evertsen J, Johnsen G (2009) In vivo and in vitro differences in chloroplast functionality in the two north Atlantic sacoglossans (Gastropoda, Opisthobranchia) *Placida dendritica* and *Elysia viridis*. Mar. Biol. 156:847–859

Falkowski PG, Dubinsky Z, Muscatine L, Porter JW (1984) Light and the bioenergetics of a symbiotic coral. Bioscience 34:705–709

Gorbunov M, Kolber Z (2001) Photosynthesis and photoprotection in symbiotic corals. Limnol. Oceanogr. 46:75–85

Govindjee (2004) Chlorophyll a fluorescence: a bit of basics and history. In: Papageorgiou GC, Govindjee (eds.) Chlorophyll a Fluorescence. A Signature of Photosynthesis. Springer, Dordrecht, pp 1–42

Hakala M, Tuominen I, Keränen M, Tyystjärvi T, Tyystjärvi E (2005) Evidence for the role of the oxygen-evolving manganese complex in photoinhibition of Photosystem II. Biochim. Biophys. Acta-Bioenerg. 1706:68–80

Iglesias-Prieto R, Beltrán VH, LaJeunesse TC, Reyes-Bonilla H, Thomé PE (2004) Different algal symbionts explain the vertical distribution of dominant reef corals in the eastern Pacific. Proc. Biol. Sci. 271:1757–1763

Iglesias-Prieto R, Trench RK (1994) Acclimation and adaptation to irradiance in symbiotic dinoflagellates. I. Responses of the photosynthetic unit to changes in photon flux density. Mar. Ecol. Prog. Ser. 113:163–175

Iglesias-Prieto R, Trench RK (1997) Acclimation and adaptation to irradiance in symbiotic dinoflagellates. II. Response of chlorophyll-protein complexes to different photon-flux densities. Mar. Biol. 130:23–33

Jeffrey S, Haxo F (1968) Photosynthetic pigments of symbiotic dinoflagellates (zooxanthellae) from corals and clams. Biol. Bull.

Johnsen G, Bricaud A, Nelson N, Prézelin BB, Bidigare RR (2011) In vivo bio-optical properties of phytoplankton pigments. In: Roy S., Llewellyn C.A., Egeland E.S., Johnsen G. (eds) Phytoplankton Pigments: Characterization, Chemotaxonomy and Applications in Oceanography. Cambridge University Press, New York, pp 496–537

Johnsen G, Nelson NB, Jovine RVM, Prézelin BB (1994) Chromoprotein- and pigment-dependent modeling of spectral light absorption in two dinoflagellates, *Prorocentrum minimum* and *Heterocapsa pygmaea*. Mar. Ecol. Prog. Ser. 114:245–258

Jokiel P (1980) Solar ultraviolet radiation and coral reef epifauna. Science 207:1069–1071

Kaniewska P, Anthony KRN, Sampayo EM, Campbell PR, Hoegh-Guldberg O (2014) Implications of geometric plasticity for maximizing photosynthesis in branching corals. Mar. Biol. 161:313–328

Karim W, Seidi A, Hill R, Chow WS, Minagawa J, Hidaka M, Takahashi S (2014) Novel characteristics of photodamage to PSII in a high-light-sensitive symbiodinium phylotype. Plant Cell Physiol. 56:1162–1171

Kirk JTO (2010) Light and photosynthesis in aquatic ecosystems, third edition. Cambridge University Press, New York

Kuffner IB (2005) Temporal variation in photosynthetic pigments and UV-absorbing compounds in shallow populations of two Hawaiian reef corals. Pac. Sci. 59:561–580

Levy O, Dubinsky Z, Achituv Y (2003) Photobehavior of stony corals: responses to light spectra and intensity. J. Exp. Biol. 206:4041–4049

Loya Y, Sakai K, Yamazato K, Sambali H, van Woesik R (2001) Coral bleaching: the winners and the losers. Ecol. Lett. 4:122–131

Maxwell K, Johnson GN (2000) Chlorophyll fluorescence - a practical guide. J. Exp. Bot. 51:659–668

Mazel CH, Lesser MP, Gorbunov MY, Barry TM, Farrell JH, Wyman KD, Falkowski PG (2003) Green-fluorescent proteins in Caribbean corals. Limnol. Oceanogr. 48:402–411

Morel A, Bricaud A (1981) Theoretical results concerning light absorption in a discrete medium, and application to specific absorption of phytoplankton. Deep. Res. 28A:1375–1393

Muscatine L, Falkowski P, Porter J, Dubinsky Z (1984) Fate of photosynthetic fixed carbon in light- and shade-adapted colonies of the symbiotic coral *Stylophora pistillata*. Proc. R. Soc. London B Biol. Sci. 222:181–202

Muscatine L, McCloskey L, Marian R (1981) Estimating the daily contribution of carbon from zooxanthellae to coral animal respiration. Limnol. Oceanogr. 26:601–611

Nelson NB, Prézelin BB (1993) Calibration of an integrating sphere for determining the absorption coefficient of scattering suspensions. Appl. Opt. 32:6710–6717

Ohnishi N, Allakhverdiev SI, Takahashi S, Higashi S, Watanabe M, Nishiyama Y, Murata N (2005) Two-step mechanism of photodamage to photosystem II: Step 1 occurs at the oxygen-evolving complex and step 2 occurs at the photochemical reaction center. Biochemistry 44:8494–8499

Palmer C V, Modi CK, Mydlarz LD (2009a) Coral fluorescent proteins as antioxidants. PLoS One 4:e7298

Palmer C V, Roth MS, Gates RD (2009b) Red fluorescent protein responsible for pigmentation in trematode-infected *Porites compressa* tissues. Biol. Bull. 216:68–74

Pearse VBV, Muscatine L (1971) Role of symbiotic algae (zooxanthellae) in coral calcification. Biol. Bull. 141:350–363

Platt T, Gallegos CL, Harrison WG (1980) Photoinibition of photosynthesis in natural assemblages of marine phytoplankton. J. Mar. Res. 38:687–701

Prescott M, Ling M, Beddoe T, Oakley AJ, Dove S, Hoegh-Guldberg O, Devenish RJ, Rossjohn J (2003) The 2.2 A crystal structure of a pocilloporin pigment reveals a nonplanar chromophore conformation. Structure 11:275–284

Roy S, Llewellyn C, Egeland ES, Johnsen G (2013) Phytoplankton Pigments: Characterization, Chemotaxonomy and Applications in Oceanography. Cambridge University Press, New York

Sakshaug E, Bricaud A, Dandonneau Y, Falkowski P, Kiefer D (1997) Parameters of photosynthesis: definitions, theory and interpretation of results. J. Plankton Res. 19:1637–1670

Salih A, Hoegh-Guldberg O, Cox G (1997a) Photoprotection of symbiotic dinoflagellates by fluorescent pigments in reef corals. 217–230

Salih A, Hoegh-Guldberg O, Cox G (1997b) Bleaching responses of symbiotic dinoflagellates in corals: the effects of light and elevated temperature on their morphology and physiology. Proc. Aust. Coral Reef Soc. 75th Anniv. Conf. 199–216

Salih A, Larkum A, Cox G, Kühl M, Hoegh-Guldberg O (2000) Fluorescent pigments in corals are photoprotective. Nature 408:850–3

Scheufen T, Iglesias-Prieto R, Enríquez S (2017) Changes in the number of symbionts and *Symbiodinium* cell pigmentation modulate differentially coral light absorption and photosynthetic performance. Front. Mar. Sci. 4:1–16

Schreiber U (2004) Pulse-Amplitude-Modulation (PAM) Fluorometry and Saturation Pulse Method: An Overview. In: Papageorgiou G., Govindjee (eds) Chlorophyll a Fluorescence. Springer, Dordrecht. pp 279–319

Smith E, D'Angelo C, Salih A, Wiedenmann J (2013) Screening by coral green fluorescent protein (GFP)-like chromoproteins supports a role in photoprotection of zooxanthellae. Coral Reefs 32:463–474

Stimson J (1997) The annual cycle of density of zooxanthellae in the tissues of field and laboratory-held *Pocillopora damicornis* (Linnaeus). J. Exp. Mar. Biol. Ecol. 214:35–48

Taiz L, Zeiger E (2010) Plant Physiology. Sinauer, Massachusetts

Takahashi S, Badger MR (2011) Photoprotection in plants: a new light on photosystem II damage. Trends Plant Sci. 16:53–60

Takahashi S, Milward SE, Yamori W, Evans JR, Hillier W, Badger MR (2010) The solar action spectrum of photosystem II damage. Plant Physiol. 153:988–93

Trench RK (1993) Microalgal-invertebrate symbioses: A review. Endocytobiosis Cell Res. 9:135–175

Tyystjärvi E (2008) Photoinhibition of Photosystem II and photodamage of the oxygen evolving manganese cluster. Coord. Chem. Rev. 252:361–376

Vásquez-Elizondo RM, Legaria-Moreno L, Pérez-Castro MÁ, Krämer WE, Scheufen T, Iglesias-Prieto R, Enríquez S (2017) Absorptance determinations on multicellular tissues. Photosynth. Res. 132:311–324

Verkhusha V V, Lukyanov KA (2004) The molecular properties and applications of Anthozoa fluorescent proteins and chromoproteins. Nat. Biotechnol. 22:289–96

Wakefield T, Farmer M, Kempf S (2000) Revised Description of the Fine Structure of in situ "Zooxanthellae" Genus *Symbiodinium*. Biol. Bull. 199:76–84

Van Woesik R, Sakai K, Ganase A, Loya Y (2011) Revisiting the winners and the losers a decade after coral bleaching. Mar. Ecol. Prog. Ser. 434:67–76

Yarden O, Ainsworth TD, Roff G, Leggat W, Fine M, Hoegh-Guldberg O (2007) Increased prevalence of ubiquitous ascomycetes in an acropoid coral (*Acropora formosa*) exhibiting symptoms of Brown Band syndrome and skeletal eroding band disease. Appl. Environ. Microbiol. 73:2755–2757

Tables and figures

Figure 3.1. (a) Dinoflagellate absorbance spectrum recreated with data from Johnsen et al. 1994. (b) Also from Johnsen et al. 1994, pigment constituents that constitute graph in (a). β, β-carotene was excluded due to low concentrations relative to other pigments. A=chl a, c2=chl c2, DIA=diadinoxanthin, PER=peridinin. Used with permission.
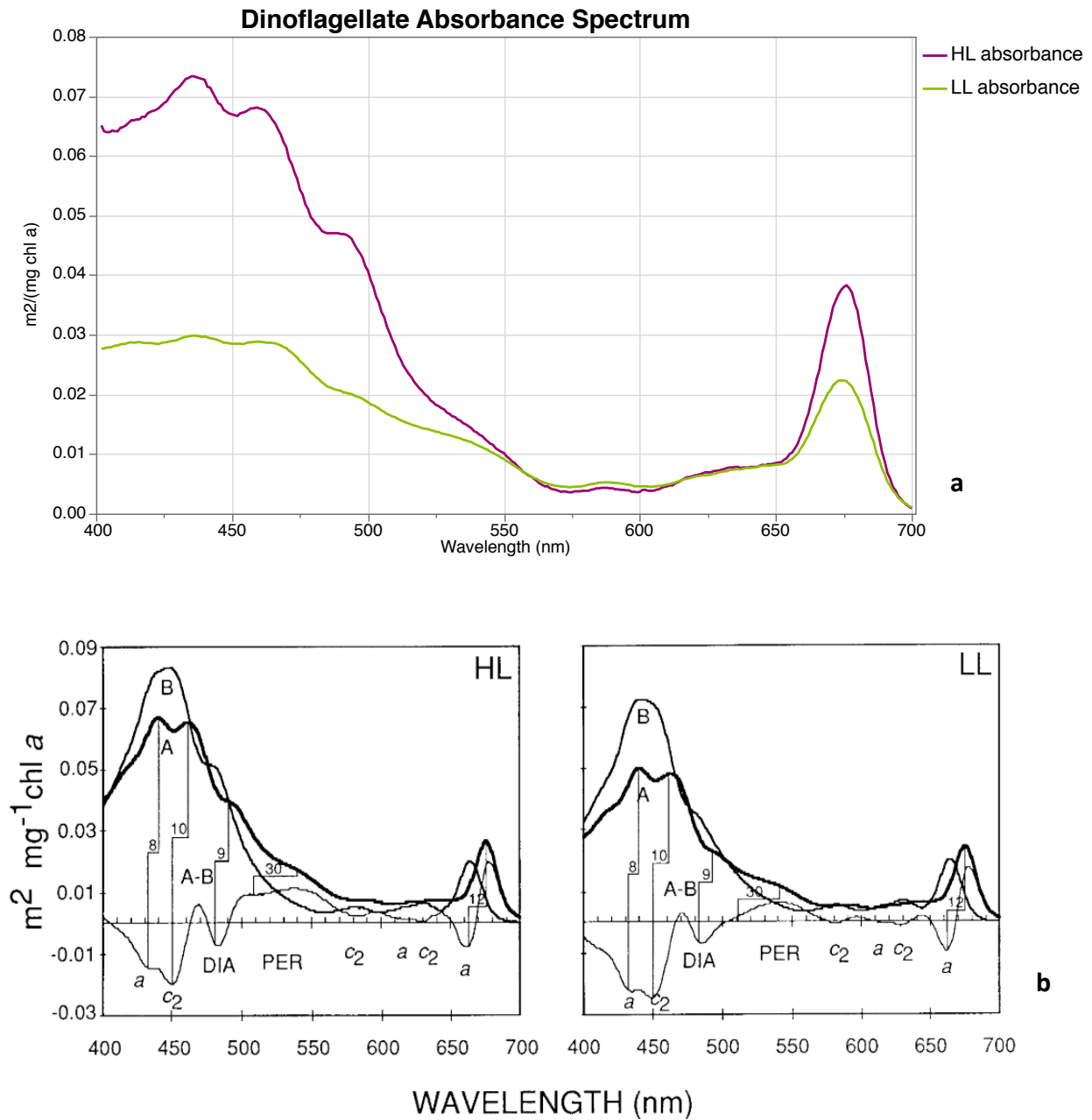
Figure 3.2. Example of a classic P vs. E curve adapted from graph by R. Iglesias-Prieto.
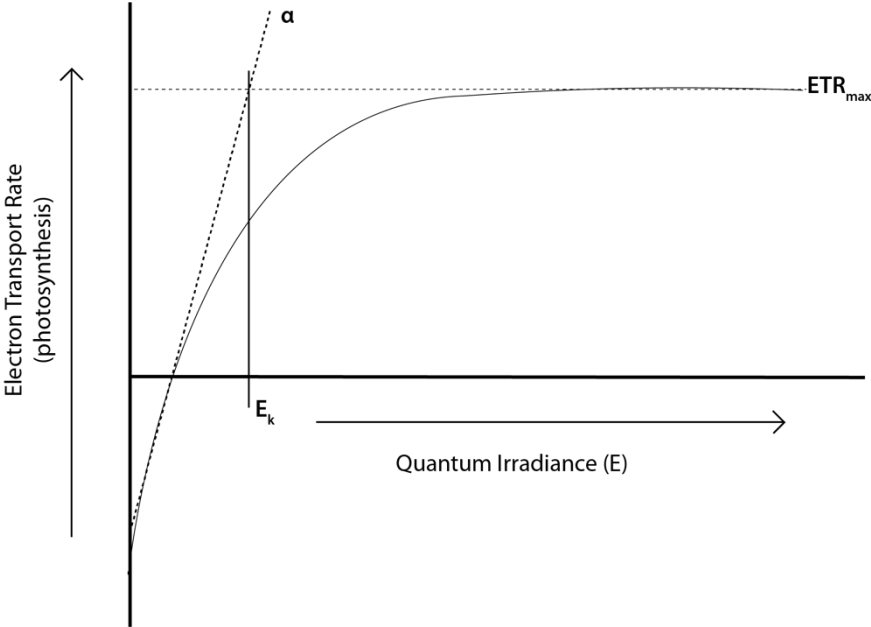
Figure 3.3. (a) Two whole coral fragments in potassium phosphate buffer with visible differences in pigmentation. (b) Pigments after 48-hour extraction time.
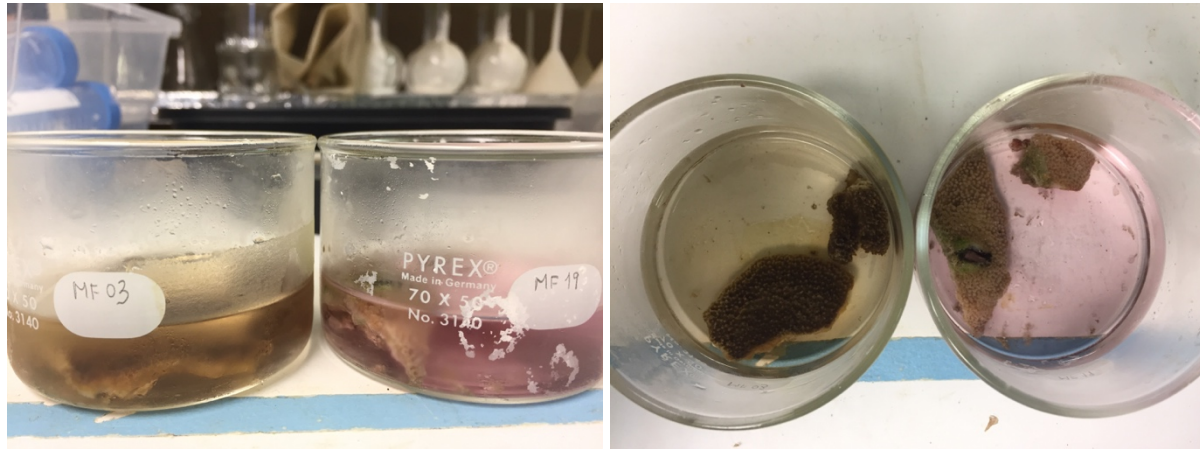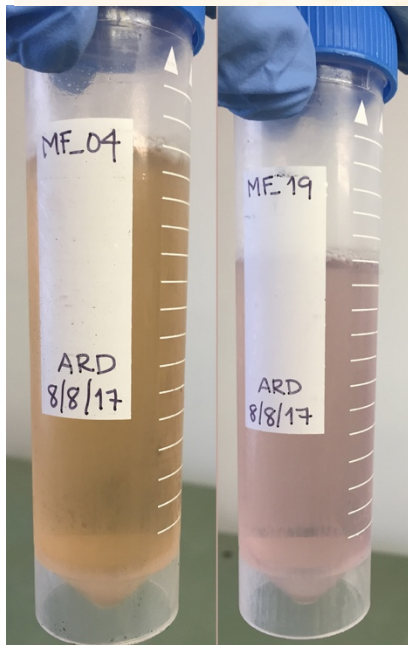
Figure 3.4. Absorptance spectra for 24 coral fragments (12 colonies) of *Montipora flabellata*. (a) All spectra normalized to 750 nm with UV included to show variation. (b) Spectra for mean colony values normalized to 700 nm, graph reduced to photosynthetically active radiation (PAR) spectrum (400-700 nm).

b
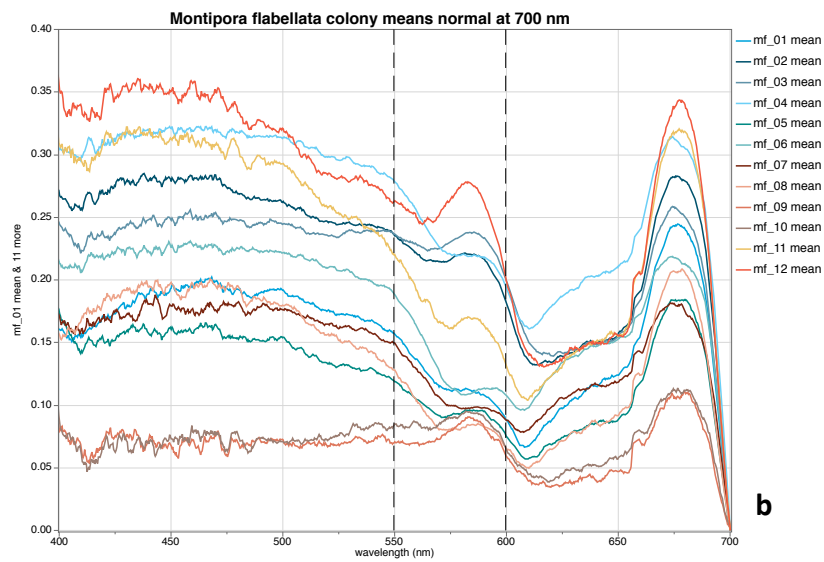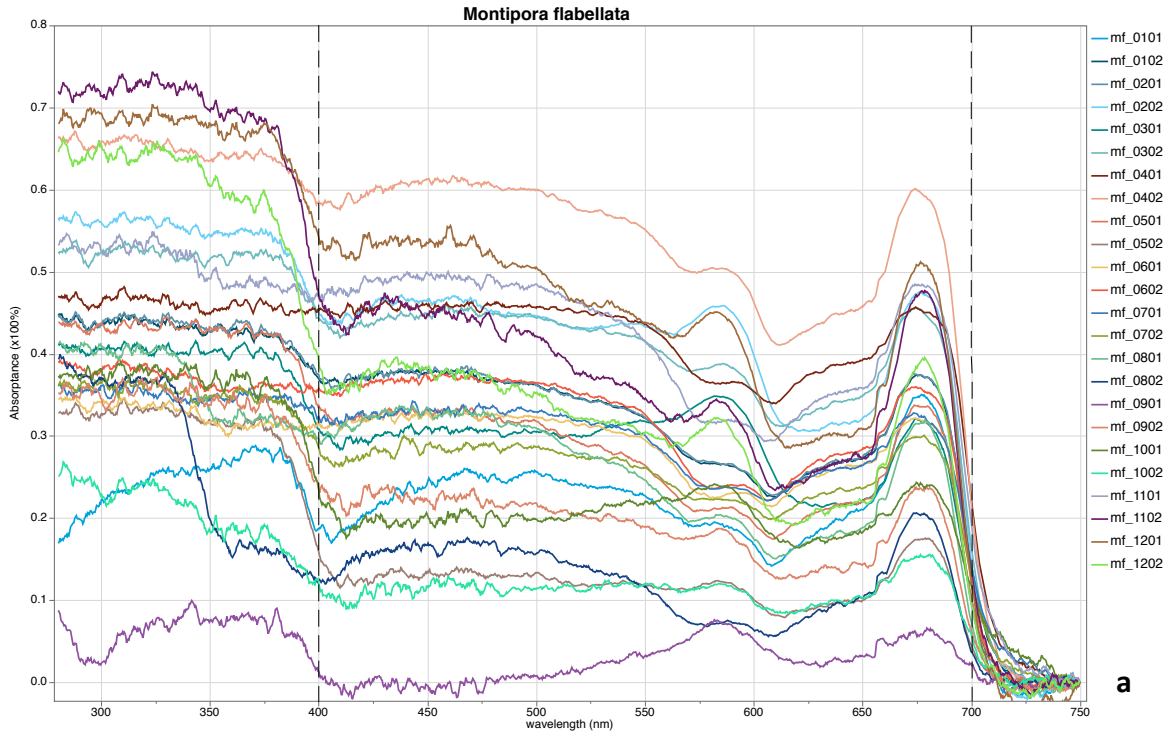
Figure 3.5. Absorptance spectra for 24 coral fragments (12 colonies) of *Montipora patula*. (a) All spectra normalized to 750 nm with UV included to show variation. (b) Spectra for mean colony values normalized to 700 nm, graph reduced to photosynthetically active radiation (PAR) spectrum (400-700 nm).
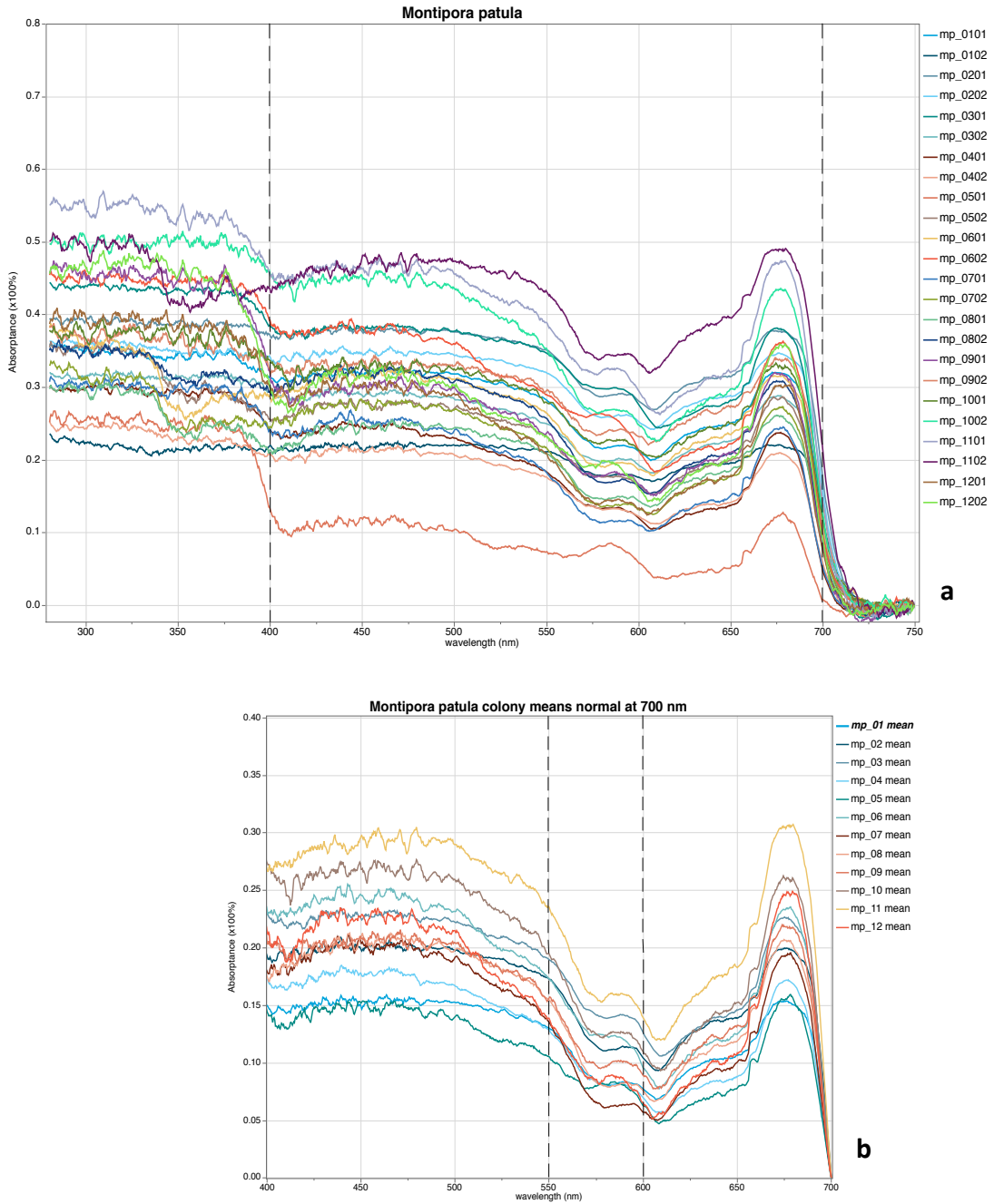
Figure 3.6. Absorptance spectra for 24 coral fragments (12 colonies) of *Leptastrea purpurea*. (a) All spectra normalized to 750 nm with UV included to show variation. (b) Spectra for mean colony values normalized to 700 nm, graph reduced to photosynthetically active radiation (PAR) spectrum (400-700 nm).
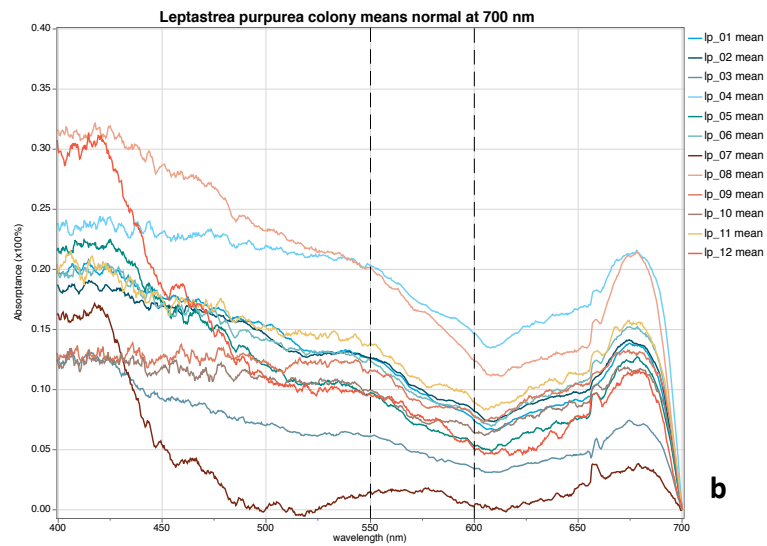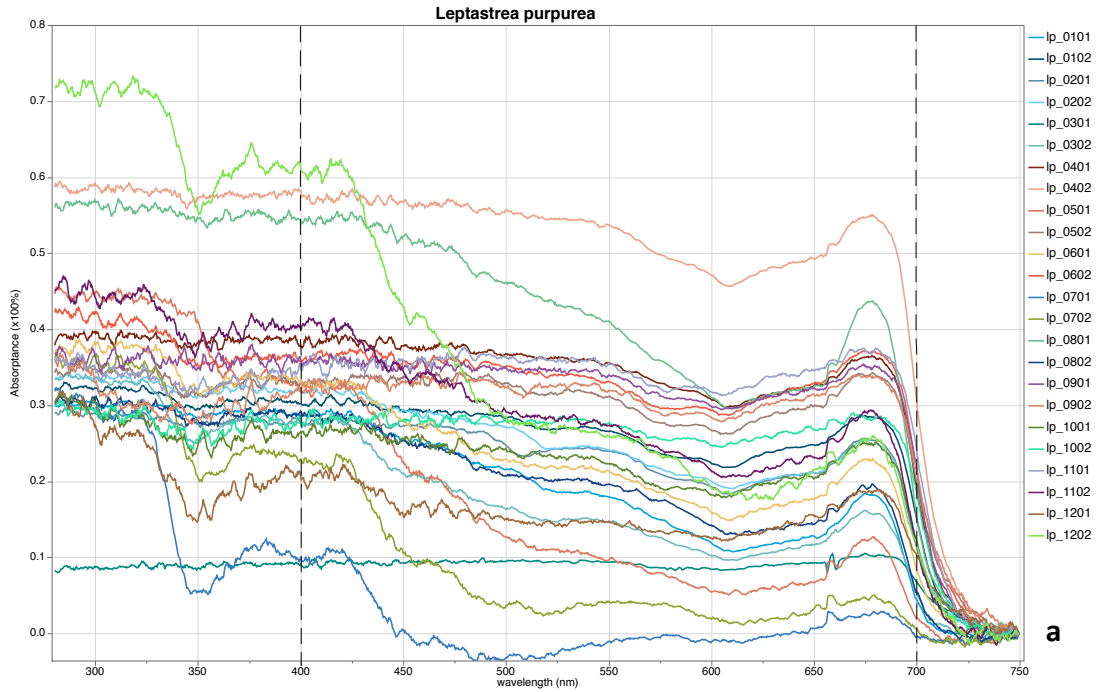
Figure 3.7. Absorptance spectra for 24 coral fragments (12 colonies) of *Porites compressa*. (a)
All spectra normalized to 750 nm with UV included to show variation. (b) Spectra for mean
colony values normalized to 700 nm, graph reduced to photosynthetically active radiation (PAR)
spectrum (400-700 nm).
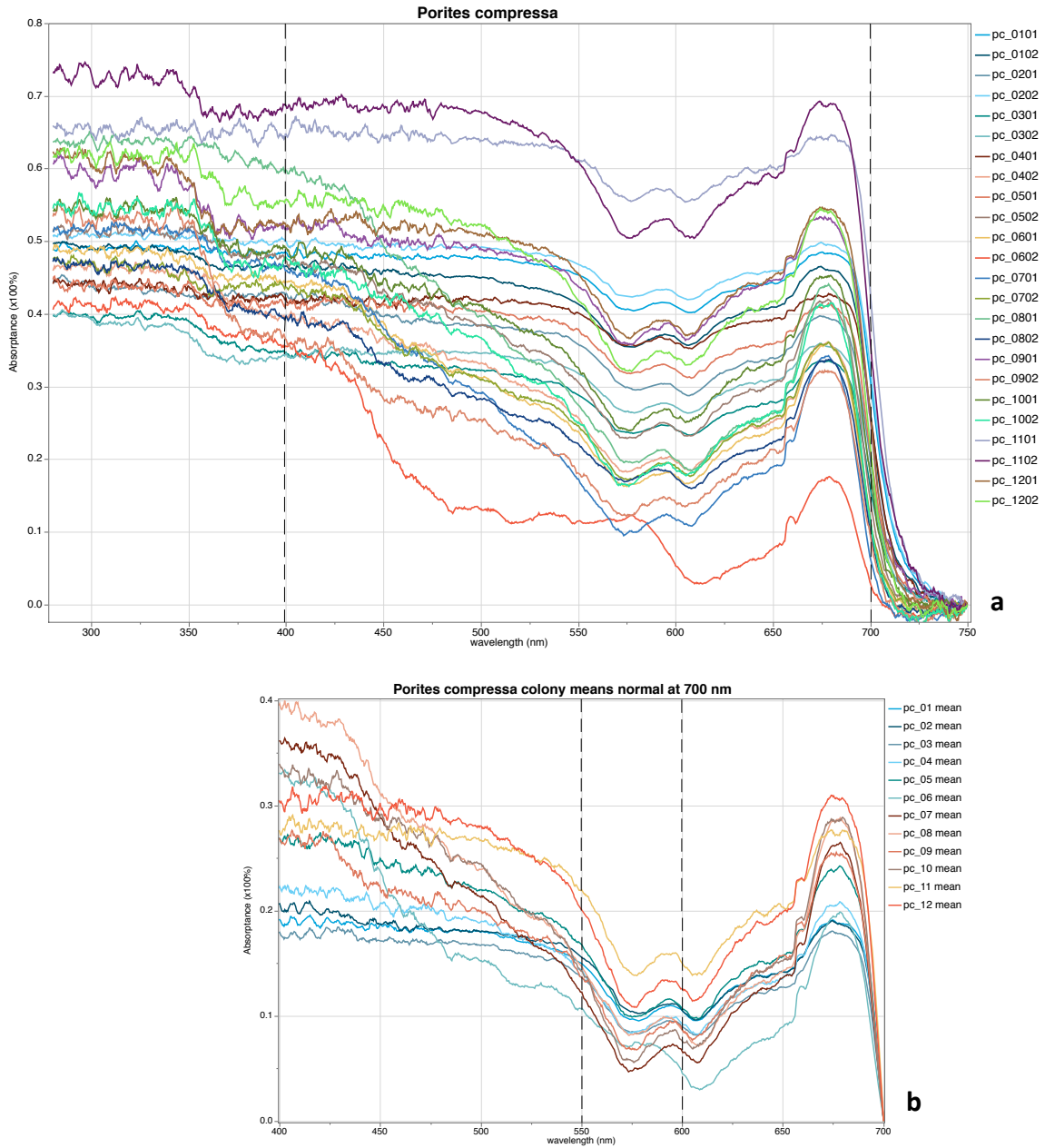
Figure 3.8. High light (HL) dinoflagellate spectrum standardized to 675 nm. All wavelengths are ratios to the value at 675 nm.
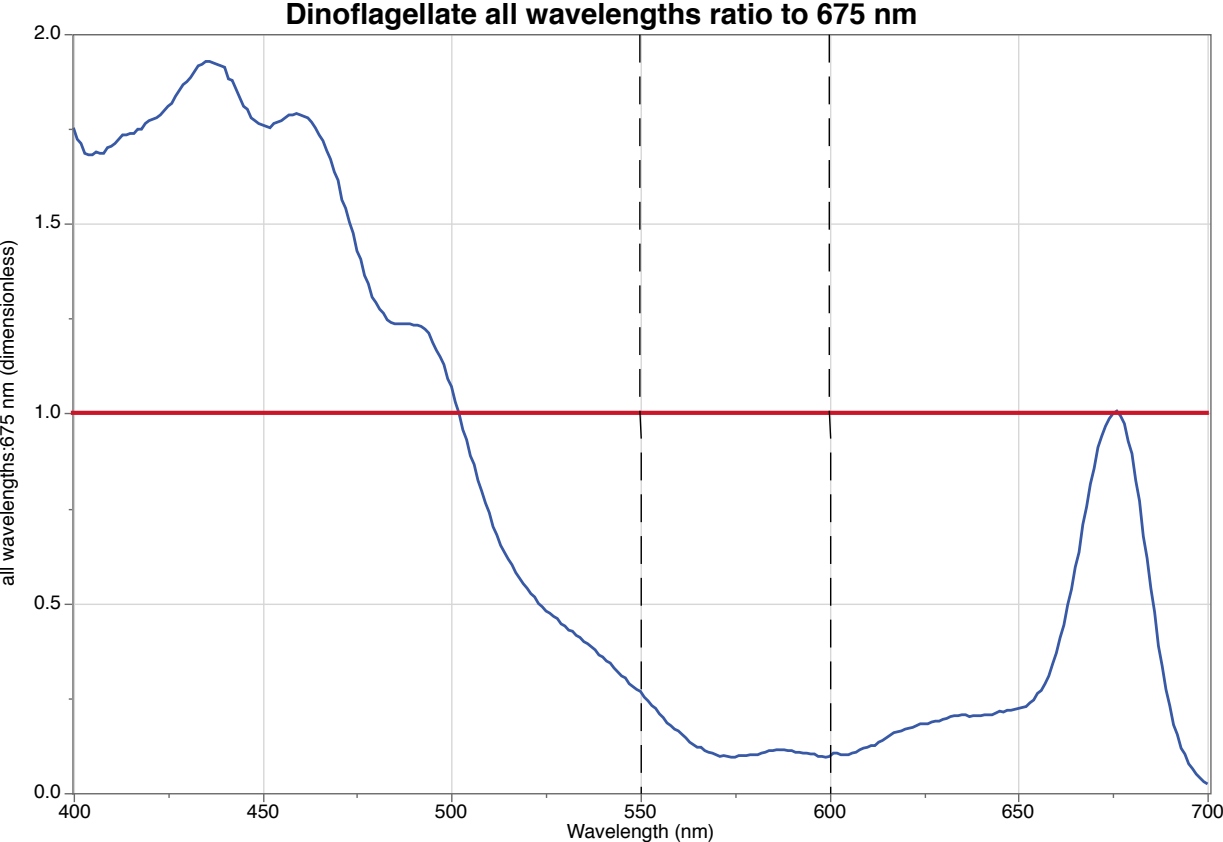
Figure 3.9. *Montipora flabellata* coral ratio to dinoflagellate ratio. Whole coral ratio of all wavelengths to value at 675 nm divided by same ratios in dinoflagellate spectrum. Resulting values are dimensionless and describe the difference between the spectra. Area of interest highlighted between 550–600 nm with dotted lines. Red line marks the value of 1 (675 nm).
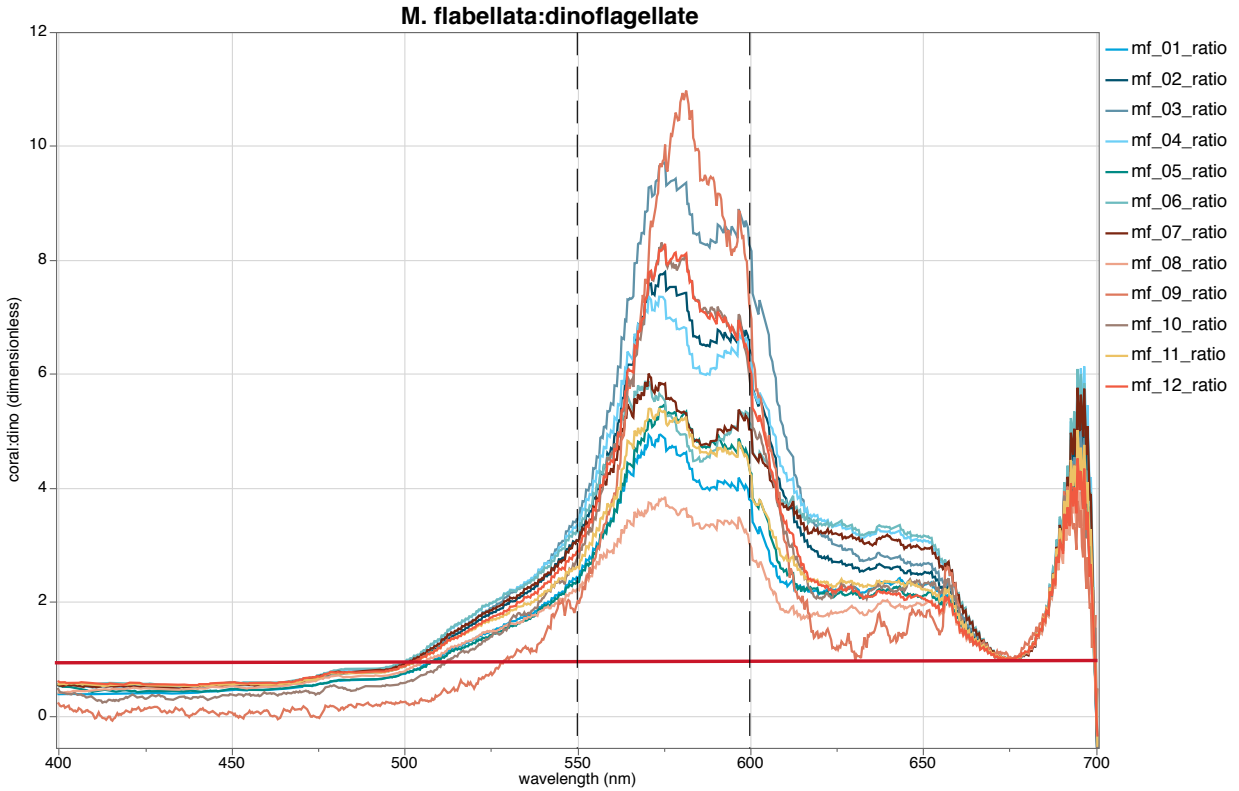
Figure 3.10. *Montipora patula* coral ratio to dinoflagellate ratio. Whole coral ratio of all wavelengths to value at 675 nm divided by same ratios in dinoflagellate spectrum. Resulting values are dimensionless and describe the difference between the spectra. Area of interest highlighted between 550–600 nm with dotted lines. Red line marks the value of 1 (675 nm).
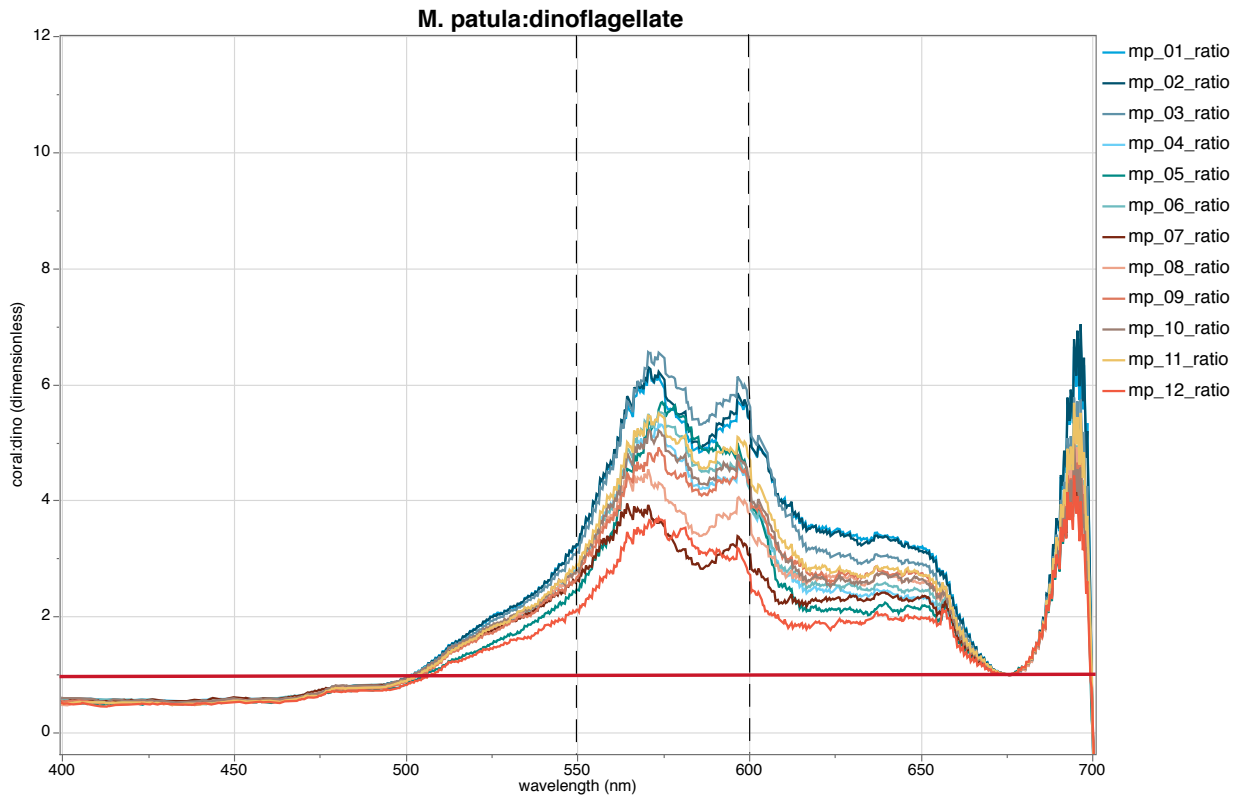
Figure 3.11. *Leptastrea purpurea* coral ratio to dinoflagellate ratio. Whole coral ratio of all wavelengths to value at 675 nm divided by same ratios in dinoflagellate spectrum. Resulting values are dimensionless and describe the difference between the spectra. Area of interest highlighted between 550–600 nm with dotted lines. Red line marks the value of 1 (675 nm).
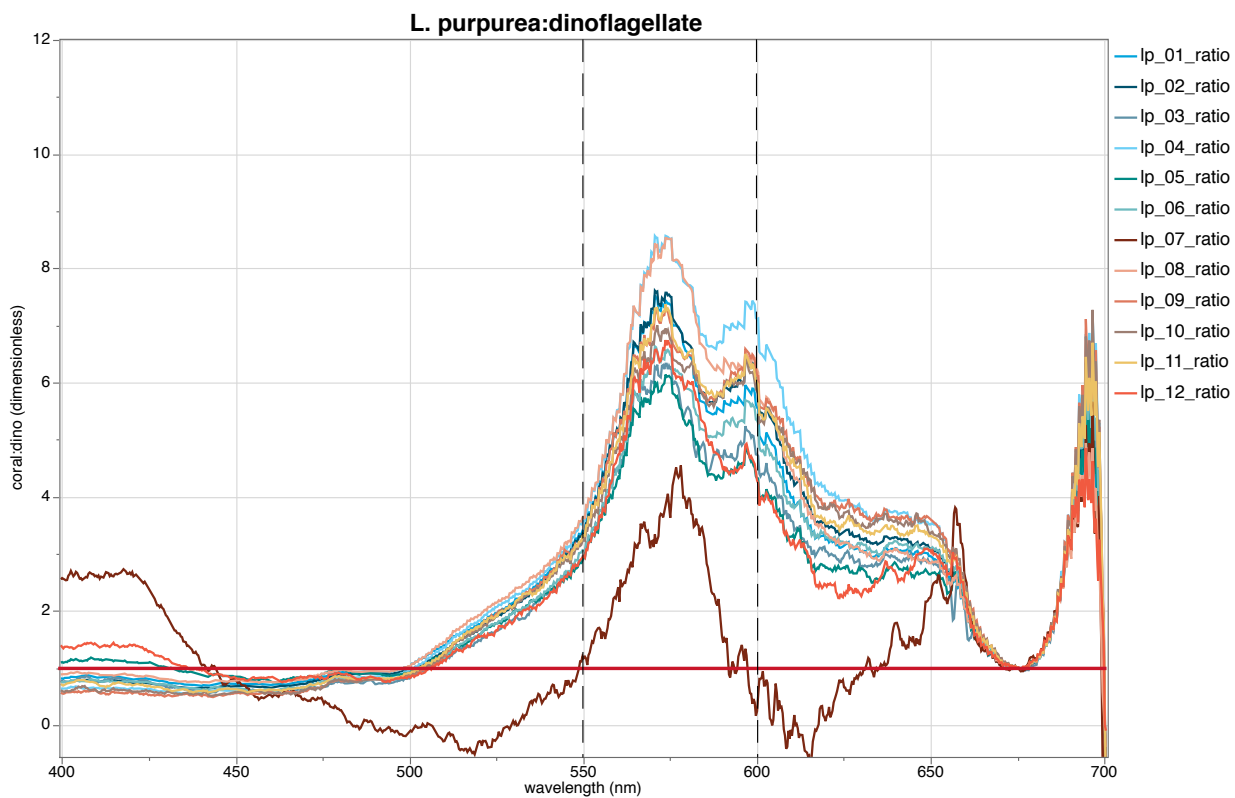
Figure 3.12. *Porites compressa* coral ratio to dinoflagellate ratio. Whole coral ratio of all wavelengths to value at 675 nm divided by same ratios in dinoflagellate spectrum. Resulting values are dimensionless and describe the difference between the spectra. Area of interest highlighted between 550–600 nm with dotted lines. Red line marks the value of 1 (675 nm).
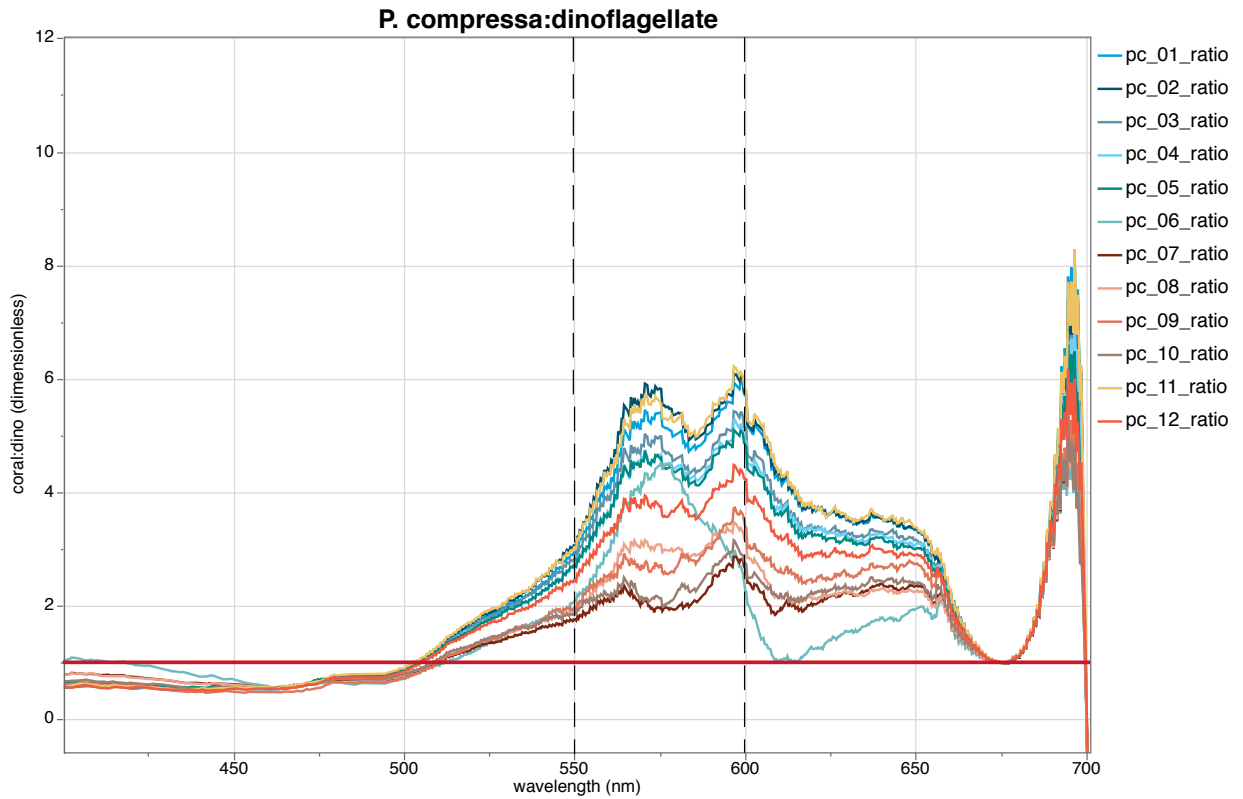
Figure 3.13. Distribution of photosynthetic parameter means (a) ΔNPQ (blue), (b) F_v/F_m (red), (c) ETR_{max} (green) with normal quantile plot by species. *Montipora flabellata* (top), *M. patula* (bottom).
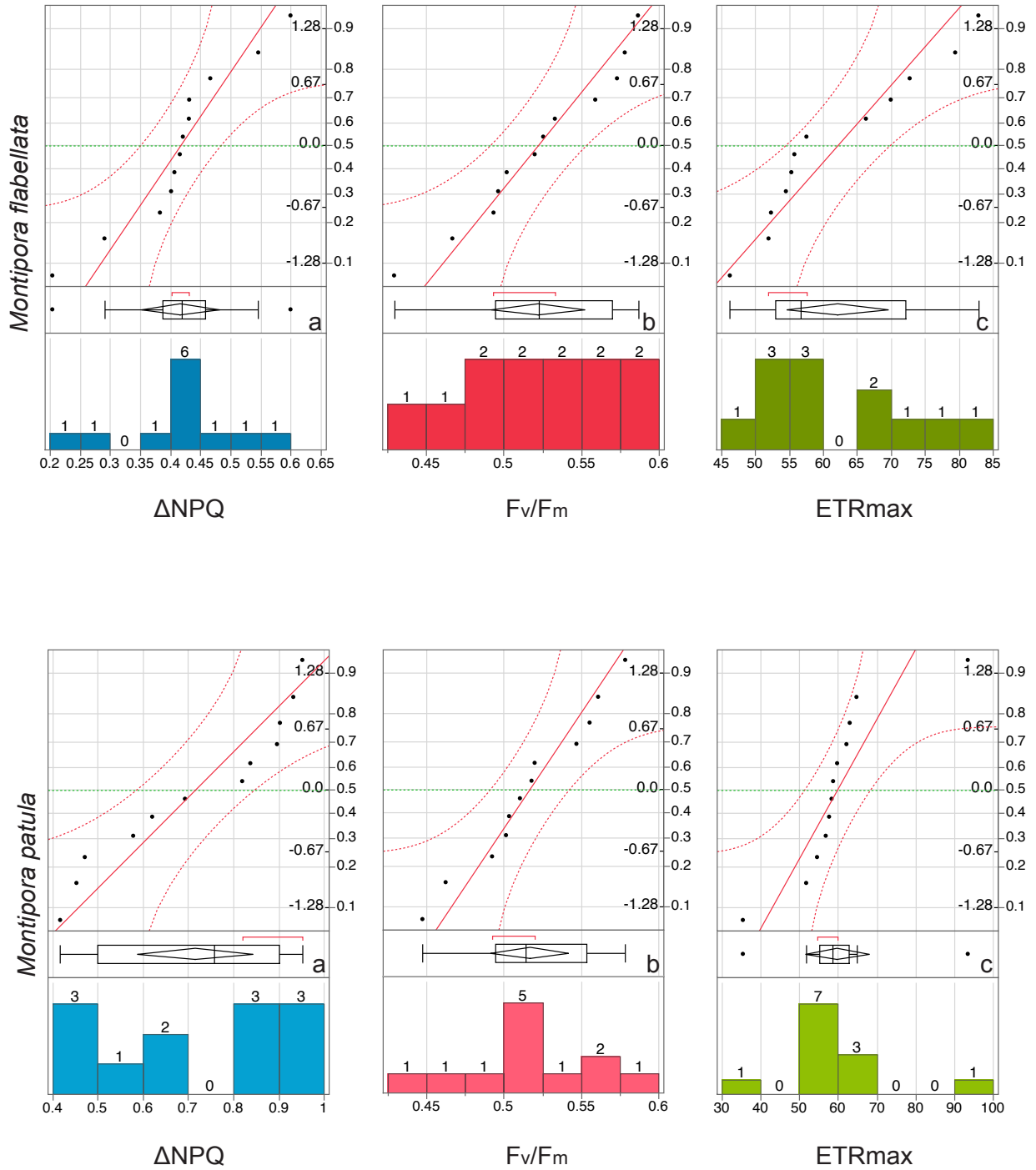
Figure 3.14. Distribution of photosynthetic parameter means (a) ΔNPQ (blue), (b) F_v/F_m (red), (c) ETR_{max} (green) with normal quantile plot by species. *Leptastrea purpurea* (top), *Porites compressa* (bottom).
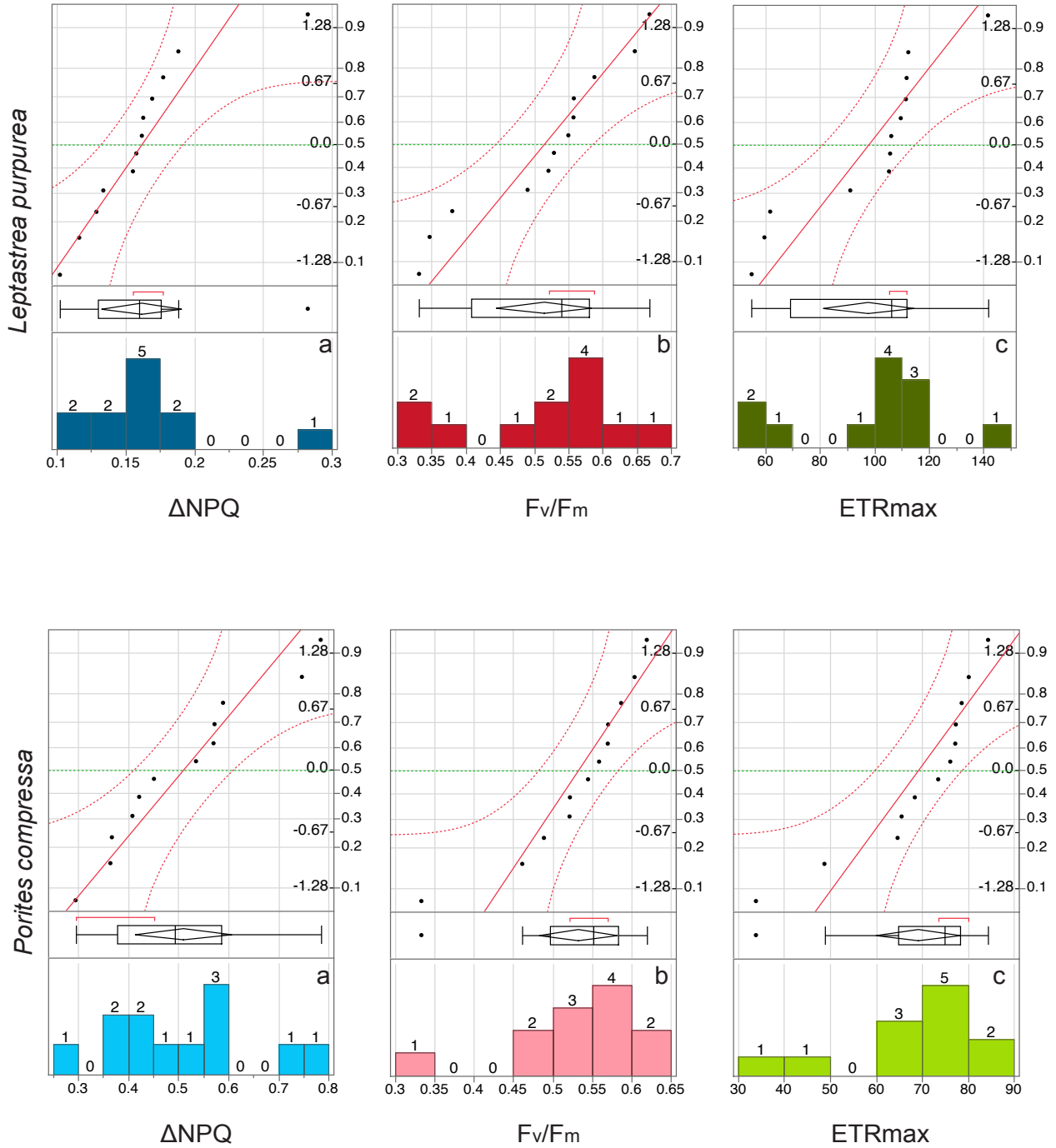
Figure 3.15. Distribution of photosynthetic parameter means for E_k (aqua) with normal quantile plot by species. *Montipora flabellata* (top left), *M. patula* (top right). *Leptastrea purpurea* (bottom left), *Porites compressa* (bottom right).
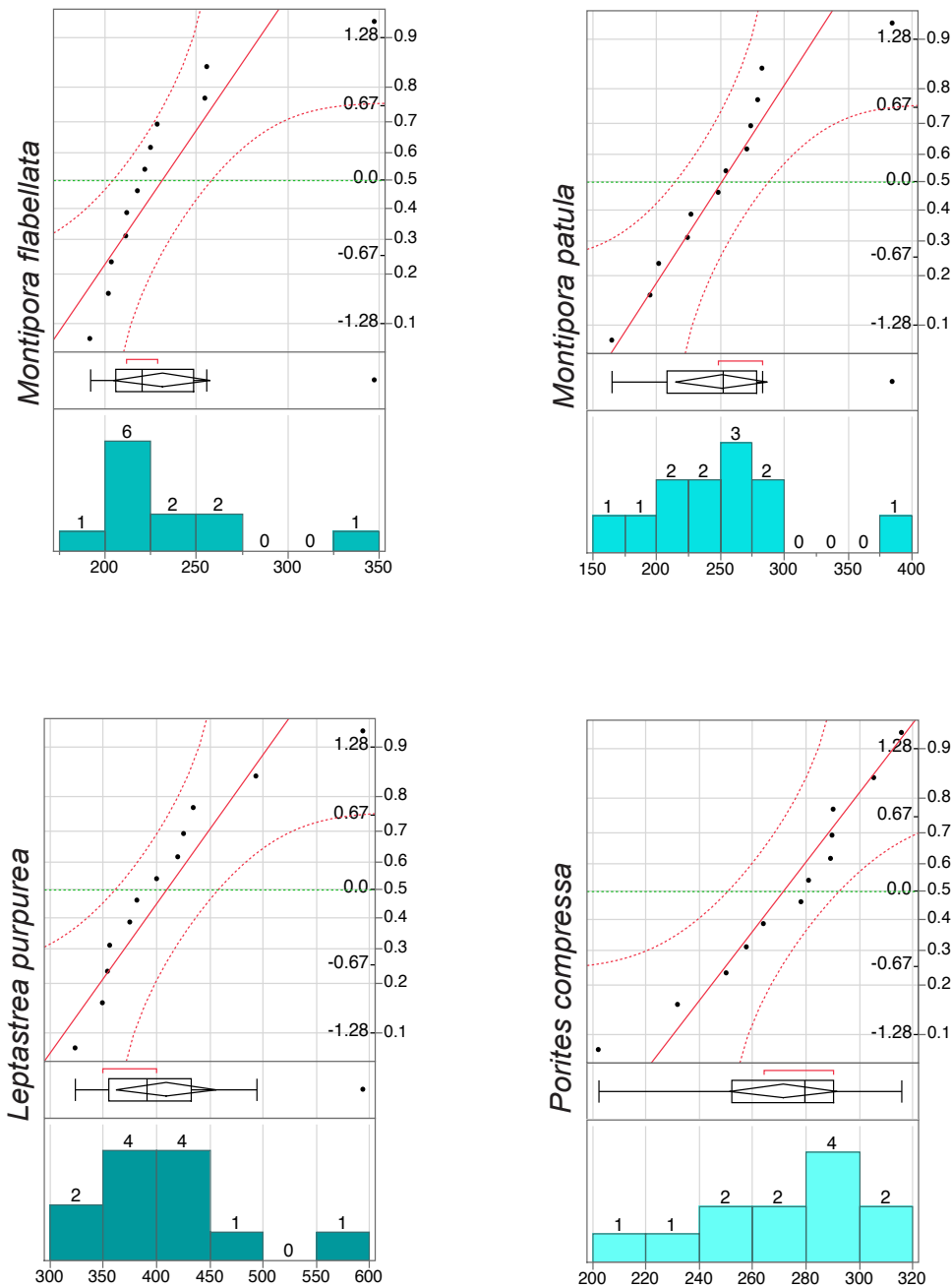
Figure 3.16. One-way ANOVA for ΔNPQ by colony means for all species (a), and Fv/Fm (b). MF = *Montipora flabellata*, MP = *Montipora patula*, LP = *Leptastrea purpurea*, PC = *Porites compressa*

Figure 3.17. One-way ANOVA for ETR$_{max}$ by colony means for all species (a), and E$_k$ (b). MF = *Montipora flabellata*, MP = *Montipora patula*, LP = *Leptastrea purpurea*, PC = *Porites compressa*
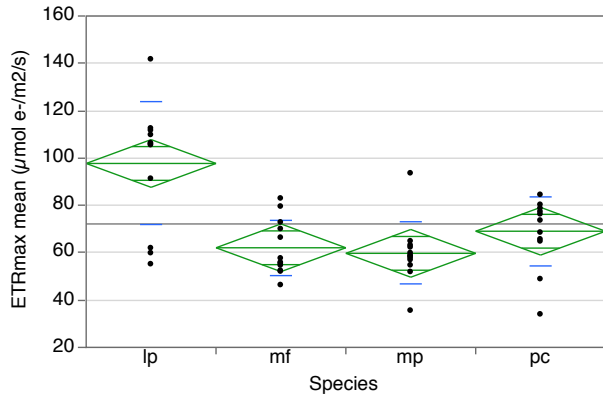
Rsquare		0.454681
Adj Rsquare		0.417501
Root Mean Square Error		17.32809
Mean of Response		72.15529
Observations (or Sum Wgts)		48

Source	DF	Sum of Squares	Mean Square	F Ratio	Prob > F
Species	3	11015.675	3671.89	12.2289	<.0001*
Error	44	13211.566	300.26		
C. Total	47	24227.241			

Level	Number	Mean	Std Error	Lower 95%	Upper 95%
lp	12	97.7100	5.0022	87.629	107.79
mf	12	62.0904	5.0022	52.009	72.17
mp	12	59.7381	5.0022	49.657	69.82
pc	12	69.0827	5.0022	59.001	79.16

Std Error uses a pooled estimate of error variance

Test	F Ratio	DFNum	DFDen	Prob > F
O'Brien[.5]	2.8357	3	44	0.0489*
Brown-Forsythe	1.4046	3	44	0.2541
Levene	3.5109	3	44	0.0228*
Bartlett	3.0472	3	.	0.0275*

Welch Anova testing Means Equal, allowing Std Devs Not Equal

F Ratio	DFNum	DFDen	Prob > F
7.0682	3	23.932	0.0014*

a
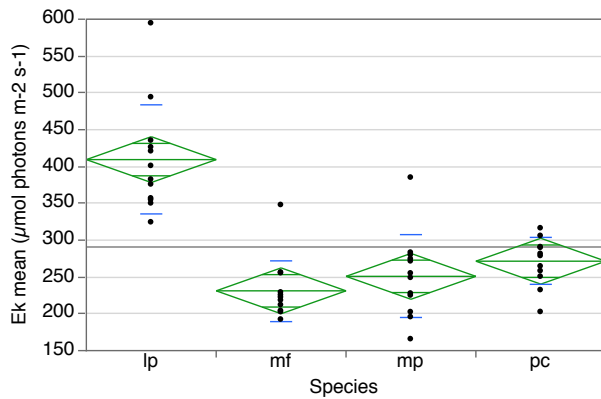
Rsquare		0.650974
Adj Rsquare		0.627177
Root Mean Square Error		53.51503
Mean of Response		290.7078
Observations (or Sum Wgts)		48

Source	DF	Sum of Squares	Mean Square	F Ratio	Prob > F
Species	3	235023.02	78341.0	27.3551	<.0001*
Error	44	126009.77	2863.9		
C. Total	47	361032.79			

Level	Number	Mean	Std Error	Lower 95%	Upper 95%
lp	12	409.373	15.448	378.24	440.51
mf	12	231.183	15.448	200.05	262.32
mp	12	250.848	15.448	219.71	281.98
pc	12	271.427	15.448	240.29	302.56

Std Error uses a pooled estimate of error variance

Test	F Ratio	DFNum	DFDen	Prob > F
O'Brien[.5]	1.0943	3	44	0.3616
Brown-Forsythe	1.4963	3	44	0.2287
Levene	1.6734	3	44	0.1865
Bartlett	2.7343	3	.	0.0420*

Welch Anova testing Means Equal, allowing Std Devs Not Equal

F Ratio	DFNum	DFDen	Prob > F
17.0154	3	23.54	<.0001*

b

Table 3.1. Dinoflagellate ratio of all wavelengths to value at **675 nm** (top row). Ratio of ratios: coral colony (left column) ratio of all wavelengths to the value at 675 nm divided by the dinoflagellate ratio in top row. mf = *Montipora flabellata*, mp = *Montipora patula*, lp = *Leptastrea purpurea*, pc = *Porites compressa*

	420 nm	440 nm	460 nm	540 nm	574 nm	578 nm	588 nm	597 nm
Dinoflagellate	1.772	1.912	1.787	0.359	0.094	0.097	0.114	0.097
mf_01	0.401	0.411	0.451	1.939	4.925	4.720	3.989	4.140
mf_02	0.540	0.520	0.557	2.394	7.740	7.526	6.498	6.889
mf_03	0.513	0.501	0.536	2.598	9.663	9.410	8.251	8.824
mf_04	0.559	0.534	0.569	2.605	7.355	6.941	5.999	6.671
mf_05	0.440	0.428	0.457	1.903	5.416	5.321	4.721	4.802
mf_06	0.561	0.533	0.583	2.540	5.630	5.172	4.549	5.341
mf_07	0.532	0.523	0.542	2.418	5.835	5.519	4.755	5.338
mf_08	0.487	0.478	0.517	1.858	3.795	3.617	3.339	3.444
mf_09	0.084	0.059	0.098	1.347	9.650	10.457	9.363	8.748
mf_10	0.330	0.327	0.394	2.067	8.239	7.898	7.069	6.981
mf_11	0.553	0.526	0.555	2.137	5.368	5.219	4.602	4.769
mf_12	0.575	0.545	0.588	2.266	8.171	8.109	6.987	6.867
mp_01	0.533	0.536	0.572	2.525	6.099	5.557	4.904	5.682
mp_02	0.542	0.545	0.559	2.524	6.183	5.640	4.983	5.804
mp_03	0.542	0.540	0.568	2.455	6.523	6.113	5.370	6.104
mp_04	0.553	0.563	0.586	2.258	5.298	4.871	4.213	4.565
mp_05	0.532	0.496	0.523	2.003	5.625	5.606	4.854	4.931
mp_06	0.571	0.552	0.596	2.241	5.516	5.261	4.496	4.722
mp_07	0.563	0.552	0.585	2.186	3.639	3.278	2.873	3.363
mp_08	0.528	0.508	0.552	2.279	4.291	3.923	3.455	4.036
mp_09	0.532	0.486	0.532	2.236	4.874	4.475	4.106	4.635
mp_10	0.546	0.547	0.585	2.290	5.185	4.771	4.286	4.764
mp_11	0.524	0.493	0.551	2.324	5.482	5.050	4.570	5.069
mp_12	0.494	0.499	0.528	1.795	3.678	3.425	3.088	3.148
lp_02	0.734	0.648	0.649	2.608	7.559	6.887	5.676	6.372
lp_03	0.761	0.583	0.585	2.309	6.298	5.582	4.738	5.187
lp_04	0.645	0.576	0.600	2.736	8.559	8.009	6.599	7.396
lp_05	1.091	0.874	0.773	2.339	6.115	5.537	4.340	4.834
lp_06	0.761	0.622	0.619	2.370	6.561	6.145	5.051	5.677
lp_07	2.659	1.091	0.531	0.556	3.949	4.393	2.221	1.168
lp_08	0.879	0.749	0.751	2.814	8.526	8.064	6.227	6.508
lp_09	0.556	0.509	0.571	2.605	7.277	6.532	5.711	6.565
lp_10	0.590	0.539	0.556	2.545	6.919	6.315	5.630	6.374
lp_11	0.699	0.590	0.617	2.557	7.311	6.574	5.749	6.458
lp_12	1.394	0.961	0.838	2.257	6.712	6.079	4.776	4.877
pc_01	0.543	0.504	0.533	2.363	5.392	5.091	4.902	5.906
pc_02	0.581	0.516	0.533	2.478	5.839	5.475	5.048	6.082
pc_03	0.544	0.502	0.528	2.331	4.970	4.662	4.446	5.426
pc_04	0.607	0.532	0.554	2.230	4.656	4.511	4.306	5.269
pc_05	0.644	0.566	0.571	2.211	4.649	4.449	4.230	5.083
pc_06	0.983	0.758	0.588	1.757	4.439	4.475	3.468	2.948
pc_07	0.756	0.637	0.563	1.615	1.967	1.949	2.204	2.870
pc_08	0.742	0.628	0.568	1.717	3.072	2.995	2.986	3.464
pc_09	0.599	0.488	0.483	1.724	2.735	2.597	2.924	3.712
pc_10	0.634	0.557	0.556	1.713	2.173	2.078	2.483	3.132
pc_11	0.591	0.536	0.572	2.491	5.663	5.331	5.162	6.201
pc_12	0.568	0.516	0.547	2.097	3.824	3.643	3.702	4.461

Figure 3.18. Distribution with normal quantile plot for ratio of coral absorbance wavelengths standardized to 675 nm from all colonies and species divided by same ratio in dinoflagellates (coral:dino ratios).

100.0%	maximum	9.646455842	Mean	5.7768507
99.5%		9.646455842	Std Dev	1.8015787
97.5%		9.642078548	Std Err Mean	0.2600355
90.0%		8.2566594051	Upper 95% Mean	6.2999747
75.0%	quartile	7.2249817085	Lower 95% Mean	5.2537268
50.0%	median	5.609827001	N	48
25.0%	quartile	4.6523166305		
10.0%		3.592110314		
2.5%		2.001165155		
0.5%		1.950809597		
0.0%	minimum	1.950809597		
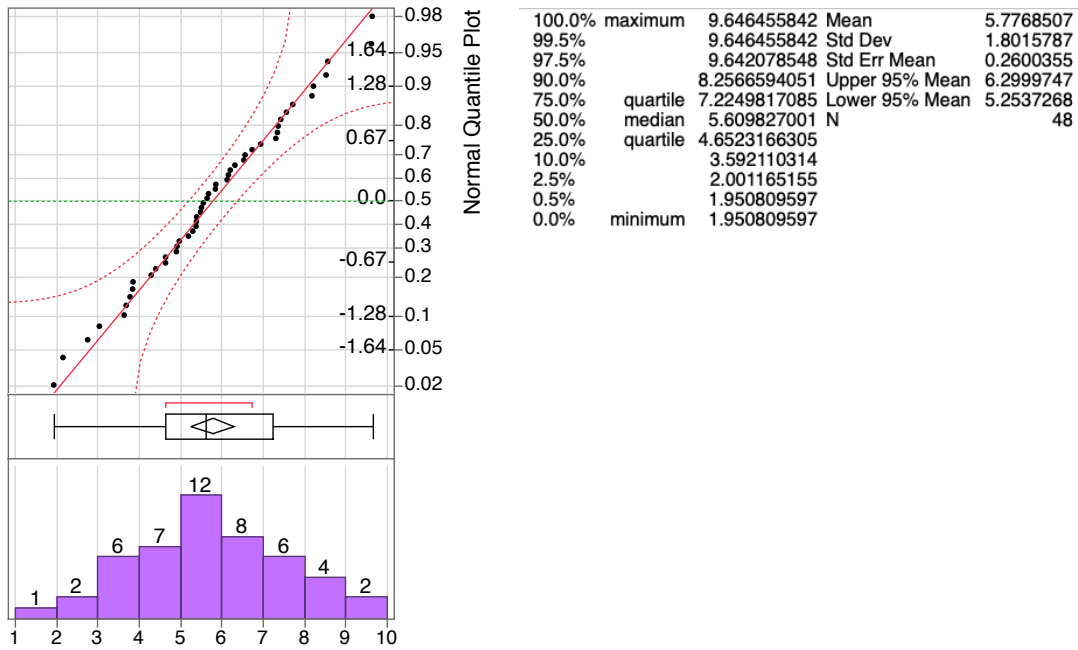
Figure 3.19. (a) Distribution of coral:dino ratios at 574 nm by species. (b) One-way ANOVA for coral:dino ratio (dimensionless) at 574 nm by species.
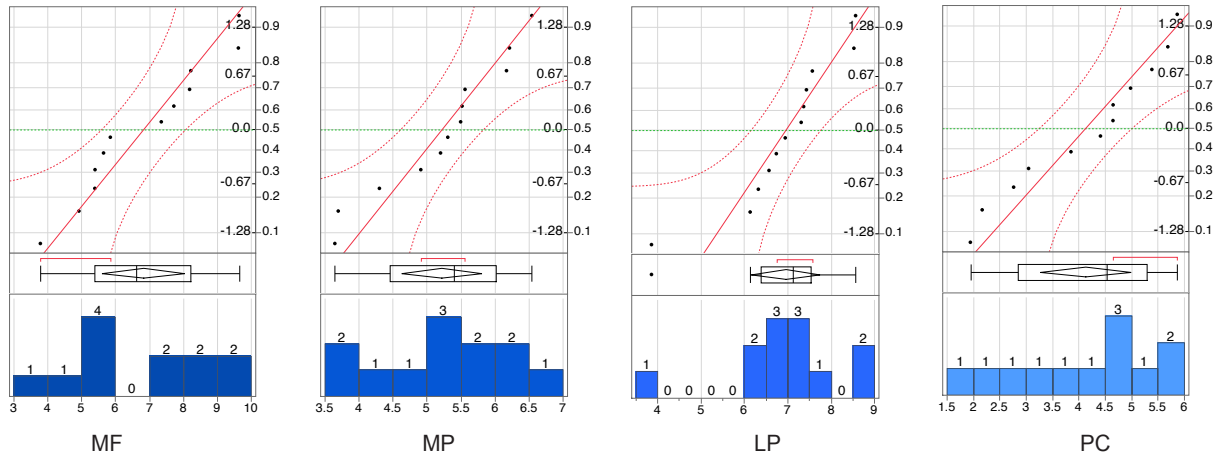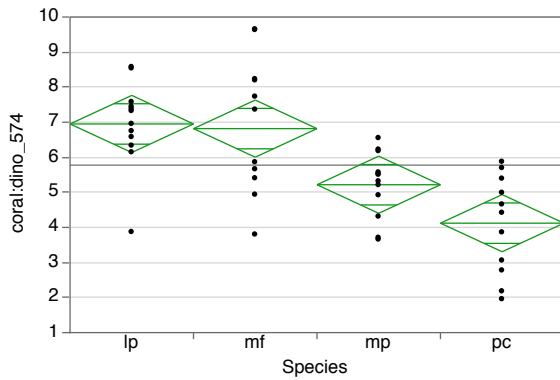
Rsquare	0.433829	
Adj Rsquare	0.395226	
Root Mean Square Error	1.401038	
Mean of Response	5.776851	
Observations (or Sum Wgts)	48	

Source	DF	Sum of Squares	Mean Square	F Ratio	Prob > F
Species	3	66.17936	22.0598	11.2383	<.0001*
Error	44	86.36788	1.9629		
C. Total	47	152.54724			

Level	Number	Mean	Std Error	Lower 95%	Upper 95%
lp	12	6.95080	0.40444	6.1357	7.7659
mf	12	6.81776	0.40444	6.0027	7.6329
mp	12	5.21736	0.40444	4.4023	6.0325
pc	12	4.12148	0.40444	3.3064	4.9366

Test	F Ratio	DFNum	DFDen	Prob > F
O'Brien[.5]	2.4665	3	44	0.0746
Brown-Forsythe	3.1619	3	44	0.0338*
Levene	3.7622	3	44	0.0173*
Bartlett	1.8277	3	.	0.1397

Welch Anova testing Means Equal, allowing Std Devs Not Equal

F Ratio	DFNum	DFDen	Prob > F
11.2487	3	23.841	<.0001*

135

Table 3.2. R-squared values for least squares regression linear fit (top) and quadratic (2) fit (bottom) for all photosynthetic parameters tested per species.

	M. flabellata	*M. patula*	*L. purpurea*	*P. compressa*
r^2 - linear				
ΔNPQ	0.0895	0.0198	0.0001	0.0006
F_v/F_m	$5.655e^{-5}$	0.0003	0.0071	0.0602
ETR_{max}	0.0443	0.1602	0.1841	0.1182
E_k	0.0949	0.3440	0.2638	0.4479
r^2 – quadratic (2)				
ΔNPQ	0.2260	0.1434	0.0002	0.2477
F_v/F_m	0.0002	0.1194	0.0134	0.2829
ETR_{max}	0.0484	0.3979	0.2997	0.3112
E_k	0.1254	0.4508	0.6431	0.4914

Figure 3.20. Linear (red line) and quadratic (2; green line) regression plots for each photosynthetic parameter tested per species. Species in columns with individual parameters in rows. MF = *Montipora flabellata*, MP = *Montipora patula*, LP = *Leptastrea purpurea*, PC = *Porites compressa*
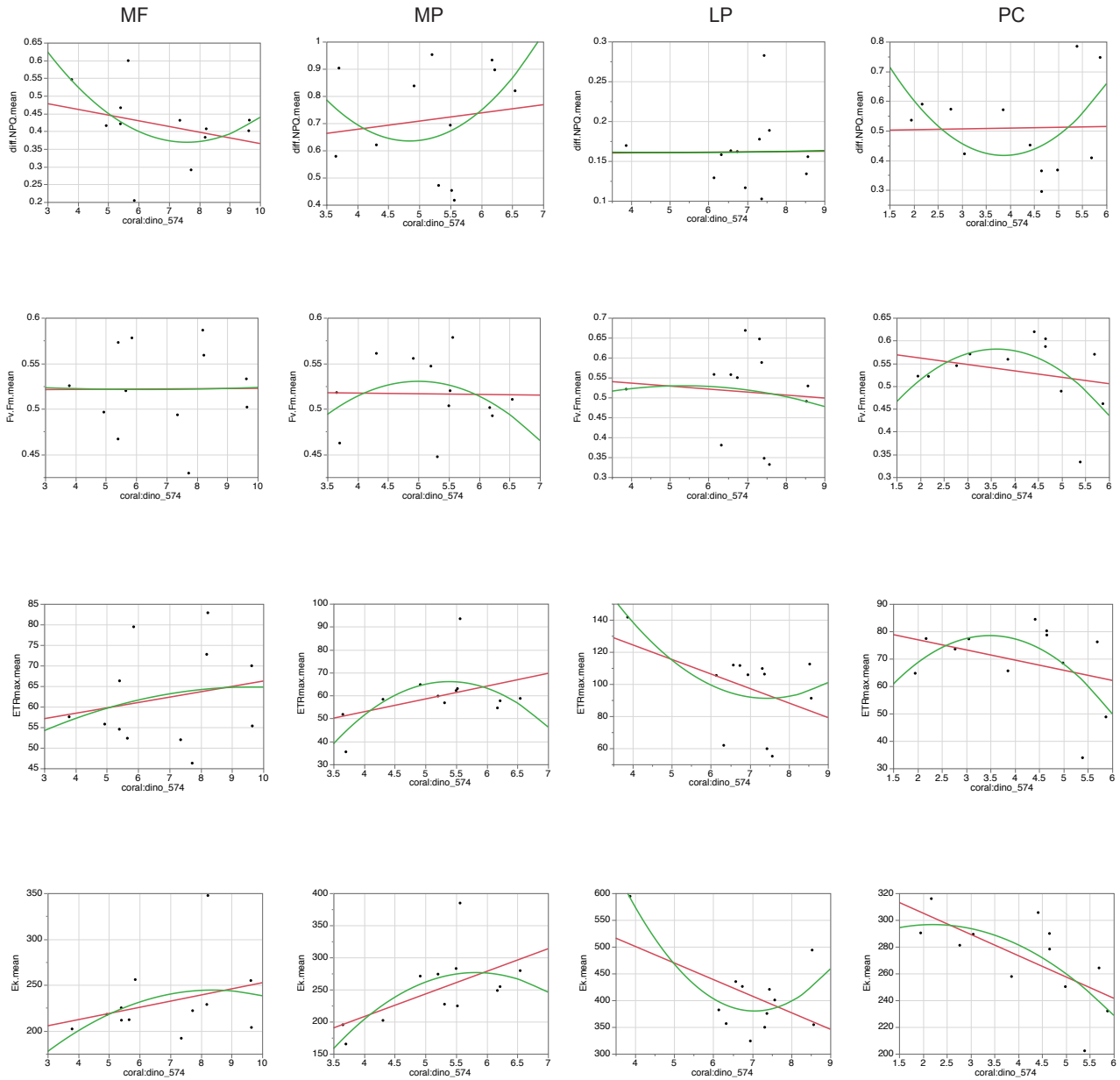
Figure 3.21. Absorbance spectra (log scale) for raw extracts from individual *M. flabellata* coral fragments. (a) Colonies 1-11, (b) colonies 12-22.
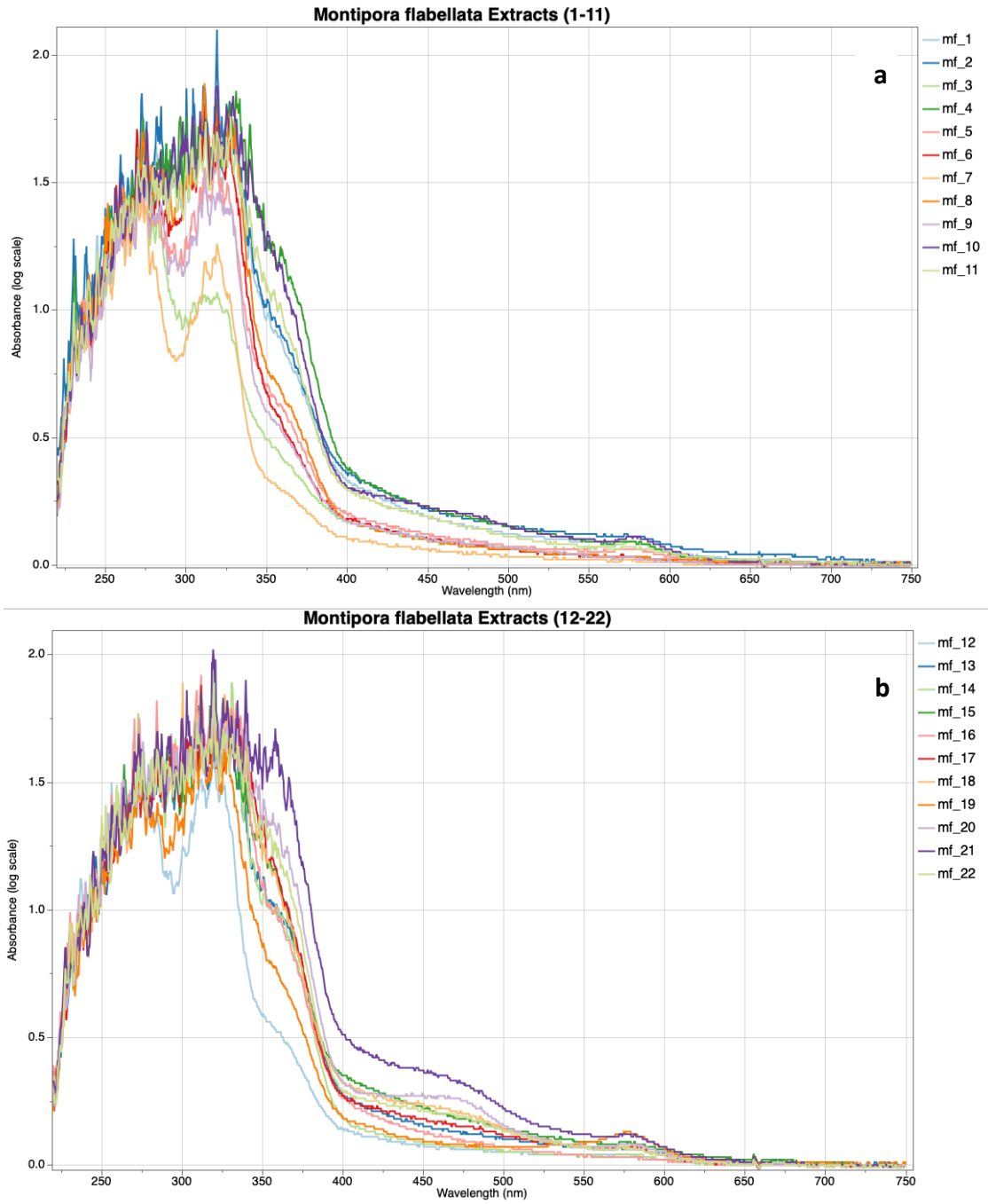
Figure 3.22. Regression plots with linear (red line) and quadratic (2; green line) fit lines for coral raw extract values at 583 nm as explanatory variable and photosynthetic parameters (a) ΔNPQ, (b) F_v/F_m, (c) ETR_{max}, and (d) E_k.
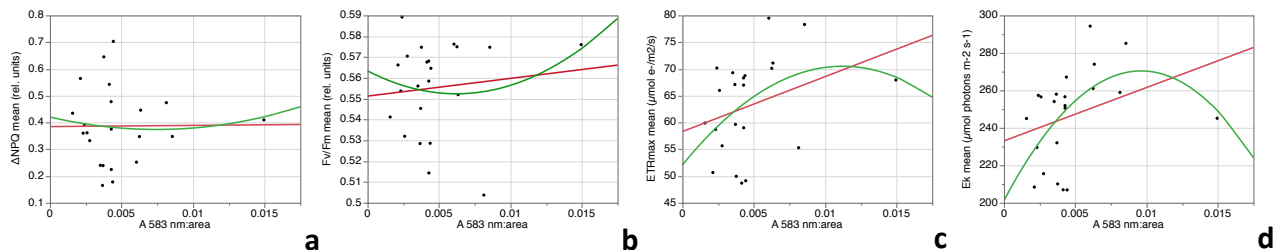
Table 3.3. Summary statistics for regression plots in Fig. 3.22.

	ΔNPQ	F_v/F_m	ETR_{max}	E_k
r^2 - linear	$8.072e^{-5}$	0.012309	0.109076	0.109807
r^2 – quadratic (2)	0.006025	0.04035	0.154519	0.263962
Mean of Response	0.387205	0.555335	63.20549	246.6263
Observations	22	22	22	22

Figure 3.23. Regression plots with linear (red line) and quadratic (2; green line) fit lines for coral raw extract values at 330 nm as explanatory variable and photosynthetic parameters (a) ΔNPQ, (b) F_v/F_m, (c) ETR_{max}, and (d) E_k.

a

b

c

d
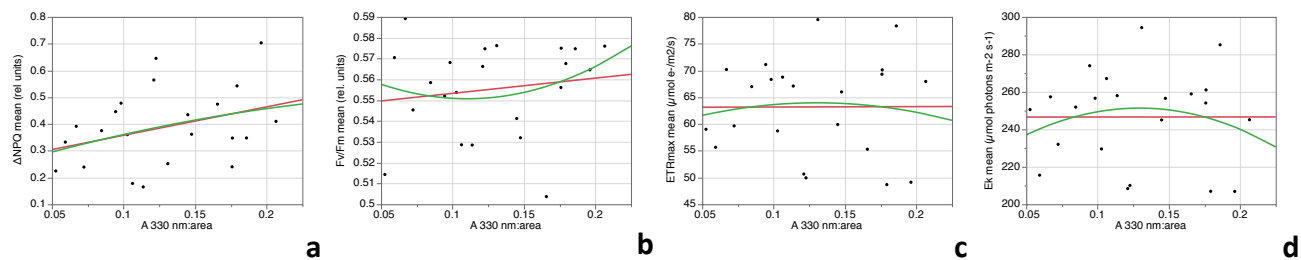
Table 3.4. Summary statistics for regression plots in Fig. 3.23.

	ΔNPQ	F_v/F_m	ETR_{max}	E_k
r² - linear	0.119988	0.023356	1.54e-5	5.749e-7
r² – quadratic (2)	0.120887	0.050892	0.006059	0.030505
Mean of Response	0.387205	0.555335	63.20549	246.6263
Observations	22	22	22	22

Figure 3.24. Absorbance spectra from Iglesias-Prieto & Trench (1997) for three cultured symbiotic dinoflagellates. Left to right: *Symbiodinium microadriaticum*, *Symbiodinium pilosum*, *Symbiodinium kawagutii*. Solid lines represent cells grown in high light, dotted lines for cells grow in low light. Used with permission.
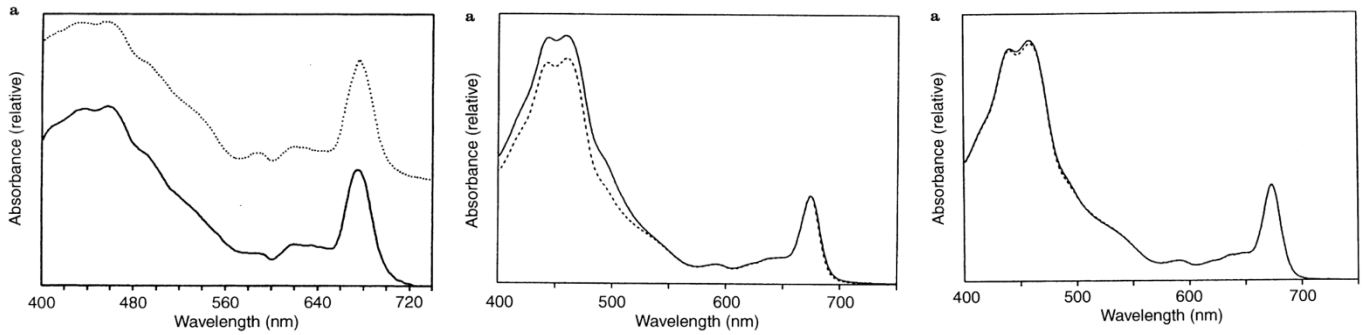
Table 3.5. Photosynthetic parameters by species. Low or high term in parenthesis reflects most efficient range for that parameter. Arrows indicate highest, lowest, or mid-range values among species. Red-filled arrows indicate criteria for highest efficiency met. Mean values for *M. flabellata* dataset 1 on top (black) and dataset 2 below (red). MF = *Montipora flabellata*, MP = *Montipora patula*, LP = *Leptastrea purpurea*, PC = *Porites compressa*

	ΔNPQ (low)	F_v/F_m (high)	ETR_{max} (high)	E_k (low)	Habitat
MF	0.417 0.387 ⟷	0.522 0.555 ⟷	62.09 63.21 ⟷	231.2 246.6 ⬇	High water flow, high to low particulate
MP	0.715 ⬆	0.517 ⟷	59.74 ⟷	250.8 ⟷	Med. water flow, med. particulate
LP	0.162 ⬇	0.514 ⟷	97.71 ⬆	409.4 ⬆	Low water flow, high suspended particulate
PC	0.509 ⟷	0. 532 ⟷	69.08 ⟷	271.2 ⟷	High to low water flow, high to low particulate

Figure 3.25. ETR vs. Irradiance (E) curve with mean ETR_{max} values plotted against mean E_k values for each species. Slope of line (α) reaches ETR_{max} at E_k.
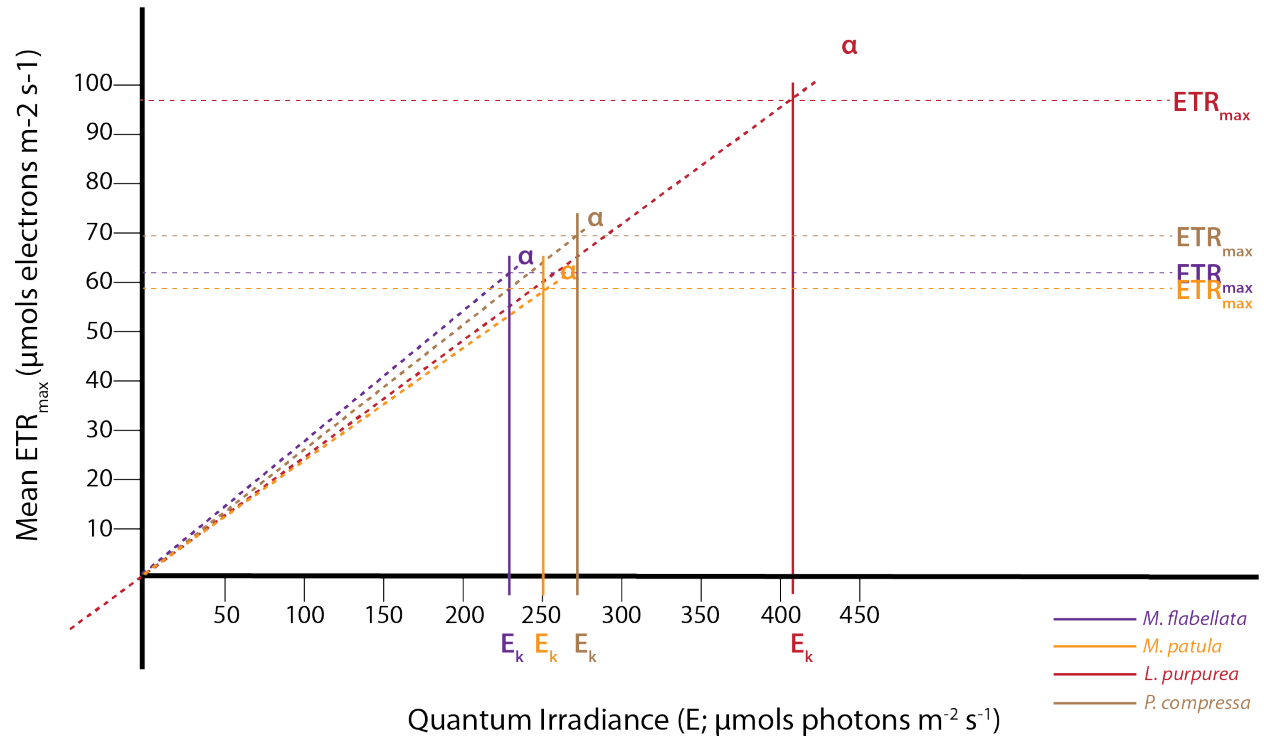
BENEFITS AND PITFALLS OF USING PULSE AMPLITUDE-MODULATED FLUOROMETRY FOR THE STUDY OF PHOTOCHEMISTRY IN CORALS

Angela Richards Donà

Abstract

Applications of Pulse Amplitude-Modulated (PAM) fluorometry for the study of photosynthesis in plants and algae are common and numerous, but its use becomes complicated when applied to corals. Light transport through the coral skeleton and across the surface can illuminate the sample several centimeters away from the light source. Coral tissue, coral host pigments, and the highly reflective skeleton may all contribute to confound the data, particularly if multiple measurements on one specimen are desired. This investigation used data from two separate experiments on several Hawaiian coral species to determine whether data from multiple, consecutive PAM measurements on an individual specimen can be accurately made despite the known light-scattering effects of coral skeletons. Experiment 1 involved following the health status of individual colony replicates over time as water temperatures were increased. Experiment 2 involved comparisons of replicates from two different light regimes. Linear mixed model results comparing multiple PAM measurements in both experiments showed no effect of a previous measurement on a subsequent measurement (three per specimen in Experiment 1 and two per specimen in Experiment 2). Importantly, most of the coral fragments were at least 5 cm^2 (both experiments) and the measurements were taken approximately 3 cm or more apart. F_v/F_m across the three measurements per individual in Experiment 1 was highly variable and best explained by random effects of the individual fragments (*Montipora flabellata* r^2 = 0.88; *Porites compressa* r^2 = 0.66; *Pocillopora meandrina* r^2 = 0.60). The high F_v/F_m variability, particularly in *M. flabellata* (n = 56), is evidence that multiple measurements should be taken to obtain a robust understanding of the specimen's photosynthetic efficiency. Experiment 2 *M. flabellata* fragments showed a significant difference in F_v/F_m between sun and shade treatments but no effect of multiple measurements in either treatment. Additionally, marked decreases in F_v/F_m were observed around midday in all species and in both experiments. This midday depression in optimal quantum yield puts a daily time limitation on PAM measurements for accurate and comparable data acquisition. These results show that multiple measurements on coral fragments are important and do not necessarily alter the dark-acclimation status at various points on individual fragments. Ideally, experimental design should include a minimum coral fragment size to allow for multiple PAM measurements and data acquisition should be planned to avoid midday depressions in photosynthetic efficiency.

Introduction

The partnership between stony corals and their intracellular, dinoflagellate symbionts is arguably the most productive partnership in coastal oceans. This intimate association has resulted in the construction of a physical ecosystem framework (Pearse and Muscatine 1971; Muscatine and Weis 1992) that supports, and has been instrumental in the evolution of, myriad species (Roberts et al. 2002; Price et al. 2011). The physiological design of this partnership is unique—unicellular algae are enclosed in membrane-bound vacuoles within coral gastrodermal cells—and entails nutrient and waste cycling that is efficient and mutually beneficial (Trench 1993; Wakefield et al. 2000; Davy et al. 2012). The algal endosymbionts translocate up to 95% of the photosynthate produced to their coral hosts (Falkowski et al. 1984; Muscatine et al. 1984; Davy et al. 2012), and in this manner up to 100% of the coral's nutritional needs are met (Muscatine et al. 1981, 1983). The symbionts, from the family Symbiodiniaceae (commonly termed "zooxanthellae"), are hosted in an exceptional light environment engineered to capture and retain incoming solar energy with high efficiency (Enrıquez et al. 2005; Kirk 2010; Marcelino et al. 2013). Unlike other algal habitats, incoming light energy that reaches the coral surface is either absorbed directly by top tier symbionts, is scattered across fractal coral skeleton surfaces (Enrıquez et al. 2005; Marcelino et al. 2013; Roth 2014; Swain et al. 2016), or is laterally transferred within tissue (Wangpraseurt et al. 2012, 2014) and diffused for eventual absorbance by lower tier symbionts. The light dynamics in the skeletal microenvironments optimize symbiont light harvesting by amplifying light thus countering the self-shading and/or "package effect" of numerous clustered chloroplasts and cells (Enrıquez et al. 2005; Kirk 2010; Marcelino et al. 2013). The number of cells is strictly controlled by the coral host whereas the number of chloroplasts is controlled by the symbionts and produced in quantities appropriate for the light environment (Muscatine et al. 1981; Kirk 2010). In high light environments, fewer cells and/or chloroplasts are required, whereas the opposite is true in lower light environments. In some coral species, skeletal microstructures (papillae or verrucae) that protrude outward from the surface of the coral aid in light-scattering and thus in optimizing light energy capture (Enriquez et al. 2005; Marcelino et al 2013; Swain et al. 2016). These and other skeletal microstructures as well as the overall colony morphology are highly influential in the species' ability to utilize incident irradiance for colony growth, reproduction, and maintenance. Coral tissue and skeleton thus play important roles in the light dynamics and by extension, the success of the coral holobiont.

Coral colony and skeletal microstructure morphologies are a function of the prevailing local environmental conditions—particularly water flow and light (Todd 2008). Colony morphology is highly variable between and within species, with forms as diverse as massive boulders and small branchlets potentially competing for reef space. Species that grow rapidly, lay down thin, skeletal frameworks that

may be highly random and interwoven. In general, rapidly-growing corals build low-density and poorly-defined skeletal features, particularly surrounding the polyps (Veron and Stafford-Smith 2000). In Hawai'i, the branching *Pocillopora meandrina* Dana and *Porites compressa* Dana, and encrusting *Montipora flabellata* Studer, represent relatively fast-growing coral species with competitive life-history strategies (Darling et al. 2012). In contrast, *Leptastrea purpurea* Dana colonies have higher skeletal densities and build well-defined walls and/or corallites. These "weedy" corals are slower-growing but tend to be highly successful in disturbed habitats such as the coastal lagoon areas of Kāne'ohe Bay. Competitive Indo-Pacific species have a mean growth rate of 47.18 mm yr^{-1} whereas weedy Indo-Pacific corals have a mean growth rate of 16.97 mm yr^{-1} (Darling et al. 2012). Although these mean growth rates apply to several species within each life-history grouping and not specifically the aforementioned Hawaiian species, the rates are good, contrasting indicators of the differences in skeletal investment, which often directly relates to light-scattering ability. Faster-growing morphologies are generally capable of longer light transport that may benefit shaded areas of the colony (Marcelino et al. 2013).

The quantity and energy of incident solar irradiance on the coral surface depend on many factors, i.e., time of day, cloud cover, depth, tides, and water clarity. Each light particle (photon) that reaches the coral surface will undergo one of three processes: photochemistry, fluorescence, or non-photochemical quenching (NPQ). These processes are in competition for photons and an efficiency increase in one process will necessarily result in a decrease in efficiency of the others (Schreiber 2004). Total chlorophyll fluorescence is small (0.5–5%), whereas photochemistry (~25–30%), and NPQ (~70-75%) are the more common pathways for absorbed photons. Photochemistry is the primary objective for photoautotrophic organisms, however, lower-energy light re-admission (fluorescence), and dissipation of light energy as heat (NPQ) are methods to rid an organism of excess energy and are important processes for organism health and stability (Schreiber 2004; Taiz and Zeiger 2010). The dependent relationship between processes allows PAM fluorometry to determine photosynthetic efficiency (Schreiber 2004) through direct measurement of chlorophyll fluorescence yield in a sample while photochemistry is transiently reduced to zero. The contribution of the third process, NPQ, is determined through simple calculation (Maxwell and Johnson 2000; Schreiber 2004).

PAM fluorometry is commonly used for corals despite the complicated nature of variable coral colony morphologies, surface complexities, and unknown densities of symbionts in the underlying epithelia. One useful technique—a rapid light curve (RLC)— involves the induction of photosynthesis at increasing levels of actinic light (AL; drives photosynthesis) over the course of time (Fig. 4.1). The levels of increasing actinic light and intervals between measurements are pre-defined, ideally with the intention of reaching a saturated electron transport rate (ETR), followed by either a plateau or a decrease in ETR. In some organisms, the decrease in ETR can indicate photoinhibition but may also indicate noise due to

147

supersaturation from high light intensities (G. Johnsen pers comm). At the start of an RLC on dark-acclimated samples, the PAM fiber optic probe emits a low frequency measuring light (ML) that is too weak to drive photosynthesis but is able to stimulate and read baseline fluorescence (F_0). This is followed by a short saturating light pulse (SP) that "closes" all Photosystem II (PSII) reaction centers (reduces photochemistry to zero). The term "closed", as it relates to PSII, is defined as the oxidized state of that reaction center since the electron has been pushed to the electron acceptor Pheophytin leaving the reaction center without a replacement. In that very brief window of time a measurement of maximum fluorescence (F_m) of a dark-acclimated sample is taken. Immediately following the saturating pulse, the first level of actinic light is applied and remains illuminated until the next saturating pulse. This process repeats generally nine to twelve times before the RLC is finished. The time between saturating pulses commonly ranges from 10 sec to over a minute, depending on the organism and the time for all PSII reaction centers to return to a relaxed or "open" stage (electron replacement has occurred). Maximum fluorescence in light (F_m') is measured at each SP after the first, since all subsequent measurements are done in actinic light. The first saturating pulse on a dark-acclimated specimen provides a measurement of the optimal quantum yield (F_v/F_m) of PSII [$(F_m – F_0)/F_m$], which is a commonly used parameter for understanding PSII efficiency (Schreiber 2004). The use of F_v/F_m is based on the Law of Conservation of Energy and a couple of assumptions: First, it is assumed that during a saturating pulse, the quantum yield of photochemistry (Φ_P) is zero and the quantum yields of fluorescence (Φ_F) and non-photochemical quenching (Φ_{NPQ}) are at their maximal values and together equal 1 ($\Phi_{Fm} + \Phi_{NPQm} = 1$, where subscript m denotes maximum). Second, it is assumed that the ratio of Φ_F to Φ_{NPQ} does not change during the brief saturation pulses, thus $\Phi_{NPQm}/\Phi_{Fm} = \Phi_{NPQ}/\Phi_F$ (Schreiber 2004). After several derivations of these equations, Φ_P can be expressed in terms of fluorescence yield. Since $\Phi_P = \Phi_{II}$, the final equation for optimal quantum yield—explicitly measured from a dark-acclimated state—is $(\Phi_{II})_{max} = (F_m – F_0)F_m = $ **F_v/F_m**. Chlorophyll fluorescence is greatest in dark-acclimated specimens and decreases with time in light (Fig. 4.1), thus a plan to make multiple measurements on a dark-acclimated sample must consider the influence of each saturating pulse and the application of increasing levels of actinic light on various regions of the sample.

Multiple-scattering in coral skeleton microenvironments complicates the application of this measurement tool since structural variability in corals may be high between species, and internal light scattering may illuminate the coral at varying distances. Additionally, illumination across the coral surface may occur depending on the presence or absence of structures such as papillae or verrucae. Unintended illumination is practically unavoidable and may affect a coral fragment at points beyond that directly in view of the probe. The problem amplifies if multiple measurements are made. Branching

colony morphologies are particularly adept at light transport (Marcelino et al. 2013) and pose the greatest challenges for researchers using PAM fluorometry.

Two experiments separated in time and by design both employed measurements of coral photosynthetic efficiency as a means to test individual hypotheses. The first experiment involved the effects of increasing temperature and the second involved effects of decreased light availability on corals. This investigation took advantage of these two experiments to test a key assumption made during both previous experiments while using PAM on corals: PAM saturating light pulses initiate multiple-scattering effects by coral skeletal structures that alter the dark-acclimated status of the coral for subsequent measurements. In both experiments, rapid light curves (RLCs) were run at different positions on each individual coral by a Diving-PAM with WinControl-3.25 software (Heinz Walz GmbH, Germany). The number of measurements per fragment depended on the overall size of the fragments and the perceived risk of unwanted illumination. This chapter explores the effects of multiple measurements on coral fragments of various sizes and species and weighs the benefits against the drawbacks of a multiple measurement approach.

Methods

Experiment 1: Photosynthetic Efficiency Measurements — Increasing Temperature Treatments

Coral Collection and Acclimation

Over fifty fragments were collected from six common Hawaiian coral species: *Pocillopora meandrina* (n = 11), *Porites compressa* (n = 10), *P. lobata* (n = 12), *P. evermanni* (n = 8), *Montipora capitata* (n = 10), and *M. flabellata* (n = 6). Unique colonies were sought from several reef locations off the north- and east-facing sides of the island of Oʻahu—Kāneʻohe Bay (inside), Mokoliʻi, Waimanalo, and Hauʻula. Each colony was subsampled into ten ~5–7 cm^2 replicates that were fastened to coral plugs with reef-safe superglue (cyanoacrylate gel; Bulk Reef Supply, USA) and labeled. Fragments were placed in one of four flow-through seawater tables at the Coral Reef Ecology Laboratory (CREL) at Hawaiʻi Institute of Marine Biology (HIMB; Fig. 4.2a). Each seawater table was equipped with one Maxi-Jet 1200 Marineland powerhead circulation pump for water flow and a bubbling stone for oxygenation. Coral fragments were acclimated to ambient water temperature in the seawater tables for 14 days before heaters were added to the tables and temperatures were scheduled to increase incrementally for the duration of the experiment until all fragments had been sampled and/or bleached white.

Rapid Light Curves

Rapid light curve (RLC) measurements were conducted on one randomly chosen fragment per colony (n=57). These RLCs determined baseline photosynthetic efficiency for each colony before the start of the experiment. Subsequently, seawater was heated and RLCs were conducted on individual coral fragments that were deemed changed in pigmentation (Fig 4.2b). Each fragment was measured only once. Coral fragments were dark-acclimated for a minimum of 20 minutes before beginning fluorescence measurements. The fiber optic probe was fitted with surgical tubing that extended 1 mm from the end to allow the probe to safely rest on the surface of the coral without causing damage to the coral or the probe. This also permitted the probe to be positioned perpendicular to the coral surface and measurement distances to be consistent. The intensity of the blue light-emitting probe (470 nm, LED, 0.05 µmol photons m^{-2} s^{-1} , 5 Hz) was set to 8 and was too low to induce fluorescence when used as a measuring light. Damp was set at 2, gain at 6, ETR-F = 0.84, saturating pulse intensity was set at 8, saturation pulse width was 1 s, and the increasing actinic light values were 0, 56, 95, 165, 225, 350, 480, 537, and 585 µmol photons m^{-2} s^{-1} (Fig. 4.3).

Three RLCs were run per fragment at three separate positions on the fragment. Initial positioning of the probe on the coral fragment was done in the dark, thus this measurement was random in terms of visible surface pigmentation. The first position was, however, intentionally selected as far from the center as possible to permit space for two subsequent RLCs. Because light from the first RLC was believed to potentially influence the measurement values of the subsequent RLCs the position for the second was selected as distant from the first as permissible and the third was distant from the first and second positions as well. On branching morphologies, first RLCs were done close to the base of the fragment whereas tips or back sides of branches were selected for the second and third RLCs. Surface morphology was visibly illuminated during RLCs with saturating pulses and actinic light making it possible to select areas where light did not visibly reach. Painstaking effort was made for each measurement to avoid skeletal light-scattering effects above and below the tissue surface. This procedure began by dark-acclimating 8–10 fragments at a time and continuing the process until RLCs for all sampled fragments were concluded. For the sake of clarity, the first position RLC for each individual fragment will be termed PAM1, the second PAM2, and the third, PAM3.

Experiment 2: Photosynthetic Efficiency Measurements — Solar Irradiance Treatments

Coral Collection and Acclimation

Coral fragments from 22 unique *M. flabellata* colonies were collected on SCUBA at patch reef 50 (PR50) in Kāneʻohe Bay in August 2017. Each fragment was approximately 10-15 cm^2 and was sectioned with a Dremel tool into eight smaller fragments of roughly equal size (~5 cm^2). Fragments were adhered to the underside of 5 cm^2 porcelain tiles with reef-safe cyanoacrylate gel (Fig. 4.4). A total of 176 fragments were placed in a 367(L) x 36(W) x 33(D) cm flume (Fig 4.5a) with four Maxi-Jet 1200 Marineland powerhead circulation pumps, positioned just below the water surface to provide unidirectional water flow to all fragments.

For the first week, the entire flume was covered with 76% shade cloth. After seven days, the 76% shade cover on the south half of the flume was removed and replaced with 58% shade cover. The north half remained shaded at 76% (Fig. 4.5b). The 58% shade screen was used to approximately simulate the ambient light at 5 m depth in Kāneʻohe Bay, the deepest point from which the corals had been collected.

Rapid Light Curves

On day seven, while all corals were shaded at the same irradiance levels, RLC measurements were conducted for one fragment per colony per sector as described previously with the same PAM settings and increasing actinic light values: 0, 56, 95, 165, 225, 350, 480, 537, and 585 µmol photons m^{-2} s^{-1}. Due to concern regarding undesired illumination beyond the area directly beneath the probe, only two RLCs were deemed prudent. To avoid light-scattering effects from the first RLC on the second, each fragment was measured at two separate areas as distant from one another as possible. Again, painstaking care was taken to maintain dark-acclimation status at the second measurement position. This procedure was done by dark-acclimating 8–10 fragments at a time and continuing the process until RLCs for all 88 fragments were measured. The same process was repeated on days 21 and 28 after the light at the south half of the flume had been reduced to 58%. The purpose of the two different shading regimes was to determine whether *M. flabellata* would acclimate to different quantities of light with a change in host pigmentation. The RLCs were done to determine the extent to which host pigment changes would yield measurable differences in photosynthetic efficiency.

Diel Changes in Photosynthetic Efficiency

During the course of both experiments it appeared that optimal quantum yield (F_v/F_m) was decreasing around midday and increasing again after ~14:00. Each RLC takes 90 seconds from first saturating pulse to last (nine total). Since each fragment was measured twice, RLCs took three minutes per fragment with approximately one minute between fragments. Approximately six hours was required to run RLCs for 88 fragments, thus the process began in the morning and continued into the afternoon or over the course of two days when needed. The process was even longer in the previous experiment because three RLCs were conducted per fragment.

To determine whether the midday depressions in F_v/F_m were occurring in the community as a whole, a brief experiment was conducted over the course of one day with a small subset of available coral fragment replicates (n = 4) that were kept in a separate 660-gallon mesocosm. RLCs were run at two positions on the coral fragment every hour beginning at 08:45 and ending at 14:45 as described above. The process took 20 minutes for dark acclimation and 15 minutes to run all RLCs, after which coral fragments were returned to the mesocosms in full sun for the remaining 25 minutes until it was time to begin again. RLCs were run at precisely the same position on the coral fragment each time.

Statistical Analyses

The statistical analyses were post-hoc in nature as the original data were collected with other hypotheses and statistical tests in mind. Statistics were analyzed in RStudio version 1.1.456 for Mac OS X version 10.14.4 and in JMP Pro version 14 by SAS. Data for each colony from three species (*M. flabellata*, *P. compressa*, *P. meandrina*) in Experiment 1 were examined for fixed effects of prior measurements on subsequent measurements, i.e., RLCs from PAM1 on PAM2 and PAM3 *and* RLCs from PAM2 on PAM3. Analysis was done for each fragment within a colony since each had been sampled at different times over the course of the experiment and loss of algal pigmentation increases skeletal reflectivity. Furthermore, these three species were chosen to represent the range of skeletal and colony morphologies present in Kāneʻohe Bay.

A logistic regression (logit model) and linear mixed model fit by the restricted maximum likelihood (REML) estimation function were used to estimate the variance components of random effects of individual fragments as well as colonies. Type III Analysis of Variance (ANOVA) with Satterthwaite's method was used for t-tests. Fixed effects were based on the F_v/F_m (first saturating pulse) from PAM1 on PAM2 and/or PAM3 and PAM2 on PAM3. The models in R were as follows:

mflab.model <- lmer(logitFvFm ~ satOrder + (1|colony) + (1|Fragment.ID), data = mflab1)

pcom.model <- lmer(logitFvFm ~ satOrder + (1|colony) + (1|Fragment.ID), data = pcom1)

pmean.model <- lmer(logitFvFm ~ satOrder + (1|colony) + (1|Fragment.ID), data = pmean1)

Experiment 2 involved only one species, *M. flabellata*, and the same fragments (with few exceptions) were measured over the course of the entire acclimation period. The statistical analysis was as previously described for experiment 1 with similar model outputs in R:

fvfm.model <- lmer(logitFvFm1 ~ satOrder + (1|colony) + (1|Fragment.ID), data = fvfm)

Additionally, a linear mixed model was fit to determine whether a difference in F_v/F_m occurred in replicates in the ambient light vs. the shaded light regimes. As previous, this model accounted for repeated measurements on the same coral fragments over time.

flume.model <- lmer(Yield ~ Light + (1|Fragment.ID), data = flume2)

Results

Experiment 1: Photosynthetic Efficiency Measurements — Increasing Temperature Treatments

Based on observations of illuminated coral surface and skeletal structures during the RLCs (Fig. 4.6a-d), it was hypothesized that previous RLCs (PAM1, PAM2) would affect the dark-acclimated status of the subsequent RLCs (PAM2, PAM3) on individual fragments for all species. Due to the compact skeletal structure, lack of protruding surface relief, and minimal light bleed during illumination, it was assumed that *P. compressa* would be least affected. In contrast, greater effect was expected in *P. meandrina* due to its branching morphology and loosely structured internal skeletal features and prominent surface verrucae (Fig. 4.6c). Furthermore, *Montipora flabellata* represents an encrusting coral with minute surface papillae and rapid skeletal growth, thus a moderate effect was predicted for this species.

Contrary to the hypotheses, PAM1 and/or PAM2 had no significant effect on PAM2 or PAM3 in any of the three species examined (*M. flabellata* p = 0.288, *P. compressa* p = 0.182, *P. meandrina* p = 0.633; Figs. 4.7, 4.8). Order of measurements explains less than 1% of the variation in F_v/F_m whereas most of the variation is explained by fragment level effects (*M. flabellata* r^2 = 0.88, *P. compressa* r^2 = 0.66, *P. meandrina* r^2 = 0.60; Table 4.1).

Experiment 2: Photosynthetic Efficiency Measurements — Solar Irradiance Treatments

Two RLCs per fragment were run for Experiment 2 because it was believed that limiting the number of total measurements would be more prudent. Therefore, it was hypothesized that there would be no effect of the first PAM RLC on the second in either sun or shade fragments at any of the time points (Fig. 4.9). As hypothesized, no significant effect of the first RLC on the second RLC was detected (Table 4.2). Random fragment effects explain most of the variability in F_v/F_m (day 7 $r^2 = 0.592$, day 21 $r^2 = 0.785$, day 28 $r^2 = 0.759$, day 48 $r^2 = 0.773$).

The first day of RLC measurements for Experiment 2 occurred several days after colony collection when ambient solar irradiance was the same for all. The second and third days of RLCs occurred after half of the replicates had been shaded, and the fourth day of RLCs occurred after all had been returned to the same, shaded, light regime. F_v/F_m in shaded corals was significantly different than in ambient corals ($p < 0.001$) although the difference (~0.06 rel. units) was small and potentially of minor biological importance. In fact, larger ranges in variability were previously described in Experiment 1 for fragments within this species and as compared to other species (Fig. 4.7). By design, differences in F_v/F_m were expected from the shaded coral replicates as compared to their ambient light (sun) controls (Fig. 4.10). From these results, it appears that by day 21, mean F_v/F_m in shaded corals increased while mean F_v/F_m in sun controls decreased. Later, the mean F_v/F_m value trends reversed by decreasing in shade corals and increasing in controls until at day 48, after several days in the same light regime, the values were again near convergence (Fig. 4.11).

Diel Changes in Photosynthetic Efficiency

High variability in mean F_v/F_m was observed at the initiation of the experiment (09:45) with a range from ~0.35 to ~0.58 (relative units). Most of the fragments increased F_v/F_m and reached a morning maximum at the second time point (10:45). All fragments decreased in F_v/F_m after the 10:45 measurement with two reaching a minimum at 12:45 and the other two at 13:45. In all fragments, the midday minimum F_v/F_m was lower than the first morning measurement and all fragments exhibited a marked increase in F_v/F_m at the time point directly following the midday minimum (Fig. 4.12).

Discussion

      Despite concern that repeated RLC measurements on individual coral fragments were altering subsequent measurements, there was no evidence found from over 300 coral fragments (both experiments combined) that a systematic effect exists. These results are likely due to a combination of very careful probe positioning during the first experiment, and a reduced number of measurements in the second. Importantly, these results show that coral fragments approximately 5 cm^2 in size, can accommodate three RLCs without F_v/F_m distortion from skeletal light-scattering. With *Pocillopora meandrina* fragments in particular, the possibility for far-reaching light transport was high and it was often necessary to run a second or third RLC on the opposite side of a branch from the first RLC. The lack of effect in this species, while surprising, may be partially explained by the nature of the probe design and the limitations to what the probe actually measures. The measurement of fluorescence entails emission of light from the probe that is absorbed at a particular wavelength and emitted at a lower wavelength. The light from the probe reaches a limited surface area and captures the signal from the emitted light from the surface chlorophyll *a* only. Presumably, reflected and/or diffuse light that is transported beyond the area being measured, will reach symbiont undersides and not affect the top surface from the opposite side of the branch where the next measurement may be taken. Additionally, *P. meandrina* tended to be in the larger size category, closer to ~6–7 cm^2, permitting multiple measurements at greater distances from one another.

      Variability in F_v/F_m was fairly consistent and relatively high between fragments of the same colony. This was expected since the experiment called for sampling fragments when a visible pigment decrease was detected. This resulted, by design, in higher values of F_v/F_m at the beginning and lower values at the end of the experiment. Interestingly, *M. flabellata* colonies exhibited lower F_v/F_m overall and higher F_v/F_m variability between fragments than other species. These results indicate notable differences in photosynthetic efficiency between species.

      In Experiment 2, the PAM measurement data was collected during the light acclimation period. The F_v/F_m values were expected to change in shaded *M. flabellata* fragments (Shade) as compared to the ambient light controls (Sun), but it was unclear whether F_v/F_m would increase or decrease. The results show that a significant change in F_v/F_m did occur in replicates of the same colonies kept in separate light regimes. After the replicates were returned to the same light regime, the difference between the F_v/F_m means decreased while variability remained quite high. High variability thus appears to be a consistent characteristic of this species. These results support the need for taking multiple measurements on individual fragments due to the potentially high variability in F_v/F_m over small distances of the same fragment.

A midday drop in F_v/F_m was noted during data collection for Experiment 1, but confirmation of this phenomenon was lacking. The brief time-series test conducted during Experiment 2 verified that there was a sharp decrease in F_v/F_m around noon in four *M. flabellata* colonies, but this has not been tested in other species. While it is likely to hold true for a number of other coral species, it would be interesting to quantify the decrease and to run RLCs on a larger number of fragments per species.

If measurements of photosynthetic efficiency in corals are part of an experimental design, it is advisable to plan coral fragment size based on an optimal number of RLC measurements, if possible. Coral fragment size and skeletal light transport capability are factors that should be accounted for in each species to determine the appropriate number of measurements on each sample. If planned properly, several RLCs can be run on one coral fragment to obtain robust photosynthetic efficiency measurements.

Conclusions

High F_v/F_m variability, particularly at a fine scale within small colony fragments, demonstrated the need to derive a mean value through multiple RLC measurements per fragment. This may not always be possible due to specimen collection size restrictions but should be carefully considered when planning experiments utilizing PAM fluorometry. Small fragments ($\sim$5 cm^2) accommodated three carefully distanced RLC measurements, despite highly reflective skeletal morphologies. It is recommended that no fewer than three RLCs per fragment should be considered, thus fragment size should be no smaller than $\sim$5 cm^2. Previous RLC measurements did not influence subsequent RLC measurements in three different coral skeletal morphologies with highly variable scattering abilities. This was particularly surprising in *Pocillopora meandrina*, a branching coral with visibly far-reaching light transport capabilities. Measured midday declines in photosynthetic efficiency exposed the importance of avoiding midday PAM measurements for accurate and comparable data acquisition. This becomes particularly important when running RLCs on large numbers of fragments and should be factored into the experimental design.

Acknowledgments

References

Darling ES, Alvarez-Filip L, Oliver TA, McClanahan TR, Côté IM (2012) Evaluating life-history strategies of reef corals from species traits. Ecol. Lett. 15:1378–86

Davy SK, Allemand D, Weis VM (2012) Cell biology of cnidarian-dinoflagellate symbiosis. Microbiol. Mol. Biol. Rev. 76:229–261

Enrıquez S, Méndez E, Iglesias-Prieto R (2005) Multiple scattering on coral skeletons enhances light absorption by symbiotic algae. Limnol. Oceanogr. 50:1025–1032

Falkowski PG, Dubinsky Z, Muscatine L, Porter JW (1984) Light and the bioenergetics of a symbiotic coral. Bioscience 34:705–709

Kirk JTO (2010) Light and photosynthesis in aquatic ecosystems, third edition. Cambridge University Press, New York, USA

Marcelino LA, Westneat MW, Stoyneva V, Henss J, Rogers JD, Radosevich A, Turzhitsky V, Siple M, Fang A, Swain TD, Fung J, Backman V (2013) Modulation of light-enhancement to symbiotic algae by light-scattering in corals and evolutionary trends in bleaching. PLoS One 8:e61492

Maxwell K, Johnson GN (2000) Chlorophyll fluorescence - a practical guide. J. Exp. Bot. 51:659–668

Muscatine L, Falkowski P, Porter J, Dubinsky Z (1984) Fate of photosynthetic fixed carbon in light- and shade-adapted colonies of the symbiotic coral *Stylophora pistillata*. Proc. R. Soc. London B Biol. Sci. 222:181–202

Muscatine L, McCloskey L, Marian R (1981) Estimating the daily contribution of carbon from zooxanthellae to coral animal respiration. Limnol. Oceanogr. 26:601–611

Pearse VBV, Muscatine L (1971) Role of symbiotic algae (zooxanthellae) in coral calcification. Biol. Bull. 141:350–363

Price SA, Holzman R, Near TJ, Wainwright PC (2011) Coral reefs promote the evolution of morphological diversity and ecological novelty in labrid fishes. Ecol. Lett. 14:462–9

Roberts CM, McClean CJ, Veron JEN, Hawkins JP, Allen GR, McAllister DE, Mittermeier CG, Schueler FW, Spalding M, Wells F, Vynne C, Werner TB (2002) Marine biodiversity hotspots and conservation priorities for tropical reefs. Science 295:1280–1284

Roth MS (2014) The engine of the reef: photobiology of the coral-algal symbiosis. Front. Microbiol. 5:422

Schreiber U (2004) Pulse-Amplitude-Modulation (PAM) Fluorometry and Saturation Pulse Method: An Overview. In: Papageorgiou G., Govindjee (eds) Chlorophyll a Fluorescence. Springer, Dordrecht, Netherlands

Swain TD, DuBois E, Gomes A, Stoyneva VP, Radosevich AJ, Henss J, Wagner ME, Derbas J, Grooms HW, Velazquez EM, Traub J, Kennedy BJ, Grigorescu AA, Westneat MW, Sanborn K, Levine S, Schick M, Parsons G, Biggs BC, Rogers JD, Backman V, Marcelino LA (2016) Skeletal light-

scattering accelerates bleaching response in reef-building corals. BMC Ecol. 16:10

Taiz L, Zeiger E (2010) Plant Physiology. 5th Ed. Sinauer. MA, USA

Todd PA (2008) Morphological plasticity in scleractinian corals. Biol. Rev. 83:315–337

Trench RK (1993) Microalgal-invertebrate symbioses: A review. Endocytobiosis Cell Res. 9:135–175

Veron JEN, Stafford-Smith M (2000) Corals of the World. Australian Institute of Marine Science, Townsville MC, Qld, Australia

Wakefield T, Farmer M, Kempf S (2000) Revised description of the fine structure of in situ "zooxanthellae" genus Symbiodinium. Biol. Bull. 199:76–84

Wangpraseurt D, Larkum AWD, Franklin J, Szabo M, Ralph PJ, Kuhl M (2014) Lateral light transfer ensures efficient resource distribution in symbiont-bearing corals. J. Exp. Biol. 217:489–498

Wangpraseurt D, Larkum AWD, Ralph PJ, Kühl M (2012) Light gradients and optical microniches in coral tissues. Front. Microbiol. 3:1–9

Tables and figures

Figure 4.1. Fluorescence rapid light curve (RLC) with saturating pulses explained in detail. F_0 = baseline or dark-acclimated fluorescence yield, F_m = maximal fluorescence yield of a dark-acclimated sample, F_v = increase in fluorescence yield during a saturating pulse, F_m' = maximal fluorescence yield of an illuminated sample, F = fluorescence yield (any time while sample is illuminated between pulses), F_0' = minimal fluorescence yield (after sample return to dark). ML = measuring light, SP = saturating pulse, AL = actinic light. At the initiation of an RLC, a measuring light captures F_0 of a dark-acclimated. A SP follows. If no actinic light is turned on that time, the fluorescence will rapidly return to or near F_0. In an RLC, immediately after the sample has received a SP, the actinic light turns on and drives photosynthesis. After a pre-determined amount of time, i.e., 10 seconds, another SP with a subsequent increase in AL occurs and repeats until the final SP. Both lights turn off. Note the decrease in F_m' with increase in actinic light intensity and number of saturating pulses. Adapted from Schreiber (2004).

Optimal quantum yield = $(F_m - F_0)/F_m = \mathbf{F_v/F_m}$

Effective quantum yield = $(F_m' - F)/F_m' = \Delta F/F_m'$
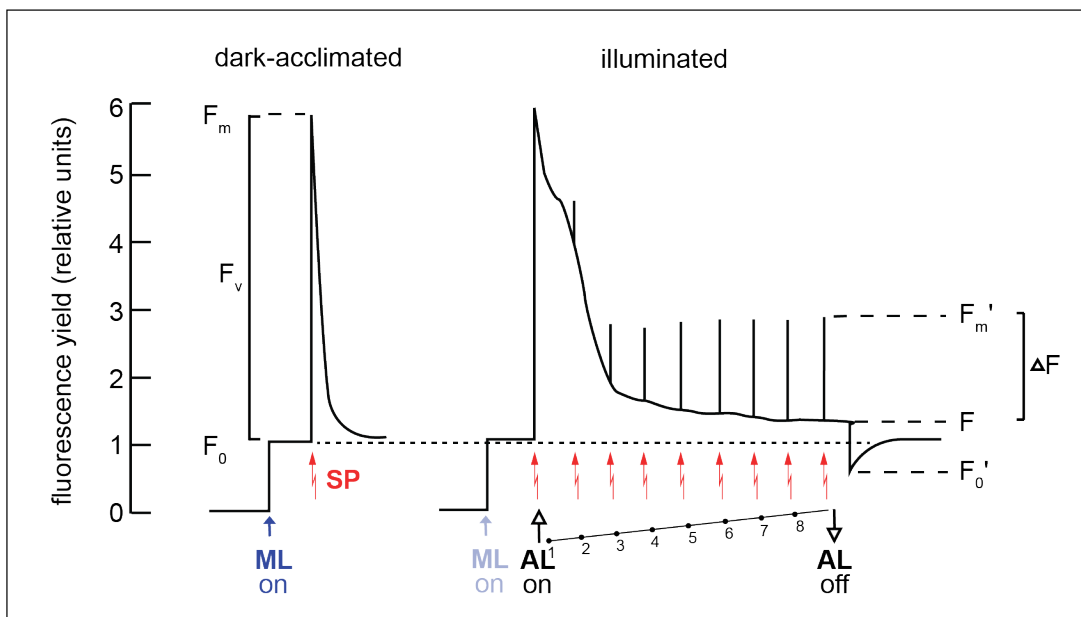
Figure 4.2. (a) Experiment 1 coral colonies from six species. Outdoor flow-through seawater tables. (b) Typical subset of coral fragments from various species prior to dark-acclimation showing variety in fragment size, color, and morphology.

Figure 4.3. WinControl software plots of RLCs for Experiment 1. ETR reaches asymptote with subsequent plateau and decrease. Fluorescence yield (green lines, Y symbol), NPQ (blue lines, box symbol), maximal fluorescence yield in light (F_m'; brown lines, X symbol), and illuminated fluorescence (F; black lines, + symbol).
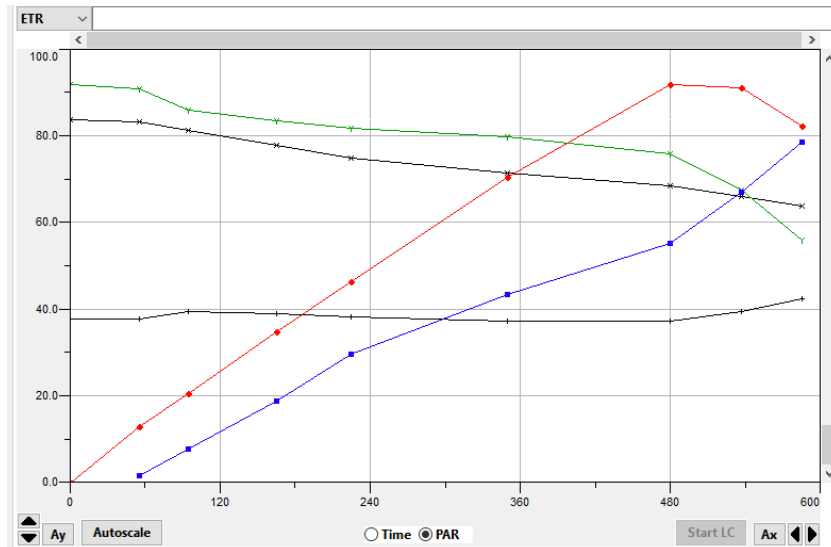
Figure 4.4. Experiment 2 *Montipora flabellata* fragments showing diversity in pigmentation, surface morphology and size. Tile size is 5 cm^2.

Figure 4.5. Experiment 2 flume demonstrating differently shaded sections. Water flow was the same for all coral fragments.

Figure 4.6. Rapid light curves on different coral species. Top inset photos taken during actinic light illumination, bottom photos taken during saturating light pulse (photos a-c, only). Probe position in top and bottom photos is exactly the same. (a) Pigmented *Montipora flabellata*, (b) Paling *M. flabellata*, (c) Paling *Pocillopora meandrina*, (d) Pigmented *Porites compressa* viewed with ambient red light. Note distance of light transport before and during saturating light pulses.
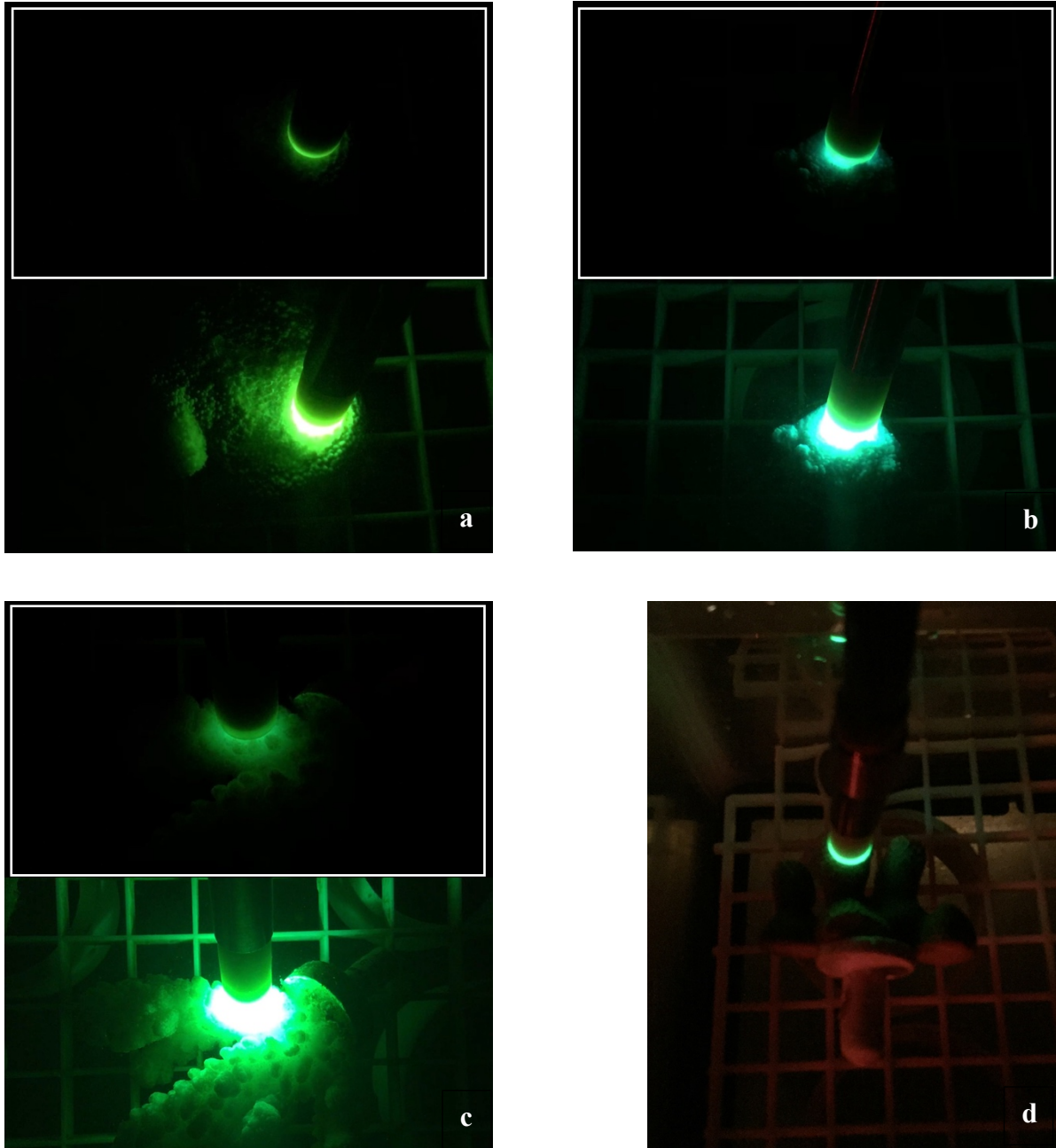
Figure 4.7. F_v/F_m plots for three coral species testing effects of previous on subsequent PAM measurements. F_v/F_m values are in relative units.
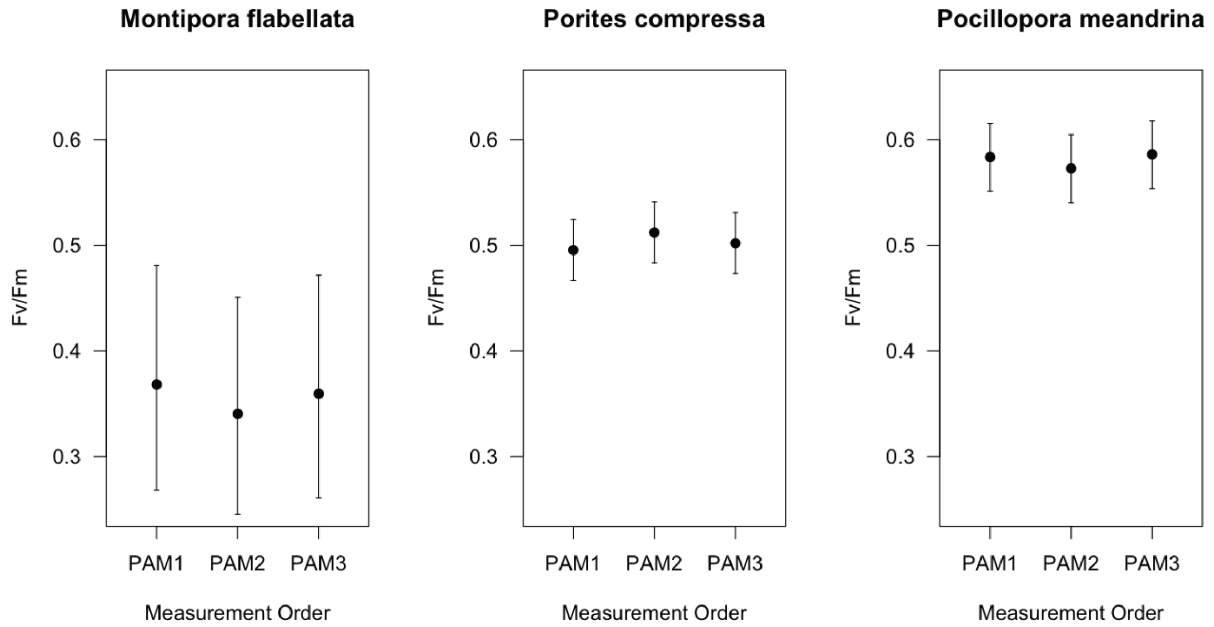
Table 4.1. Experiment 1 results of linear mixed model testing effects of previous on subsequent PAM measurements for three coral species with different skeletal light transport capabilities.

Species	Colony (n)	Frag (n)	Observ (n)	Fragment effects r^2	PAM1 on PAM2	PAM1 on PAM3 r^2	PAM2 on PAM3	Effects of PAM order Mean Sq	DF	p-value
M. flabellata	6	55	165	0.88	-0.166	-0.166	0.500	0.21141	2	0.288
P. compressa	11	99	297	0.66	-0.308	-0.308	0.500	0.11173	2	0.182
P. meandrina	11	101	301	0.60	-0.448	-0.448	0.497	0.084192	2	0.633

Figure 4.8. Plots for Experiment 1 depicting effects of previous on subsequent PAM measurements by species. A systematic decrease in F_v/F_m would appear as clusters below the 1:1 line. Instead, for all three species, clusters are spread out above and below showing no clear pattern or effect due to PAM measurement order. F_v/F_m values in relative units. Colored dots represent unique colonies.
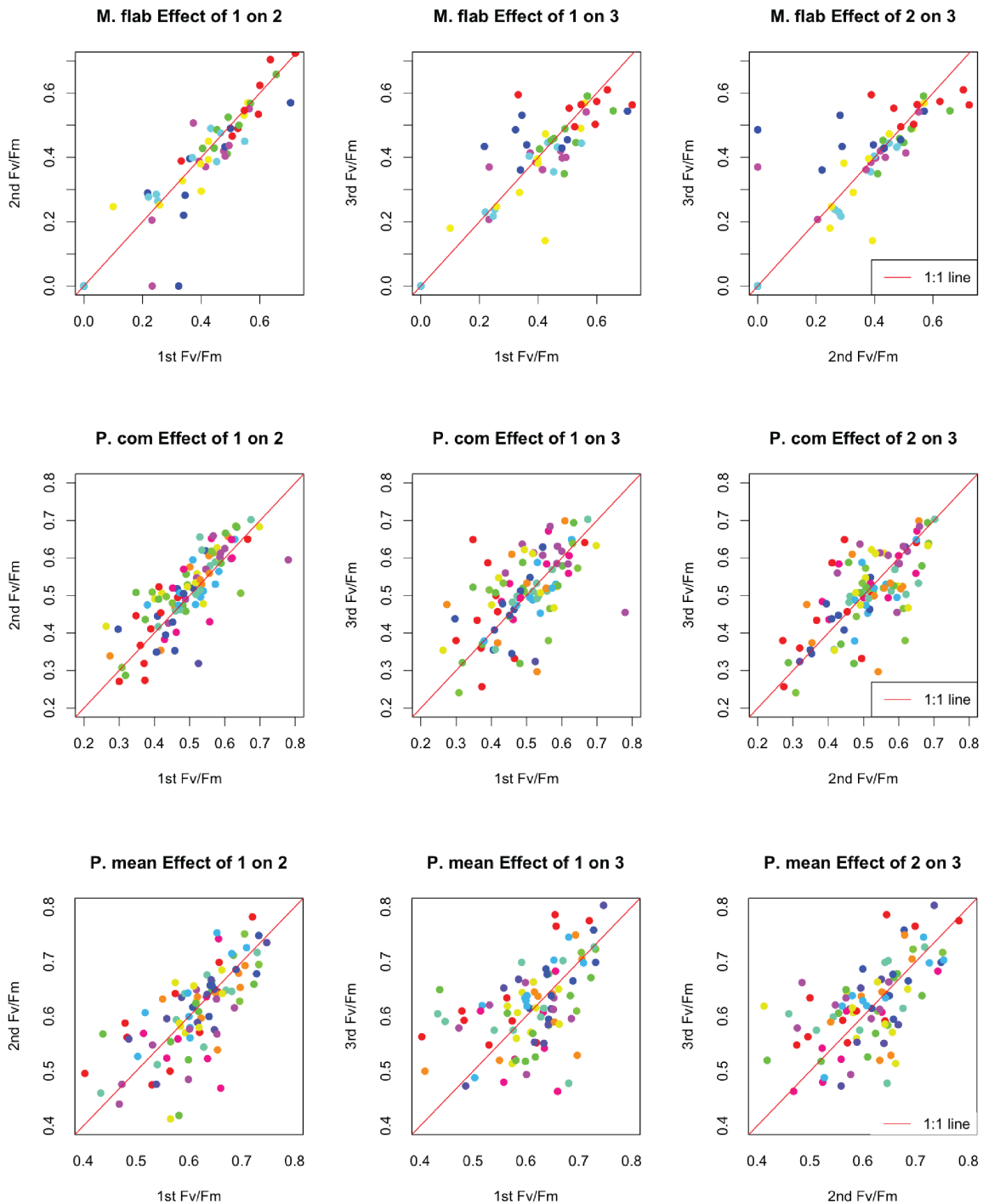
Figure 4.9. Plots for Experiment 2 depicting effects of previous on subsequent PAM measurements in *Montipora flabellata* colonies. A systematic decrease in F_v/F_m would appear as clusters below the 1:1 line. Instead, for all timepoints, clusters are spread out above and below showing no clear pattern or effect due to PAM measurement order. F_v/F_m values in relative units. Colored dots represent unique colonies.
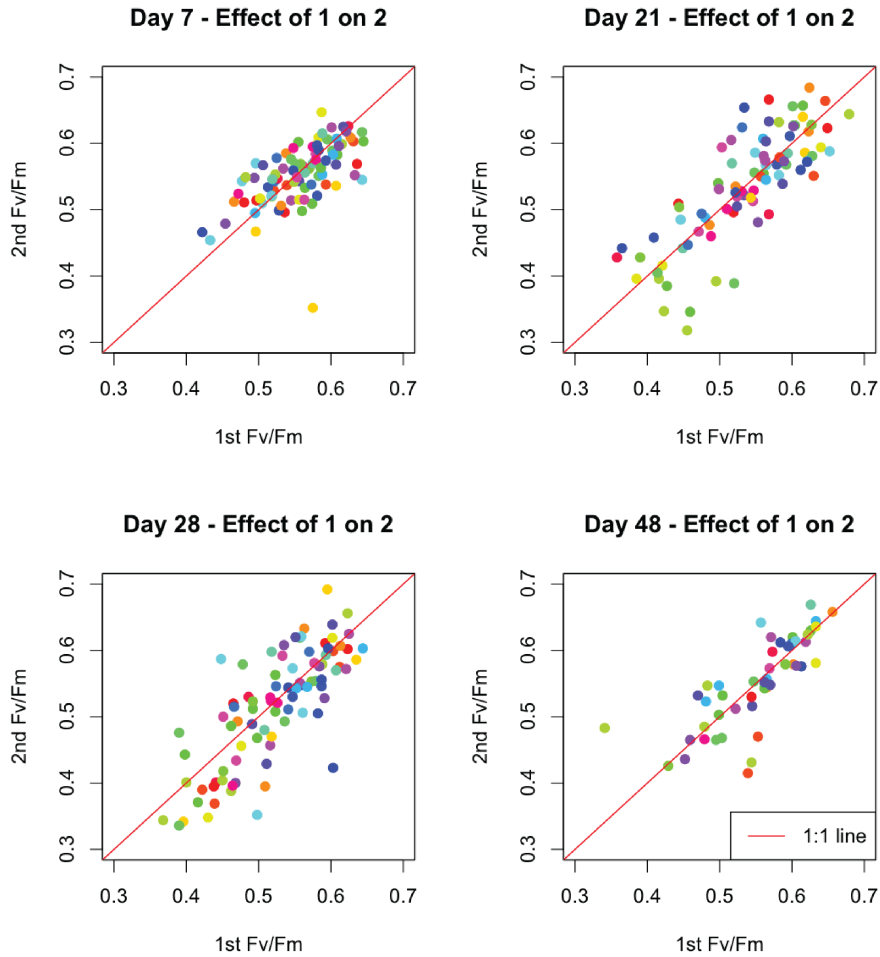
Table 4.2. Experiment 2 results of linear mixed model testing effects of previous on subsequent PAM measurements for *Montipora flabellata* colonies at four different time points.

Date	Colony (n)	Frag (n)	Observ (n)	Fragment effects r^2	PAM1 on PAM2 r^2	Effects of PAM order		
						Mean Sq	DF	p-value
Day 7	22	88	176	0.592	-0.437	0.007	1	0.504
Day 21	22	88	176	0.785	-0.328	0.008	1	0.561
Day 28	22	88	176	0.759	-0.348	0.050	1	0.153
Day 48	11	48	96	0.773	-0.337	0.0001	1	0.930

Figure 4.10. Plots of F_v/F_m from two measurements per *Montipora flabellata* fragment on Day 21 of Experiment 2. This data set shows the greatest differences in F_v/F_m between light acclimation replicates of all time points. Yellow symbols = controls (sun), grey symbols = shaded replicates. First (PAM1) measurements represented by squares and second measurements (PAM2) represented by circles. Fragments within a colony (MF_01, etc.) were randomly assigned to sun or shade acclimation.
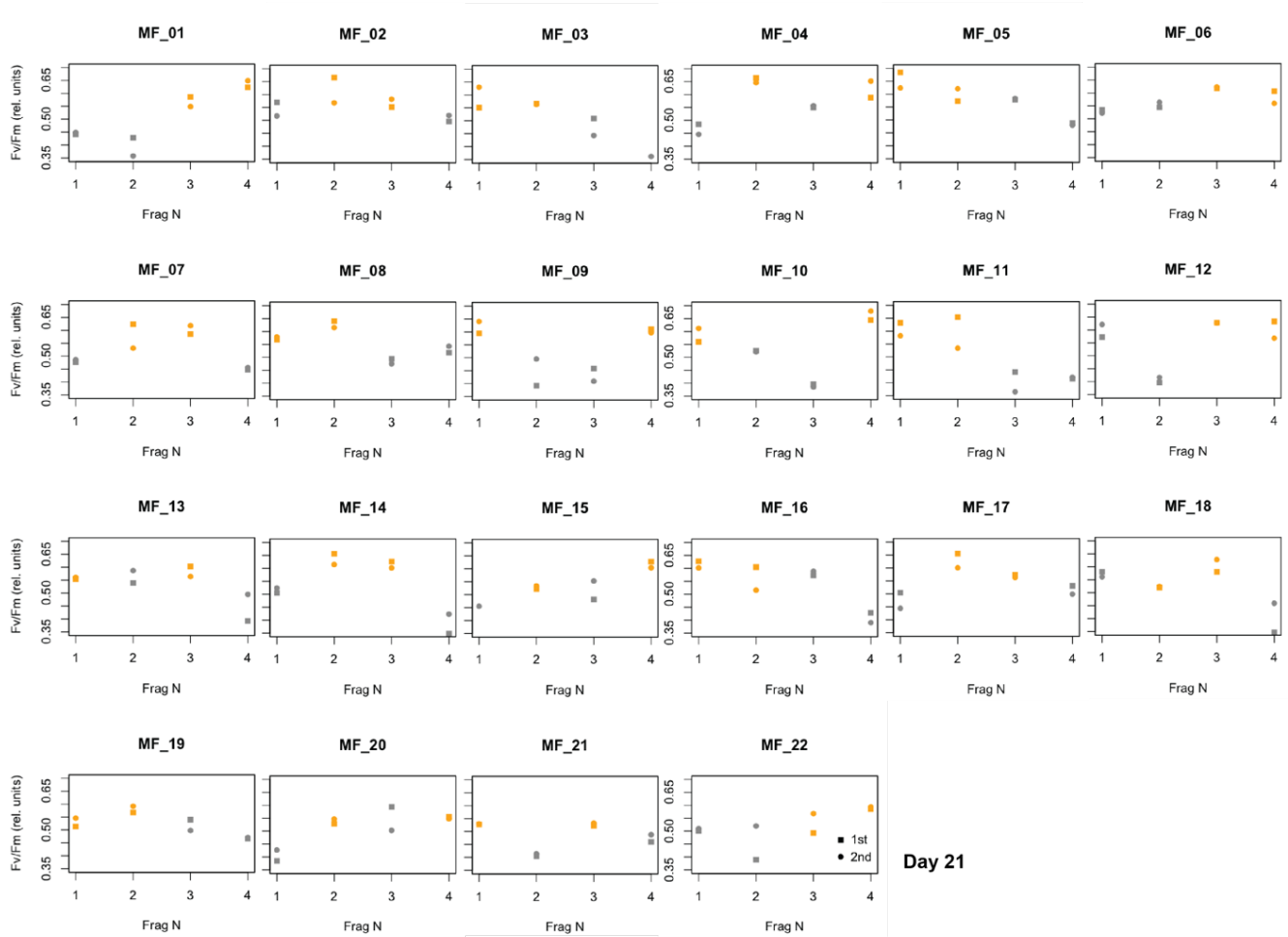
Figure 4.11. (a) F_v/F_m (relative units) plot for *Montipora flabellata* colony replicates from Experiment 2, (b) mean difference in F_v/F_m between sun and shade acclimation replicates.
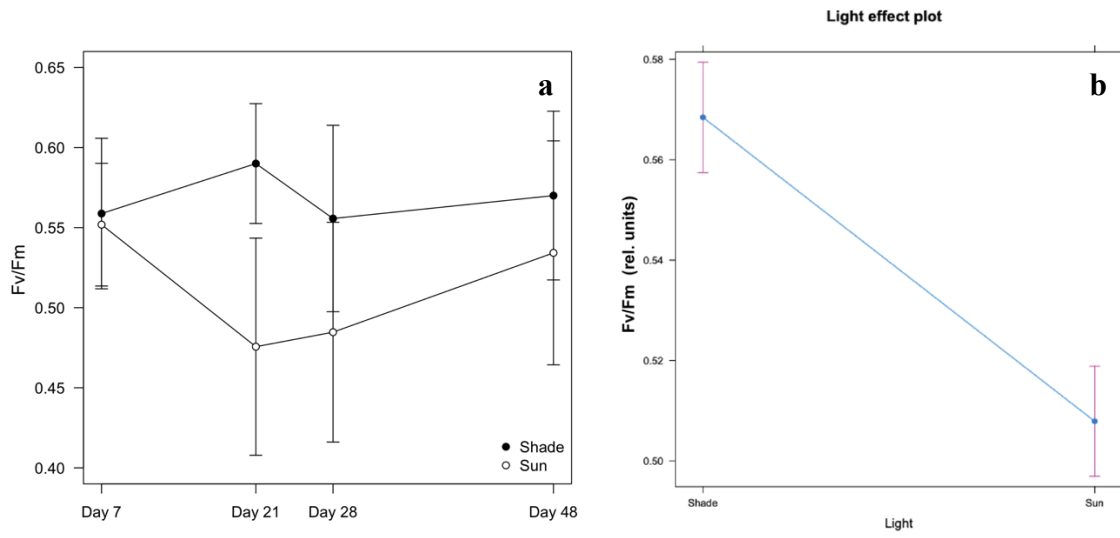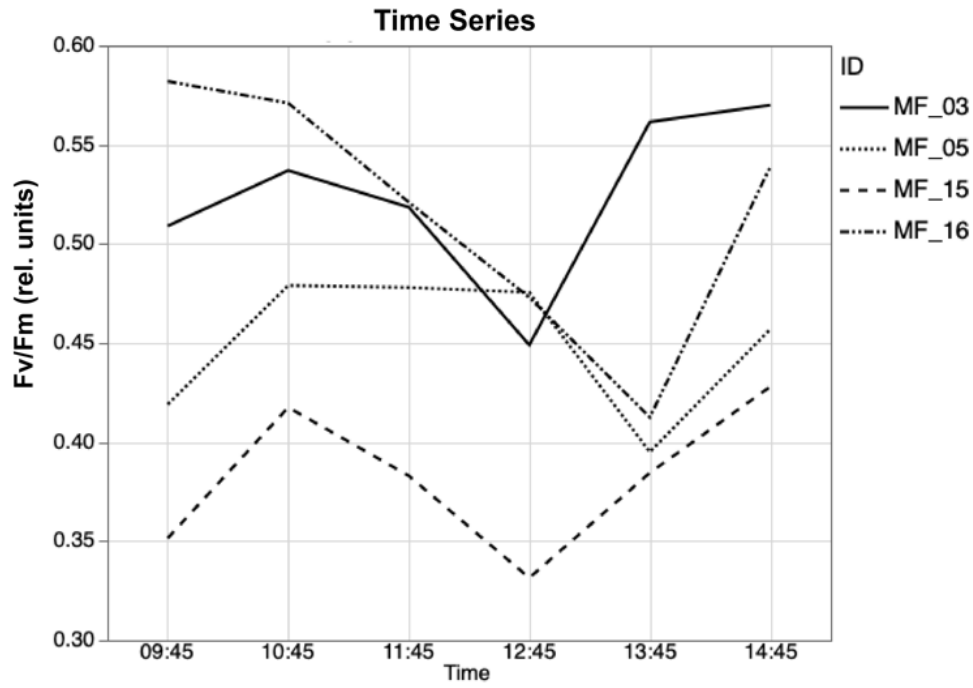
Figure 4.12. Plot of mean F_v/F_m (two measurements) from four *Montipora flabellata* colony fragments at hourly time points during one day.

CONCLUSIONS

The results from this investigation support the role of photoprotection for the chromoproteins in *Montipora flabellata*. Thick sheaths of CPs were found located in the coral epidermis with a low number or near lack of mucocytes as compared to the other species that were investigated. The low mucocyte count suggests an energy trade-off that places the requirements of photoprotection over the numerous, beneficial functions carried out in the surface mucus layer in most corals. This can be explained by colony distribution and water flow and sedimentation results, which showed that *M. flabellata* colonies are present in Kāne'ohe Bay lagoon areas near the channels where suspended particulate and water flow are high. These habitat conditions likely remove the need for mucus production in *M. flabellata* under normal conditions and are consistent with a high water flow requirement in *M. flabellata* to prevent particles from settling or to remove them when settling occurs.

Fluorescent proteins were found in the epidermis in several species, supporting a photoprotective role for some but not all FPs in these Hawaiian species. RFPs were consistently found within surface structures; epidermis of polyps, tentacles, coenenchyme, but these should be more thoroughly explored.

The minimally invasive, non-destructive approach to determine whether CPs and/or RFPs have an effect on photosynthetic efficiency in the four Hawaiian coral species showed no correlation between high CP absorbance and any of the photosynthetic parameters measured. These results do not provide supporting evidence of a photoprotective function, however, they also do not exclude the possibility. It is conceivable that the only way to measure photoprotection in corals is to cause light stress and measure differences between treatments and controls. Since this investigation explicitly sought methods that avoided stress experiments, it can only be concluded that CPs and RFPs do not affect photosynthesis under normal conditions, or that CP and RFP concentrations were not high and/or variable enough to make this determination. Future attempts to repeat this or a similar experiment would likely benefit from fragment collection at a time when CPs are highly prominent.

The results did provide important insight into how each species functions in their particular irradiance habitats. For example, the photosynthetic parameter E_k—minimum saturating irradiance— illustrated that *M. flabellata* operates under supersaturating irradiance for most hours of each day. The extensive work conducted with PAM fluorometry during this investigation showed that coral F_v/F_m can be highly variable across the colony surface and that several measurements and mean values should be utilized whenever fragment size permits. Concerns regarding effects of previous rapid light curve (RLC) measurements on subsequent RLC measurements were unfounded as no effect was observed in three different coral skeletal morphologies with highly variable light-scattering abilities.

PAM fluorometry is commonly used for the study of plants and algae, but it is not widely used for corals, perhaps due to the complicated coral skeletal structures and poor understanding of the information PAM can provide. When used for corals, most investigations provide data on F_v/F_m only, however, this is not always the most informative parameter. RLCs provide powerful photophysiological information that improves our understanding of how corals use and are affected by irradiance. Because irradiance exacerbates thermal stress and accelerates symbiont loss, understanding the photobiological capabilities and limitations of all coral species when conditions are normal will help us predict which species will be most vulnerable when periods of thermal stress occur. This knowledge may aid management to determine where best to focus protection efforts to meet the challenges of rising seawater temperatures due to global climate change.